U. S. DEPARTMENT OF COMMERCE
Charles Sawyer, Secretary
NATIONAL BUREAU OF STANDARDS
E. U. Condon, Director

JUNE 1948
VOLUME 40
NUMBER 6

JOURNAL OF RESEARCH

of the

NATIONAL BUREAU OF STANDARDS

Contents

		Page
887.	Resin bonding and strength development in offset papers. Charles G. Weber, Merle B. Shaw, Martin J. O'Leary, and Joshua K. Missimer. (Price 10 cents)	427
888.	Metastable transitions in mass spectra of fifty-six hydrocarbons. Evelyn G. Bloom, Fred L. Mohler, Jonathan H. Lengel, and C. Edward Wise. (Price 10 cents)	437
889.	Determination of small amounts of oxygen in organic compounds. William W. Walton, Francis W. McCulloch, and W. Harold Smith. (Price 10 cents)	443
890.	Infrared emission spectra of flames. Earle K. Plyler and Curtis J. Humphreys. (Price 10 cents)	449
891.	Pressure-volume-temperature data for oxygen. Cyril H. Meyers. (Price 10 cents)	457
892.	Reduction of sphero-chromatic aberration in catadioptric systems. Robert E. Stephens. (Price 5 cents)	467
893.	Some energy relations in the systems PbO–B_2O_3 and Pb–SiO_2. Leo Shartsis and Edwin S. Newman. (Price 10 cents)	471
894.	Divided flow, low-temperature humidity test apparatus. Arnold Wexler. (Price 10 cents)	479
895.	Gradual damping of solitary waves. Garbis H. Keulegan. (Price 10 cents)	487
	Index to volume 40 (January to June 1948, Research Papers RP1850 to RP1895).	499

Sale by the Superintendent of Documents, U. S. Government Printing Office, Washington 25, D. C. - Price 50 cents
$4.50 per year on subscription

UNITED STATES GOVERNMENT PRINTING OFFICE, WASHINGTON : 1948

S. Department of Commerce
ational Bureau of Standards

Research Paper RP1887
Volume 40, June 1948

Part of the Journal of Research of the National Bureau of Standards

Resin Bonding and Strength Development in Offset Papers

By Charles G. Weber, Merle B. Shaw, Martin J. O'Leary, and Joshua K. Missimer

A series of experimental offset papers was made in which the strength and resistance to surface pick were developed mainly by bonding the fibers with a synthetic resin instead of by the conventional beating. The papers were made from three widely different furnishes of commercial wood pulps, and the principal bonding agent was melamine-formaldehyde resin. In all instances, the resin-bonded papers were superior with respect to curling, oil absorption, folding endurance, and resistance to tear to gel-bonded control papers with comparable bursting strength and resistance to pick. Expansion also was improved in sulfite-soda papers. Only small amounts of resin were required to greatly improve the strength of papers composed principally of short-fibered filler pulps.

I. Introduction

Maximum strength in wood-fiber papers is cus-marily developed by beating with the formation gel-like bonds formed by the hydration asso-ated with beating. For the best results in fset printing, paper must be made with a mini-um of beating, because the formation of gel on e fibers must be carefully controlled. The velopment of maximum strength by hydration omotes some of the most troublesome proper ies paper encountered in offset printing, namely, gh expansion, excessive curling, slow oil absorp-on, and low opacity.

In experimental manufacture of offset papers at e National Bureau of Standards the use of a nthetic resin, widely used for imparting wet rength to paper, has been extended to a new eld. Resin bonds between the fibers are sub-ituted for the conventional gel-like bonds formed hydration. The resin bonding made it pos-ble to develop suitable strength with a minimum adverse effect on the other properties of the aper.

Maximum strength was developed in wood-fiber apers by resin bonding with only a fraction of the eating required to develop comparable strength beating alone.

By using resin it was also possible to develop suitable strength when using high contents of filler pulps that do not lend themselves readily to hydration. This is important because these pulps contribute to low curl and expansivity and good oil absorption in paper.

It was possible to obtain much higher folding endurance, a very desirable property, without the undesirable effects that accompany the building up of folding strength by hydration. The results were secured in experimental papers made in the Bureau's semicommercial-scale paper mill by using different combinations of typical commercial wood pulps. A series of papers was made from each fiber furnished, with controlled variations in beating, with and without synthetic-resin bonding. The work was carried on with the counsel of an advisory committee of technical representatives under the chairmansbip of R. F. Reed, director of research, Lithographic Technical Foundation. Previous publications resulting from research work at the Bureau with the cooperation of the advisory committee contain information on the manufacture and treatment of offset papers for optimum results in offset printing [1 to 10].[1]

[1] Figures in brackets indicate the literature references at the end of this paper.

II. Experimental Paper-making Equipment

The paper-making equipment at the Bureau is semicommercial in size, and is adapted to the experimental manufacture of papers under conditions that simulate those of typical industrial plants. Detailed descriptions and photographs of the essential equipment are contained in previous publications [11, 12, 13]. The equipment used in this particular work consisted essentially of a 50-lb beater with copper-lined tub and manganese-bronze bars and plate; a jordan refiner with bars of bronze and steel alloy, a four-plate, flat screen; a 29-in. Fourdrinier paper-making machine with a wire 33 ft. long, two presses, nine 15-in. dryers, a machine calender stack of seven rolls, and a reel; and a five-roll supercalender.

III. Fibrous Raw Materials

Inasmuch as the purpose of this investigation was to explore the possibilities of substituting resin bonding for the effects of hydration in developing strength, only three types of commercial wood pulps were used. The following pulps were chosen:

1. Bleached sulfite, made by cooking eastern spruce wood in a solution of calcium bisulfite. This was a relatively standard quality of pulp such as is widely used in offset papers. It is composed of relatively long, strong fibers that hydrate rather readily with beating.

TABLE 1.—*Test data on pulps used in experimental papers*

Kind of pulp	Alpha cellulose	Beta cellulose	Gamma cellulose	Pentosans	Copper number	Ash	Natural resin	Acidity (glass electrode) hot-water extraction
	Percent	*Percent*	*Percent*	*Percent*		*Percent*	*Percent*	*pH*
Sulfite	84.4	3.6	12.0	4.2	1.3	0.2	0.4	5.5
Deciduous wood sulfite	83.6	10.9	5.5	6.0	1.0	.2	.1	6.2
Soda	80.7	16.2	3.1	15.1	1.5	1.8	.4	8.5

2. Bleached deciduous-wood sulfite, a short-fibered filler type of pulp made by cooking deciduous woods in a solution of calcium bisulfite. The fibers are soft and resilient and impart desirable resilience and absorptiveness to printing papers. However, they are tender and are inclined to break up rather than to hydrate during beating.

3. Soda pulp, another filler pulp made by cooking deciduous woods in a solution of caustic soda. The fibers are characteristically soft and bulky, comparable to deciduous-wood sulfite, but somewhat stronger and less resilient. They do not hydrate readily.

The chemical characteristics of these pulps are given in table 1.

IV. Manufacturing Procedure

The general procedure comprised the making of papers with strengths developed by controlled variations in beating, without resin and with synthetic-resin binders. The comparative results with a number of different resins were first investigated with the more nearly conventional beater furnish of 75-percent sulfite–25-percent soda pulps. Subsequently other furnishes were explored in a similar manner.

Fifty pounds of pulp was used for each machine run. Before the stock was furnished to the beater, in each instance, the roll was raised above the bedplate a definite number of turns. The position of the beater roll is expressed as the number of turns of the handwheel above (+) or below zero setting, which is the point of contact between the roll and the bedplate. One turn moves the roll 0.008 inch. The beating pattern with respect to sequence and time intervals of roll settings is shown in figure 1.

The beaten stock was dropped directly to the chest from where it was pumped via the stuff box through the jordan and screen to the machine without the use of a machine chest. The stuff box was of the regulating type with constant head over an adjustable orifice. The jordan was used as a mixer only, with the same setting for all papers.

Melamine-formaldehyde resin was the standard bonding agent. It was added in the form of a colloidal solution made by dissolving the powdered resin in warm water acidified with hydrochloric acid. The solution was added continuously at a uniform rate to the paper-making stock just before it entered the head box of the paper machine. The temperature of the stock was maintained at 90° ±2° F. One percent of rosin size was used in each of the papers, hence sizing

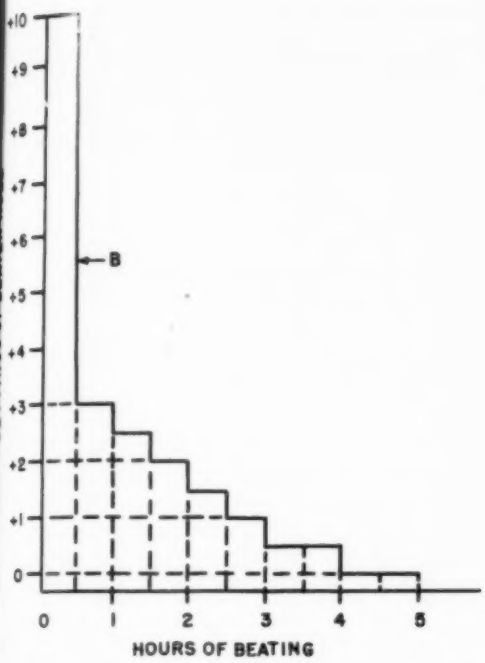

FIGURE 1. *Standard practice of lowering the beater roll for all experimental papers.*

Pattern of beating curve for all papers. Value for roll settings are turns of the handwheel above (+) contact (0) of roll with bedplate. One turn moves the roll 0.008 in. Lighter bar down at start.

was not a variable. It was precipitated with papermaker's alum, $Al_2(SO_4)_3$, which was used to control the pH of the stock. No filler was used. The finish imparted by the small machine calender was relatively low; therefore, the papers were given light supercalendering to obtain a smoothness comparable to commercial "machine finish."

V. Sampling and Testing

The method of sampling paper from a machine run in the paper mill was as follows: The paper wound on the reel of the paper machine during the test period was slit across the web, thereby being converted into a stack of sheets. The stack was then cut so as to give an entire cross section of the sheets for sampling. The resultant stack was divided into seven parts. From the first part, 13 sheets were laid out as the first sheets of 13 packs to be built up. From the second part, 13 sheets were likewise distributed as the second sheets of the packs. From each of the seven parts a sheet was added to each pack. The procedure was then repeated until all the paper had been distributed into the 13 packs. The odd-numbered (1–3–5–7–9–11–13) packs were then assembled, one above the other, to make one bundle of paper, and similarly the even-numbered packs to make another. From these bundles, sheets were taken for the test samples.

All physical and chemical tests of the pulps and papers referred to herein were made in accordance with the Standard Methods of the Technical Association of the Pulp & Paper Industry,[2] except air permeability. This property was determined with a Carson Precision Permeability Tester [14], which measures the rate of air flow through the paper per unit of area with a pressure difference of 1 g/cm.[2] The pH of mill waters at the beater, stuff box, and head box was determined electrometrically with a quinhydrone electrode.

A Set of the papers comprising sheets from each machine run was printed in six colors by the offset process at the Coast and Geodetic Survey to get information on relative printing qualities. The papers were conditioned in accordance with the best recommended practice for control of moisture in multicolor printing [4] and printed in a press room with controlled humidity and temperature.

VI. Description of Experimental Papers

Papers were made of 75-percent-sulfite–25-percent-soda pulps, 75-percent-soda–25-percent-sulfite pulps, and 75-percent-deciduous-wood sulfite–25-percent-standard-sulfite pulps. The procedure was to make control papers from each furnish with three different degrees of beating, and then repeat each control run several times with different amounts of bonding resin. Four synthetic resins were tried in exploratory machine runs. Since appreciably better results were obtained with melamine-formaldehyde resin than with the others, that resin was selected as the standard bonding agent for this investigation.

The properties of the typical papers made are shown in table 2.

[2] Available from the Association headquarters at 122 East Forty-Second Street, New York 17, N. Y. The methods specify the number of specimens for each test as well as other details of testing.

TABLE 2. *Properties of experimental offset papers*

Paper number	Fiber furnish	Melamine-formaldehyde resin added	Beating time	Bursting strength	Surface pick (wax No.)	Curl	Folding endurance (double folds) MIT		Tearing strength		Tensile strength		Moisture expansion per 10% relative humidity change	
							Machine	Cross	Machine	Cross	Machine	Cross	Machine	Cross
		Percent	*hr*	*Points*		*Degrees*			*g*	*g*	*kg*	*kg*	*Percent*	*Percent*
1452	75% sulfite–25% soda	None	1¼	13	3A	40	12	6	63	69	4.3	2.2	0.05	0.14
1467	do	½	1½	14	5A	35	21	9	63	68	4.6	2.5	.05	.15
1466	do	1	1½	21	10A	38	108	40	60	64	6.1	3.3	.05	.13
1463	do	2	1½	23	12A	48	140	51	52	59	7.1	4.2	.05	.16
1453	do	3	1½	25	16A	52	251	67	46	46	7.8	4.0	.06	.18
1455	do	None	5½	18	8A	52	44	17	55	64	6.3	3.0	.06	.17
1469	do	½	5½	21	9A	40	61	24	62	70	6.5	3.3	.06	.16
1468	do	1	5½	24	12A	41	88	34	69	72	6.7	4.0	.06	.18
1464	do	2	5½	27	15A	51	218	110	50	53	7.6	4.6	.07	.19
1456	do	3	5½	29	17A	61	340	94	48	48	8.4	4.7	.07	.2
1458	do	None	9½	25	14A	122	136	60	47	48	7.6	4.4	.07	.2
1459	do	3	9½	35	23A	96	704	512	39	40	9.4	6.1	.08	.2
1480	75% deciduous–25% coniferous sulfite.	None	1½	6	2A–	33	1	1	44	47	1.9	1.2	.06	.1
1483	do	1	1½	10	2A–	36	3	2	44	44	3.1	1.9	.06	.1
1481	do	3	1½	12	4A	41	6	4	40	42	3.5	2.3	.08	.1
1484	do	None	5½	8	2A–	42	2	1	42	46	2.4	1.6	.06	.1
1486	do	1	5½	14	6A	46	9	5	41	43	3.9	2.5	.07	.1
1485	do	3	5½	16	10A	56	11	9	37	37	4.2	2.9	.07	.2
1488	do	None	9½	15	6A	78	6	6	36	38	4.3	2.6	.07	.2
1504	75% soda–25% sulfite	None	1¼	12	2A–	36	5	3	51	55	4.0	2.4	.06	.1
1505	do	1	1½	18	6A	37	14	9	51	55	5.4	3.5	.06	.1
1506	do	2	1½	18	10A	42	24	14	49	48	5.4	3.8	.07	.1
1507	do	3	1½	22	10A	43	24	16	44	44	6.0	4.0	.07	.1
1511	do	None	5½	15	6A	45	9	6	48	50	4.7	3.0	.07	.1
1512	do	1	5½	21	11A	55	39	29	49	53	6.3	3.9	.07	.1
1513	do	2	5½	22	13A	50	42	28	44	48	6.3	4.1	.07	.1
1514	do	3	5½	23	13A	58	28	29	41	46	6.3	4.6	.07	.1
1515	do	None	9½	20	11A	60	22	17	44	47	5.8	3.9	.07	.1

Paper number	Permeability to air	Oil penetration time	Sizing value, dry indicator	Opacity	Smoothness bekk	Thickness	Weight 25×40-500	Results of printing tests	
								Picking	Feeder performance
	cm³ sec	*sec*	*sec*	*Percent*	*sec*	*inch*	*lb*		
1452	568	26	72	86	87	0.0034	53	Yes	Wrinkle.
1467	550	28	72	87	60	.0040	57	Yes	Satisfactory.
1466	464	31	68	87	67	.0038	57	No	Do.
1463	363	45	70	86	80	.0039	57	No	Do.
1453	327	44	63	85	59	.0036	56	No	Do.
1455	228	44	67	87	106	.0036	56	No	Do.
1469	339	47	62	87	68	.0038	56	No	Do.
1468	306	40	72	86	64	.0036	55	No	Do.
1464	210	55	70	85	58	.0037	55	No	Do.
1456	183	53	77	85	81	.0038	56	No	Do.
1458	33	174	71	83	77	.0033	55	No	Do.
1459	26	228	73	81	54	.0035	54	No	Do.
1480	781	20	58	90	154	.0034	55	Yes	Split.
1483	736	22	69	89	110	.0037	54	Yes	Poor.
1481	693	22	71	87	98	.0037	55	Yes	Do.
1484	623	21	62	89	124	.0036	54	Yes	Do.
1486	500	23	68	88	112	.0034	54	No	Satisfactory.
1485	396	27	69	87	155	.0033	53	No	Do.
1488	160	57	73	88	182	.0038	55	No	Do.
1504	457	33	69	90	76	.0040	56	Yes	Poor.
1505	366	33	62	89	69	.0042	56	No	Satisfactory.
1506	339	43	47	88	118	.0037	54	No	Do.
1507	300	44	50	88	88	.0038	55	No	Do.
1511	307	47	57	89	97	.0037	54	No	Do.
1512	206	63	50	88	124	.0035	55	No	Do.
1513	194	64	60	88	169	.0033	53	No	Do.
1514	143	86	58	88	188	.0031	54	No	Do.
1515	80	151	65	88	139	.0033	55	No	Do.

[a] Tests made in accordance with the Standard Methods of the Technical Association of the Pulp and Paper Industry, 122 East Forty-Second Street, New York 17, N. Y.

VII. Interpretation and Discussion of Data

The first objective of this work was to find the possible advantages of developing strength by resin bonding over the development of comparable strength by "hydration." By referring to the data on the 75-percent-sulfite–25-percent-soda papers in table 2, it will be seen that 2 percent of bonding resin and only 1½ hours of beating, which amounted to mixing only, developed bursting strength and surface pick comparable to those achieved by 9½ hours of beating without resin. One and one half hours of beating with 3 percent of resin achieved far better strength than was obtained by hydration alone, even with the most drastic beating.

The advantages of resin-bonding versus gel-bonding, or hydration, for developing strength in printing papers are shown graphically in figures 2 and 3. In figure 2, three papers of like bursting strength are compared graphically. The bursting strength of paper C was developed by 9½ hr of beating. For paper R_3, the bursting strength was developed with 3 percent of resin and only 1½ hr of beating, and for paper R_1, with 1 percent of resin and 5½ hr of beating.

The graph shows the important degree to which resin bonding in this type of fiber furnish produces strength, without the objectionable effects of hydration on expansion, oil resistance, and increased tendency to curl. The importance of these properties in printing papers is well known.

The resistance of the surface to picking, as measured by the wax test, is an important property in offset papers. The surface fibers must resist the strong pull of tacky inks in printing. Figure 3, shows the relationship between the surface pick of the sulfite-soda papers and the tendency to curl. One advantage of resin bonding is demonstrated rather clearly here.

For the papers made of 75-percent-soda–25-percent-sulfite furnish, resin bonding was a rela-

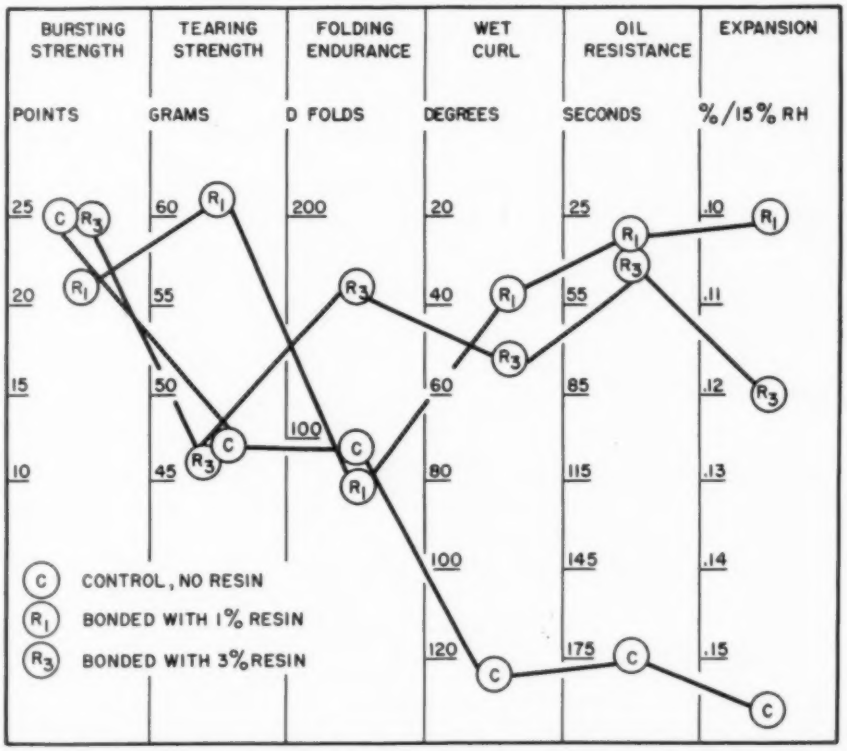

FIGURE 2. *Relative properties of papers having comparable bursting strength developed by: 9½ hr of beating (C); 5½ hr of beating plus 1 percent of resin (R_1); and 1½ hr of beating plus 3 percent of resin (R_3).*

Seventy-five-percent-sulfite–25-percent-soda papers.

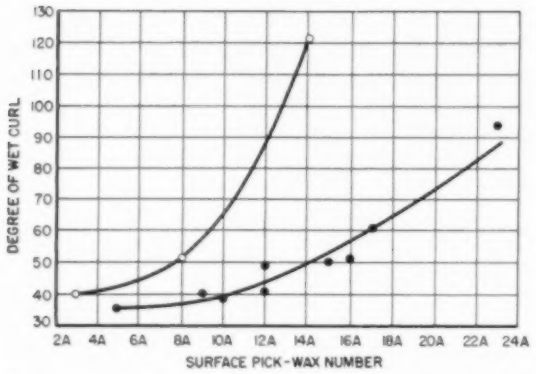

FIGURE 3. *Relationship between surface pick and tendency to curl for 75-percent-sulfite–25-percent-soda papers, strength developed by beating alone and by resin bonding.*

○, No resin; ●, resin bonded.

tively greater aid to strength development than with higher sulfite content. The effects of resin bonding with this furnish are shown in figure 4.

Beating intervals of 5½ hours with 1 percent resin, and only 1½ hours with 2 percent of resi produced papers superior in strength, oil absor tion, and tendency to curl to the control pap with maximum beating time. With this ty of furnish, hydration plays a smaller part th when more sulfite is present, consequently e cessive beating has less deleterious effect on expa sion. It does, however, produce excessive cu to about the same degree as with the papers co taining 75 percent of sulfite. Hence, the te dency to curl accompanying excessive beati cannot be ascribed entirely to hydration. Th "fines" formed in the beater doubtless play a important part.

Deciduous-wood sulfite pulp hydrates ver little during beating, and the papers containin 75 percent of this pulp developed strength ver slowly with beating. The effects of resin bondin are shown in figure 5. It is of interest that he again drastic beating had little effect on expa

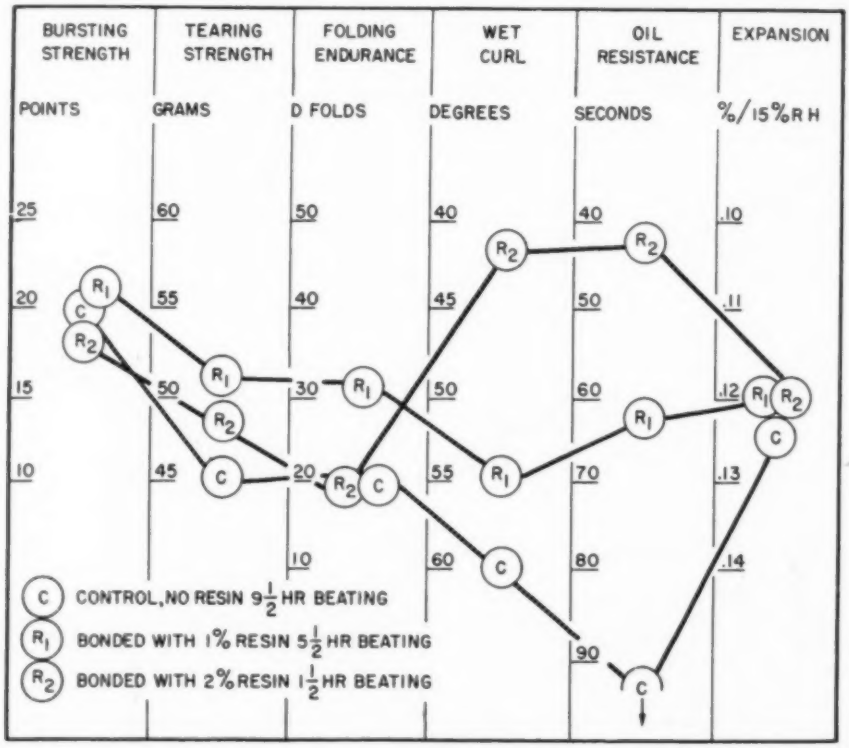

FIGURE 4. *Relative properties of 75-percent-soda–25-percent-sulfite papers of comparable bursting strength, with and without resin bonding.*

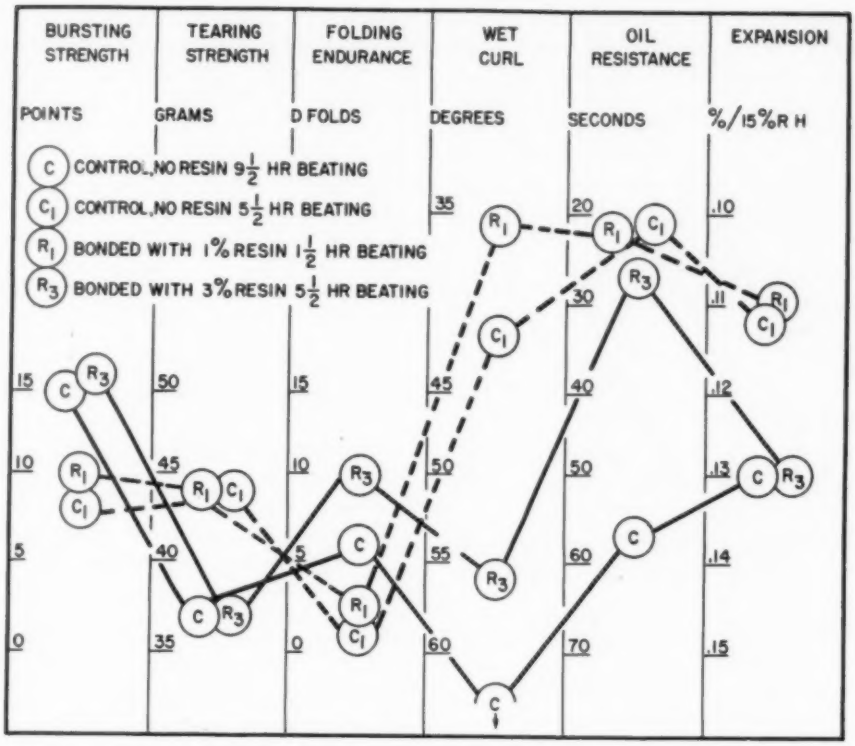

FIGURE 5. *Relative properties of papers containing 75-percent deciduous-wood sulfite of comparable bursting strength developed with and without bonding resin.*

sion, which is closely associated with hydration. Beating 9½ hours without bonding resin and 5½ hours with 3 percent of resin produced papers with comparable strength as did beating 5½ hours without resin and 1½ hours with 1 percent of resin. In both instances the resin-bonded paper had more desirable oil resistance and curling characteristics. This difference is illustrated in figure 6. The straight-line relationships in this graph, as compared to the curves in figure 3, are doubtless accounted for by the relative absence of hydration in beating deciduous-wood sulfite.

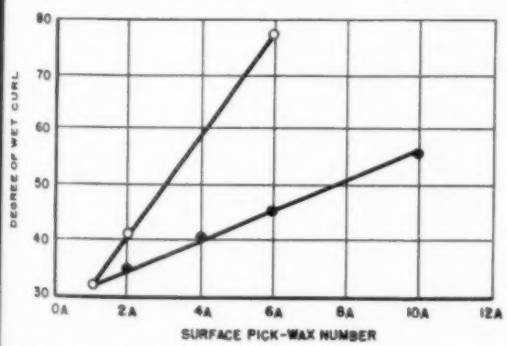

FIGURE 6. *Effects of increasing resistance to surface pick on tendency to curl resin bonding versus hydration.*

Fiber furnish: 75-percent deciduous-wood sulfite; 25-percent-standard sulfite. ○, No resin; ●, resin-bonded.

Further evidence of the different effects of hydration on these two furnishes are indicated in figure 7. This shows that bursting-strength–expansivity relationships fall on the same straight line regardless of how the strength was developed, in the instance of deciduous-wood papers, which do not hydrate readily. The conventional 75-percent sulfite–25-percent-soda papers form two straight lines, parallel but separated by approximately 8 points of burting strength. Thus a resin-bonded paper of this type with a burst of 25 points has no greater expansion than the gel-bonded control paper with a bursting strength of only 17 points.

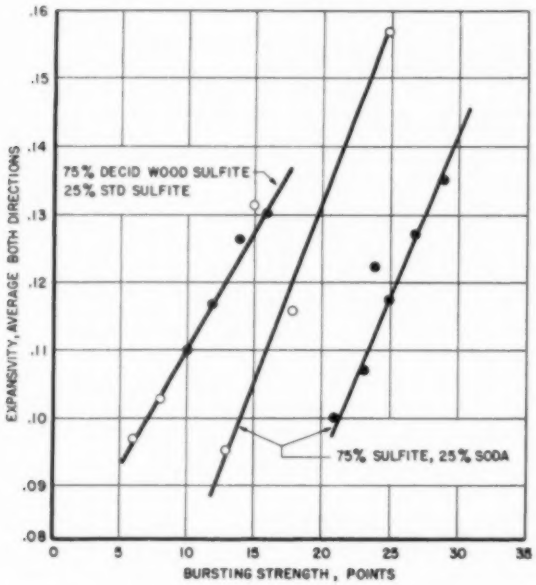

FIGURE 7. *Bursting-strength–expansivity relationships for two different types of furnishes, with and without resin bonding.*

○, Blank, no resin; ●, with resin bonding.

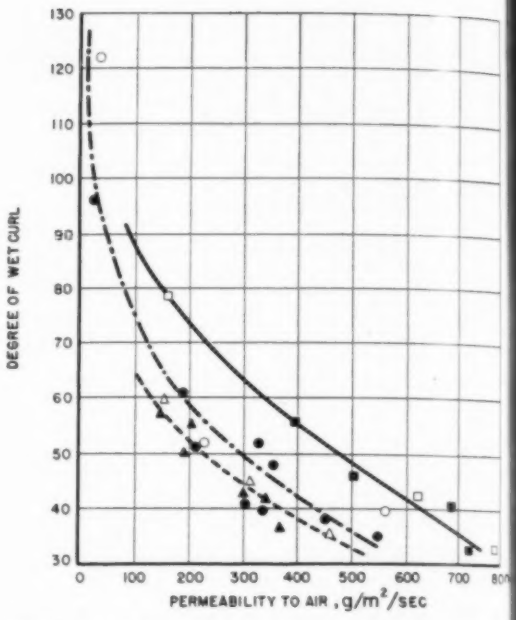

FIGURE 8. *Relationship between permeability to air (porosity), and tendency to curl; all experimental papers.*

——, seventy-five-percent sulfite–25-percent soda; ○, no resin; ●, resin bonded. —, 25-percent sulfite–75-percent soda; △, no resin; ▲, resin bonded. —, 75-percent deciduous-wood sulfite, 25-percent sulfite (standard); □, no resin; ■, resin bonded.

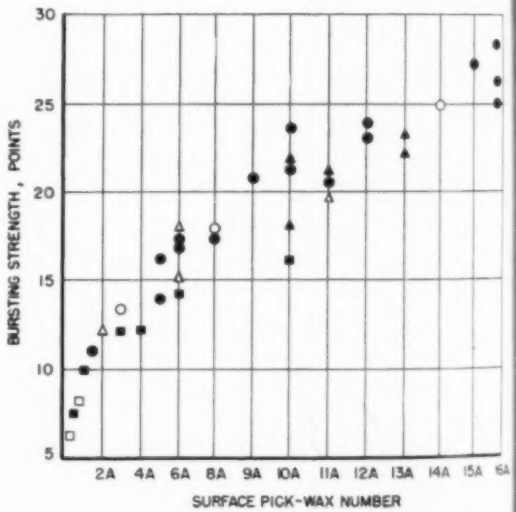

FIGURE 9. *Relation of resistance to surface pick to bursting strength; all experimental papers.*

□, Seventy-five-percent-deciduous-wood sulfite, 25-percent-standard sulfite, no resin; ■, same resin bonded. ○, Seventy-five-percent sulfite–25-percent-soda, no resin; ●, same resin bonded. △, Seventy-five-percent soda–25-percent sulfite, no resin; ▲, same resin bonded.

The permeability of paper to air is an important property when considering printing papers, mainly because it determines the behavior of the sheet with respect to curl and oil absorption. It has been noted that the three types of papers dealt with developed curl rapidly with increased beating, regardless of the rate of strength increase or apparent hydration. This is probably the result of "closing the sheet" or reducing the voids, whether it is by gel-formation, as in hydration of sulfite, or the formation of fines as in the instance of the filler pulps, soda and deciduous-wood sulfite, which are not readily hydrated. The relationship between permeability to air and degree of curl are shown in figure 8.

High resistance to pick is essential in offset printing papers. The surface fibers must resist the pull necessary to transfer tacky ink from the rubber blanket to the paper without lifting or being themselves transferred to the blanket. A fiber or bundle of fibers loosened by the pull of the ink not only leaves a blemish in the printed image on the sheet where the "picking" occurs, but it clings to the blanket where it becomes moistened and repels ink to print white spots on succeeding

sheets. Surface strength is closely allied to bursting strength (see fig. 9), and is improved to about the same degree by resin bonding. The results of printing tests are shown in the two right-hand columns of table 2. It will be seen that a pick test of less than 6A resulted in some picking on the press and gave feeder trouble, apparently because of a "limpness." The printing was otherwise satisfactory, except for misregister that accompanied feeder trouble.

VIII. Summary and Conclusions

By adding 1 to 3 percent of melamine formaldehyde resin, maximum strength and resistance to surface picking was developed in offset papers with a minimum of beating. The development of high strength by hydration or gel-formation affects adversely such properties as expansivity, curling, and oil absorption, which are particularly important in offset printing.

The bonding resin was very effective in developing strength in papers containing high percentages of soda and deciduous-wood sulfite pulps, which do not develop strength readily by beating alone. As little as 2 percent of resin, with a minimum of beating produced strength and surface bonding superior to any obtained without resin, even with the maximum of beating.

Using three different wood-fiber furnishes, considerably better all-around printing papers were obtained with resin-bonding than without, and the indicated savings of beating time and power were important.

The application of resin bonding apparently provides a means of using higher contents of short filler-types of fibers than is possible when developing strength by beater action only. This is important from the standpoint of conservation of fibrous raw materials and availability of pulps. The short-fibered pulp woods are not fully utilized, while the supply of long-fibered softwoods is becoming critical.

IX. References

[1] C. G. Weber and R. M. Cobb, BS J. Research **9,** 427 (1940) RP480.

[2] C. G. Weber and L. W. Snyder, BS J. Research **12,** 53 (1934) RP633.

[3] C. G. Weber, J. Research NBS **13,** 609 (1934), RP730.

[4] C. G. Weber and M. N. Geib, J. Research NBS **16,** 93 (1936) RP859.

[5] C. G. Weber, Paper Trade J. **109,** 205 (Oct. 19, 1939).

[6] C. G. Weber, Air conditioning in printing, Refrigerating Data Book, chap. 56 (Society of Refrigerating Engineers, New York, N. Y., 1940).

[7] C. G. Weber and M. N. Geib, Method of conditioning paper for multicolor offset printing, Tech. Bul. **3** (Lithographic Technical Foundation, Inc., New York, N. Y., 1940).

[8] C. G. Weber, Paper Trade J. **112,** 119 (March 6, 1941).

[9] C. G. Weber, M. B. Shaw, M. N. Geib, and M. J. O'Leary, J. Research NBS **28,** 241 (1942) RP1455.

[10] C. G. Weber, M. B. Shaw, and M. J. O'Leary, J. Research NBS **30,** 267 (1943) RP1532.

[11] M. B. Shaw and G. W. Bicking, Tech. Pap. BS **21,** 338 (1927) T340.

[12] M. B. Shaw and G. W. Bicking, BS J. Research **3,** 904 (1929) RP121.

[13] M. B. Shaw, Paper Trade J. **89,** No. 19, 60 (1929).

[14] F. T. Carson, BS J. Research **12,** 567 (1934) RP681.

WASHINGTON, January 9, 1948.

U. S. Department of Commerce
National Bureau of Standards

Research Paper RP1888
Volume 40, June 1948

Part of the Journal of Research of the National Bureau of Standards

Metastable Transitions in Mass Spectra of Fifty-Six Hydrocarbons

By Evelyn G. Bloom, Fred L. Mohler, Jonathan H. Lengel, and C. Edward Wise

In the mass spectra of 56 saturated and unsaturated hydrocarbons, all the observable metastable transitions have been identified. In 362 cases, there are 32 different transitions involving loss of masses 2, 15, 16, 26, 27, 28, 29, 30, 42, and 44. The occurrence of a metastable transition depends on the intensity of both the initial ion peak and the final ion peak.

I. Introduction

The mass spectrum of a hydrocarbon as obtained in a gas analysis mass spectrometer shows peaks at integral mass numbers equal to the molecular weight of the compound and its dissociation products. In addition to these peaks there are commonly found some small and abnormally wide peaks with maxima that are in general at nonintegral mass numbers. Hipple, Fox, and Condon [1, 2] have made a detailed experimental study of these abnormal peaks and have given a theoretical explanation. They arise from ions that dissociate after they have traversed the ion-accelerating field. If an ion of mass m_i dissociates immediately after traversing the electric field into an ion of mass m_f and a neutral particle, then the apparent mass m_a of the ion is given by the relation

$$m_a = m_f^2/m_i. \tag{1}$$

Because the initial ion does not dissociate at a definite point but over a range of positions, the resulting ion peak is broad and diffuse. Hipple, et al.[1] verified this theory by showing that the kinetic energy of the final ion was reduced in proportion to the mass lost by measuring the stopping potential applied to the ion collector that would reduce the diffuse peak to zero. Thus, if the ion-accelerating potential is V and the ion breaks in half, then a stopping potential of $V/2$ is sufficient to stop the ionized fragment that has only half of the kinetic energy. They ascribed this dissociation phenomenon to excited states of the initial ion, which spontaneously go to the dissociated state with a rather long "life" according to the relation

$$n_t = n_0 e^{-t/\tau}, \tag{2}$$

where n_0 and n_t are the number in the initial state at zero time and time t. Hipple [3] has measured values of the life τ by measuring relative peak heights with different electric fields drawing ions from the ionization chamber and finds values of the order of 10^{-6} second. The dissociating ions are termed metastable ions, because the life of the initial state is long compared to most radiative transitions.

The authors have been making systematic measurements of mass spectra of pure hydrocarbons and tabulating results in the form of tables published by the American Petroleum Institute, Research Project 44.[4] The tables present intensities of mass peaks relative to a value 100 for the maximum peak in the spectrum and include all peaks of intensity 0.01 or greater. Spectra at ionizing voltages of 50 and 70 volts are given. All measurable peaks involving metastable transitions have been recorded, and it has been possible to identify the transitions involved in nearly every case. Mass spectra of 56 compounds have been published to date.

The following compounds have been included in this study: All saturated isomers (40 in all) from

[1] J. A. Hipple, R. E. Fox, and E. U. Condon, Phys Rev. **69**, 347 (1946).
[2] J. A. Hipple and E. U. Condon, Phys. Rev. **68**, 54 (1945).
[3] J. A. Hipple, Phys. Rev. **71**, 594 (1947).
[4] Catalog of mass spectral data, tables 1 to 56, American Petroleum Institute, Research Project 44, National Bureau of Standards.

methane through the C eights; unsaturated compounds—ethylene, propylene, four butenes, six pentenes, two butadienes, and two butynes. All these compounds except methane show from 1 to 11 metastable transitions. In all, 362 have been recorded and the transitions identified. This paper is a survey of the detailed data that have been published in the API catalog (see footnote 4). Enough cases have been covered to permit some general conclusions to be drawn concerning the occurrence of metastable transitions.

II. Experimental Conditions

A consolidated mass spectrometer has been used in this research, and spectra have been obtained with uniform procedures described in detail in a descriptive sheet published with the API catalog of mass spectra (see footnote 4). In this spectrometer, ions produced by an electron beam at 50 or 70 volts are drawn out of the ionization chamber by a small field, accelerated by an ion-accelerating voltage and bent through 180° in a homogeneous magnetic field. In obtaining the spectra, the magnetic field is held constant and the ion-accelerating voltage varied. The small draw-out potential is about 1 percent of the ion-accelerating voltage. That is, it is a variable potential varying inversely as the apparent mass of the ion.

The ion current is recorded by four galvanometers with sensitivities in the ratios 1 to 1/3 to 1/10 to 1/30. A compound is run at a pressure to give nearly full-scale deflection for the maximum peak on the 1/30 scale and a peak of 0.01 percent of maximum is detectable under optimum conditions. Figure 1 illustrates a part of the record of the *n*-butane spectrum showing the four galvanom-

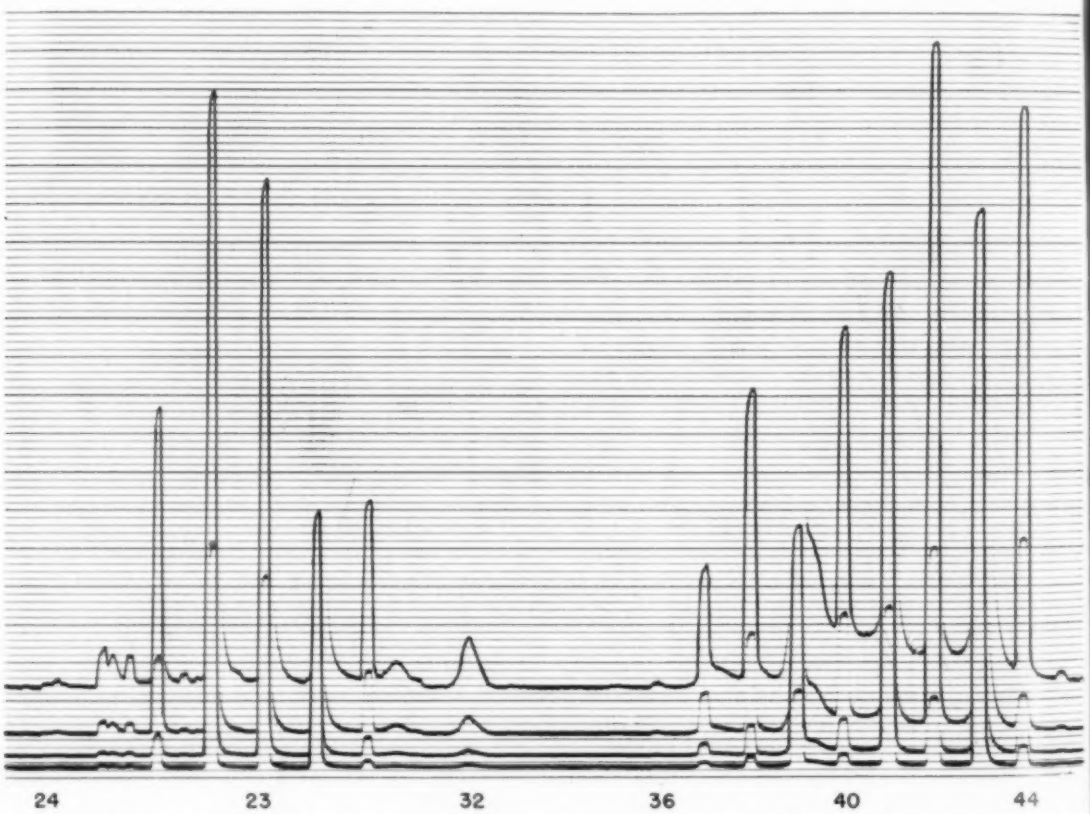

FIGURE 1. *Part of n-butane mass spectrum showing metastable transition peaks at mass numbers 25.1, 30.4, 31.9, and 39.1 and smaller peaks at 24.1 and 37.1.*

er traces in decreasing order of sensitivity from op to bottom. The 43 peak is the maximum eak. There are four conspicuous metastable ransition peaks in this range (25.1, 30.4, 31.9, nd 39.2) and three other small ones (24.1, 35.1, nd 37.1) that require careful measurement and omparison with other spectra for their verifica- ion. The peak at 31.9 is a good example of the haracteristic appearance of these peaks. It is bout three times the normal peak width. The eak at 39.2 is the largest of these, but it is incom- letely resolved from the large 39 peak so that the alue of the peak height is more uncertain than n the other cases.

This interference between normal peaks and etastable transition peaks occurs frequently and an give rise to a large uncertainty in the peak eight. However, because of the abnormal width f the metastable transition peaks a rough estimate f peak height can often be made even when a mall normal peak is exactly coincident with it. Hipple's analysis (see footnote 3) shows that the elative height of a metastable peak will depend n the draw-out potential, which is in this spec- rometer a variable inversely proportional to the mass. It also depends on the resolving power of he spectrometer.

III. Intensity Relations

The relation (eq 1) between apparent mass and he initial and final masses is theoretically suffi- ient to determine both m_i and m_f, because there s the additional condition that m_f and m_i are ntegers equal to or less than the molecular eight. In practice, m_a is not always known with ufficient accuracy to give a unique answer. An mportant guiding principle has been the fact that herever a metastable transition is observed m_f nd m_i correspond to relatively large mass peaks n the mass spectrum.

We have looked for a quantitative intensity ule. The ratio R of the observed intensity at m_a to the product of the intensities at m_f and m_i,

$$R = I(m_a)/I(m_f) \times I(m_i), \qquad (3)$$

s usually of the order of magnitude 0.01 when I's are expressed on the basis of the maximum peak qual to unity. One would expect variations for nstrumental reasons where different values of m_a are compared. There is, however, a nearly equal range of variation when one compares the same transition in different compounds. The average value of R for all observations is about 0.01, and this furnishes a criterion for estimating whether or not observable metastable peaks are to be expected. Metastable transition peaks very rarely exceed 1 percent of the maximum intensity, and this is consistent with the average value of R.

The identification of transitions has been aided by going systematically from simple to more complicated molecules in each series. In the saturated series, C_nH_{2n+2}, it is only the parent peak that is uniquely characteristic of the particular n value. The other peaks can also come from dissociation of heavier molecules. Correspondingly, metastable transitions keep recurring in successive members of the series except for cases where m_i is the parent mass.

IV. Results

The 362 metastable transitions observed in 55 compounds involve 32 different transitions insofar as initial and final masses are concerned. If the transitions are classified according to the neutral mass lost, there are 10 classes involving loss of mass 2, 15, 16, 26, 27, 28, 29, 30, 42, and 44, or H_2, CH_3, CH_4, C_2H_2, C_2H_3, C_2H_4, C_2H_5, C_2H_6, C_3H_6, and C_3H_8.

Loss of mass 2.—Loss of mass 2 is by far the most frequent type of transition. Eight different transitions involving loss of mass 2 are listed in table 1. The last metastable transition is unique insofar as relative intensity is concerned. The ratio of the peak at 110 to the product of the peak heights at 114 and 112 is 7.3. The average

TABLE 1. *Metastable transitions involving loss of mass 2*

Apparent mass	Initial mass	Final mass	Occurrence
24.1	28	26	Ethane, propane, *n*-butane, ethylene, butenes, butadienes, and butynes.
25.1	29	27	Saturated hydrocarbons C_2 to C_4, butenes and pentenes.
35.1	39	37	Butanes and mono-olefins C_3 to C_5, butadienes, and 1-butyne.
37.1	41	39	Saturated hydrocarbons C_4 to C_5 and propene, butenes, and pentenes.
39.2	43	41	Propane, butanes, 2 pentanes, hexanes, heptanes, octanes.
51.1	55	53	Pentenes.
26.1	30	28	Ethane (30 is parent ion).
110.0	114	112	2,5-Dimethylhexane (114 is parent ion).

value for this ratio is 0.01, and values exceeding 0.1 are very rare. The peak at 112 is very small in all other octanes so there is nothing unusual in the failure to observe a 110 peak in other cases. Figure 2 shows the 110, 112, and 114 peaks in 2,5-dimethylhexane.

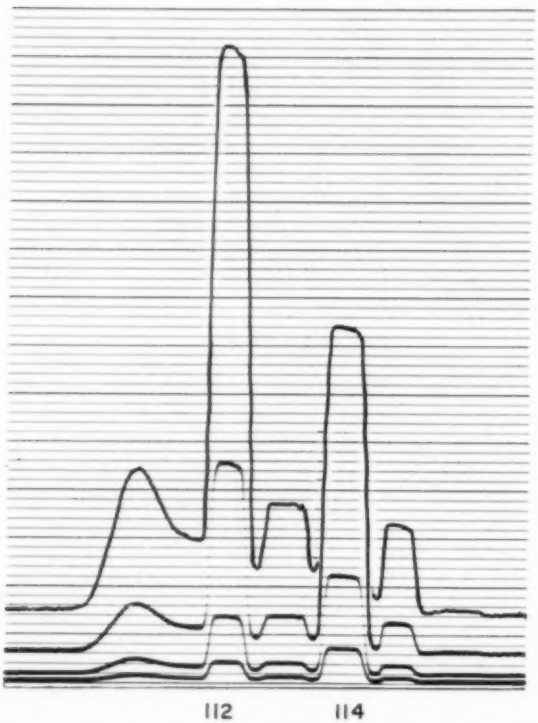

FIGURE 2. *Part of mass spectrum of 2,5-dimethylhexane showing the peak at 110 from the transition* $114^+ \rightarrow 112^+ + 2$.

Loss of mass 15.—Seven different transitions involving loss of CH_3 have been observed (see table 2). In all these cases the initial ion is the parent molecule ion. The first transition is of interest, because in 1,3-butadiene there are no CH_3 radicals, yet the metastable transition is very strong. In 1,2-butadiene there is a CH_3 radical but the 28.2 peak is not observed. According to the intensity rule, one would expect to find this peak in both butadienes as well as in the butynes. Similar transitions involving dissociation of the parent ion are found in all the butenes and pentenes. In the saturated hydrocarbons, there are only scattered instances of loss of 15 by the parent ion and in most of these cases it occurs with abnormally high intensity. In the heptanes and octanes the nonoccurrence of this transition in all the other isomers conforms to the intensity rule. Failure to observe a 58.6 peak in *n*-hexane is an exception to this rule. Except in *n*-butane there is a $(CH_3)_2CH$ group at one or both ends of the saturated molecules in all cases where this metastable transition occurs. Hipple, Fox, and Condon (see footnote 1) note that one might expect to find a transition $72^+ \rightarrow 57^+ + 15$ in *n*-pentane but it is not observed.

TABLE 2.—*Metastable transitions involving loss of mass 15*

Apparent mass	Initial mass	Final mass	Occurrence
28.2	54	39	1,3-Butadiene and butynes.
30.0	56	41	Butenes.
43.2	70	55	Pentenes.
31.9	58	43	*n*-Butane (fig. 1).
58.6	86	71	2,3-Dimethylbutane.
72.3	100	85	2-Methylhexane.
86.0	114	99	2-Methylheptane and 2,5-dimethylhexane.

Loss of mass 16.—The loss of CH_4 from a hydrocarbon involves either a double dissociation or a rearrangement of hydrogen atoms in the initial ion before it dissociates. However, 35 cases of this have been observed in three different transitions listed in table 3. The 30.4 peak of *n*-butane is the only case involving a parent ion, and it occurs with abnormally high intensity. The nonoccurrence of 29.5 in one hexane, two heptanes, and two octanes is consistent with the intensity rule, as the product of the peak heights at 57^+ and 41^+ is small in these cases.

TABLE 3. *Metastable transitions involving loss of mass 16*

Apparent mass	Initial mass	Final mass	Occurrence
27.7	55	39	Pentenes.
29.5	57	41	Pentanes, 4 hexanes, 7 heptanes, and 16 octanes
30.4	58	42	*n*-Butane (fig. 1).

Loss of mass 26.—The loss of C_2H_2 occurs in only one transition that is observed in 41 hydrocarbons:

$$m_a = 15.3 \qquad 55^+ \rightarrow 29^+ + 26.$$

This is found in all hexanes and octanes and all but one heptane and also in all butenes and pen-

tenes. Its occurrence conforms to the intensity rule.

Loss of mass 27.—Loss of C_2H_3 is observed in one transition from parent ions:

$$m_a=13.5 \qquad 54^+ \rightarrow 27^+ + 27.$$

It occurs in both butadienes and in 2-butyne. It is abnormally weak according to the intensity rule. The unsymmetrical molecule 1-butyne does not show a 13.5 peak, although this peak is found in 1,2-butadiene, which is also unsymmetrical and requires a rearrangement of hydrogen atoms to break in half.

Loss of mass 28.—Loss of C_2H_4 appears in two transitions that recur in many saturated hydrocarbons:

$m_a=26.0$ $\quad 71^+ \rightarrow 43^+ + 28$ occurs in hexanes, 5 heptanes and 11 octanes.

$m_a=38.2$ $\quad 85^+ \rightarrow 57^+ + 28$ occurs in 5 heptanes and in 9 octanes. The appearance or nonappearance of these transitions in general conforms to the intensity rule.

Loss of mass 29.—Loss of C_2H_5 only occurs from parent ions and is observed in three transitions listed in table 4.

TABLE 4. *Metastable transitions involving loss of mass 29 from the parent ion*

Apparent mass	Initial mass	Final mass	Occurence
24.0	70	41	5 Pentenes.
30.4	100	71	*n*-Heptane.
63.4	114	85	*n*-Octane and 3,4-dimethylhexane.

Loss of mass 30.—Loss of C_2H_6 can only occur from a double dissociation or by a rearrangement. As the dissociating ion is always the parent ion, double dissociation is indicated. Table 5 lists the four transitions observed. The intensity of 61.9 relative to the product of the intensities at 114 and 84 is high in the octanes.

TABLE 5. *Metastable transitions involving loss of mass 30*

Apparent mass	Initial mass	Final mass	Occurence
28.5	72	42	*n*-Pentane.
36.5	86	56	*n*-Hexane.
49.0	100	70	5 Heptanes.
61.9	114	84	5 Octanes.

Loss of mass 42.—Loss of C_3H_6 occurs in two transitions in heptanes and octanes:

$m_a=21.7$ $\quad 85^+ \rightarrow 43^+ + 42$ in 8 heptanes and 11 octanes;

$m_a=32.8$ $\quad 99^+ \rightarrow 57^+ + 42$ in 17 octanes.

The occurrence of 21.7 conforms to the intensity rule, but the relative intensity of 32.8 is abnormally high.

Loss of mass 44.—A peak at mass 31.4 in three heptanes has been tentatively ascribed to the following transition:

$$m_a=31.4 \qquad 100^+ \rightarrow 56^+ + 44.$$

It is observed in *n*-heptane, 2,4-dimethylpentane and 2,3-dimethylpentane. Its occurrence does not conform entirely to the intensity rule.

V. Summary

On the basis of momentum considerations, it is believed that the process of ionization by electron collision consists in removing an electron from the molecule, and that the molecule ion may be left in a highly excited state and subsequently dissociate into various fragments. Because of the fact that some of the dissociation processes occur with a time delay of the order of 10^{-6} second, we have direct experimental evidence as to the nature of the dissociation processes. The great variety of metastable transitions show that molecule ions may dissociate step by step (in all cases where the initial ion is not the parent ion) or by losing a rather large mass from the parent ion. It is natural to assume that loss of masses CH_3, C_2H_4, C_2H_5, and C_3H_6 involve a single dissociation process, insofar as these are natural units of the hydrocarbon molecule. On the other hand, loss of masses CH_4 and C_2H_6 necessarily involve more complicated processes, either double dissociation or a rearrangement of hydrogen atoms.

The generality of the relation that the intensity of the metastable transition depends on the intensity of the initial and final ion peaks is interesting and in some respects surprising. Consider transitions involving parent ions. Where the parent peaks are small, dissociation of the parent ions is most probable; yet, these are the cases where metastable transitions are not observed. This is not a paradox because long life of an excited state implies low probability of transition. Many

785784—48——2

transitions must take place with "half lives" much less than 10^{-6} second.

Hipple (see footnote 3) has measured the half life of the two transitions from the parent ion in *n*-butane

$$58^+ \rightarrow 43^+ + 15,$$

$$58^+ \rightarrow 42^+ + 16,$$

and estimated the fraction of 58^+ ions that are in the two initial states for these two transitions at time zero. The estimate is that roughly 9 percent of the 58^+ ions are in these two initial states. The 58^+ peak is 12.6 percent of the maximum peak and accounts for about 4 percent of all the ions in *n*-butane. If all are initially ions of mass 58, then 96 percent of the original ions dissociate with a very short life, 3.6 percent are stable or at least have a half life much longer than 10^{-6} second and 0.4 percent are in two states, each of half life about 2×10^{-6} second.

The nonoccurrence of a metastable transition involving loss of CH_2 is significant, for mass spectra indicate that loss of the structural unit CH_2 must be very frequent. It is concluded that the transition is always short lived.

The transitions involving loss of mass 2 are by far the most probable type of metastable transitions, and it is of interest that losses of mass 1 or mass 3 are never observed in hydrocarbons. Loss of mass 2 occurs in almost every case where the are two large peaks separated by two mass uni with only a few exceptions. No such generaliz tion can be made for loss of larger masses.

It follows from the intensity rule that isome having similar normal mass spectra in gener show the same metastable peaks. The occurren of a peak at 28.2 in 1,3-butadiene and not in 1, butadiene is an exception to this. Dibeler, Wi and Mohler [5] have found another exception amo the isomers of monochloropropene. In gener though, the metastable peaks will not be useful chemical analysis of unknown mixtures for th merely reflect features of the normal spectrum.

The compilation of mass spectra and the ident fication of metastable transitions is continuin and data will appear in the API catalog (s footnote 4).

We acknowledge the assistance of Dorothy Thompson and Laura Williamson in making tabl of possible values of m_e. V. H. Dibeler and J. Hipple have given valuable help and advice this project.

WASHINGTON, January 8, 1948.

[5] V. H. Dibeler, C. E. Wise, and F. L. Mohler. Phys. Rev. 71, 38 (1

U. S. Department of Commerce
National Bureau of Standards

Research Paper RP1889
Volume 40, June 1948

Part of the Journal of Research of the National Bureau of Standards

Determination of Small Amounts of Oxygen in Organic Compounds

By William W. Walton, Francis W. McCulloch, and W. Harold Smith

A method based on the Unterzaucher procedure has been developed for the determination of small amounts of oxygen in organic compounds. The method involves the pyrolysis of the sample in an atmosphere of helium, conversion of the oxygen compounds that are formed to carbon monoxide by passage of the products over pellets of carbon at a temperature of 1,120° C, and collection of the carbon monoxide in a flask of known volume. Interfering substances are removed by passage of the gas through a liquid-air or potassium-hydroxide trap before collection of the gas. The percentage of carbon monoxide in the collected gas is determined through use of the NBS colorimetric indicating gel. As little as 0.01 percent of oxygen can be determined readily.

I. Introduction

In investigations of natural [1][1] and synthetic rubbers, of plastics, of petroleum products, and other organic materials, a direct method for the accurate determination of small amounts of oxygen was needed. Such a method has many applications, for example, the determination of traces of oxygen-containing compounds (water, etc.) in purified substances, or in studies of rate of oxidation.

Elving and Ligett [2] critically reviewed methods that have been proposed to determine oxygen in organic compounds and favor a procedure proposed by Schütze [3, 4, 5], which was later modified by Unterzaucher [6]. The essentials of the method are the thermal decomposition of the sample in an atmosphere of oxygen-free nitrogen, passage of the resulting products over carbon heated to 1120° C to convert to carbon monoxide the compounds of oxygen that have been formed, absorption of interfering gases by solid potassium hydroxide, and oxidation of the carbon monoxide to carbon dioxide by iodine pentoxide at a temperature of 118° C. An important feature of Unterzaucher's apparatus is an arrangement whereby the nitrogen can be passed through the furnace in reverse to flush out any air that is introduced with the sample.

The accuracy claimed by Unterzaucher for his method has not been obtained by other workers. After a critical investigation of this method, Aluise, Hall, Staats, and Becker [7] recommend the procedure as a satisfactory method for the determination of oxygen in organic compounds, but they state that the results obtained in their laboratory show over-all precision and accuracy somewhat less than those now obtained in carbon and hydrogen analyses. Unpublished work by members of the staff of the National Bureau of Standards has disclosed a number of disadvantages in the use of iodine pentoxide in the determination of small amounts of carbon monoxide—it is difficult to obtain samples of iodine pentoxide that yield low blanks, and frequently samples of iodine pentoxide that are satisfactory will suddenly develop large blanks during use. For the accurate determination of small amounts of oxygen such variability cannot be tolerated.

Recently the Gas Chemistry Section of the National Bureau of Standards developed a colorimetric indicating gel for the detection and estimation of small amounts of carbon monoxide [8]. It is possible by this method to detect and estimate less than 1 part of carbon monoxide in 1,000,000 parts of air. This sensitivity is far greater than

[1] Figures in brackets indicate the literature references at the end of this paper.

needed for estimating the carbon monoxide formed in the Unterzaucher procedure even with very small amounts of oxygen—20 milligrams of a sample containing 0.01 percent of oxygen would yield a concentration of carbon monoxide equal to about 1 part in 300,000 if collected in a 1-liter flask.

A procedure was developed for the determination of oxygen based on the Unterzaucher method for converting the oxygen to carbon monoxide and determination of the amount of carbon monoxide with NBS colorimetric indicating gel.*

II. Description of the Apparatus and Method

A general view of the apparatus is given in figure 1, and the details are shown in a schematic drawing, figure 2.

FIGURE 1. *Apparatus for the determination of small amounts of oxygen in organic compounds.*

The rubber connections used by Unterzaucher were avoided, because water and oxygen diffuse through rubber. Helium was substituted for nitrogen because of its inertness, its greater freedom from oxygen, and the possibility that it would be more efficient in the removal of adsorbed oxygen.

Furnace (5, in fig. 2) is a Nichrome-wire-wound type, 22 cm in length, and is operated at a temperature of 400° C. The tube in this furnace is made of 10-mm Pyrex glass tubing and is about 32 cm long. It is sealed to the U-tube through a two-way stopcock that allows the gases to be passed either through the U-tube or to the atmosphere, and it is filled with small copper spirals to remove any oxygen that may be in the helium. Any oxide formed on the copper spirals is reduced when necessary by passing a stream of hydrogen through the heated tube and out to the atmosphere through the two-way stopcock (8, in fig. 2).

The U-tube (10, in fig. 2) has an outside diameter of 25 mm and a height of 30 cm. The arm of the U-tube, connected to stopcock 8, is packed with ascarite; and the arm connected to stopcock 12 is packed with anhydrous magnesium perchlorate.

Furnace (17, in fig. 2) consists of a cast-iron pipe, with a diameter of 20 cm and a length of 25 cm, and is closed at both ends with transite board. The transite boards are 20 mm thick and are drilled to hold the quartz tube and a central core. This central core is an Alundum tube, 1 in. in diameter with grooves of $\frac{1}{12}$-in. pitch. It is wound with about 30 feet of 90-percent platinum-

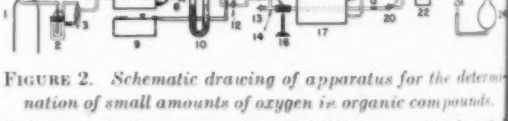

FIGURE 2. *Schematic drawing of apparatus for the determination of small amounts of oxygen in organic compounds.*

(1) Helium tank; (2) pressure regulator; (3) bubble counter; (4) tube packed with copper spirals; (5) furnace heated to 400° C; (6) variable transformer for furnace (5); (7) thermocouple for furnace (5); (8) two-way stopcock; (9) potentiometer for measuring the temperatures of furnaces (5) and (17); (10) U-tube filled with ascarite and anhydrous magnesium perchlorate; (11) two-way thermocouple switch; (12) three-way stopcock; (13) stopcock; (14) quartz tube packed with gas-black pellets; (15) wire gauze mantle; (16) burner; (17) furnace heated to 1,120° C; (18) thermocouple for furnace (17); (19) variable transformer for furnace (17); (20) three-way stopcock; (21) liquid air trap; (22) Dewar flask; (23) collecting flask; (24) water container; (G) graded quartz to pyrex seal.

10-percent rhodium wire, 0.8 mm in diameter. The windings should be closer at the ends of the tube than they are at the center. The furnace is insulated with a packing of Santocel and is operated at a temperature of 1,120° C. Equilibrium, if reached, would leave only a negligible fraction of the oxygen in compounds other than carbon monoxide at any temperature above about 1,000° C. To be sure of approaching equilibrium during the time that the gases are in the heated zone, a higher temperature is needed. Too high a temperature increases the difficulties with the apparatus. The temperature selected by Unterzaucher was found to be satisfactory.

The liquid-air trap (21, in fig. 2) is a spiral formed from 5-mm glass tubing and has a diameter of 4 cm. and a length of 25 cm.

The collecting flask is a round flask fitted at both ends with capillary stopcocks. The upper stopcock is sealed to a standard spherical ground-glass joint. Both 1-liter and 2-liter flasks have been used. They are calibrated by filling them with water, draining to a mark on the lower capillary, and weighing the water.

The quartz tube is shown in detail in figure 3. It is 66.5 cm long, with an outside diameter of 13 mm and a wall thickness of 2 mm. Quartz to Pyrex graded seals are used at points 3 and 7 shown in the drawing. The end of the quartz tube through which the sample is introduced is ground to receive a ground-glass joint (2, in fig. 3), which is fitted with a capillary stopcock (1, in fig. 3). The quartz tube is packed with carbon pellets (5, in fig. 3) for a length of 10 cm, starting at a point 31 cm from the capillary sidearm. The packing is held in place with rolls of platinum gauze (4 and 6, in fig. 3) or quartz wool. Carbon from the products of pyrolysis slowly deposits on the platinum gauze (4, in fig. 3) and interferes with the free passage of helium. This deposit is readily removed by withdrawing the platinum gauze and igniting it over a burner.

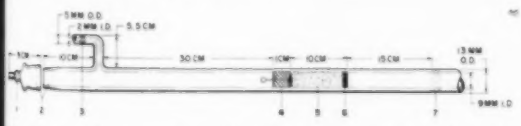

FIGURE 3. *Quartz tube used in the apparatus for the determination of oxygen.*

(1) Micro stopcock; (2) ground-glass joint; (3) quartz to Pyrex graded seal; (4) platinum gauze or quartz wool; (5) carbon pellets; (6) platinum gauze or quartz wool; (7) quartz to Pyrex graded seal.

Detailed directions for the use of the indicating gel tubes and the preparation of the necessary materials are given by Shepherd [8]. The indicating gel tubes are made of 7-mm Pyrex glass tubing and are about 12 cm long. The packing consists of a small piece of Fiberglas tape,[2] 4.5 cm of guard gel, 14 mm of indicating gel, 2.5 cm of guard gel, and a second piece of Fiberglas tape. The guard gel is purified silica gel. The indicating gel is purified silica gel impregnated with a palladium and a molybdenum solution. The purification and preparation of the materials must be done with great care.

After the apparatus is assembled, the air is swept out of the system with a stream of helium and the furnaces are heated to the proper temperatures. The helium gas is then replaced with a stream of hydrogen to remove adsorbed oxygen from the carbon packing. When helium was used, about 1 to 2 weeks were required before a satisfactory blank was obtained, but with hydrogen a low blank was obtained in 24 hours. The flow of hydrogen is continued overnight and then replaced with helium. After the apparatus is ready for use, a slow stream of helium is maintained continuously, but the temperature of furnace (17, in fig. 2) is reduced to about 900° C overnight.

The sample is weighed in a platinum boat and introduced through the ground joint at (13, in fig. 2) into the quartz tube. The stopcocks (12), (20), and (13) are adjusted so that a stream of helium flows in reverse through furnace (17) and out at (13). After 2 hours of flushing, stopcock (13) is closed and stopcocks (12) and (20) are changed so that the gas flows forward through the furnace and out through the liquid air trap. The Dewar flask is filled with liquid air and placed around the glass spiral (21). The collecting flask (23) is filled with water and connected to the liquid-air trap. The flask (24) is lowered, and the lower stopcock on the collecting vessel is adjusted so that the rate of flow of helium is about 30 ml per minute. The sample is then carefully decomposed by slowly advancing the burner and the gauze mantle over the section of the quartz tube that contains the platinum boat. The ignition requires from 10 to 15 minutes and is repeated to insure complete decomposition of any

[2] Cotton is preferable if the tubes are used the same day they are packed.

particles that may have sublimed to other parts of the tube. The second ignition requires only 10 minutes. The flow of gas is maintained until the water level in the collecting flask reaches a mark on the lower capillary arm, and then both the lower and upper stopcocks are closed. The collecting flask is disconnected from the apparatus and the upper stopcock opened momentarily to allow a small amount of air to flow into the flask to restore atmospheric pressure—oxygen introduced at this point does not interfere with the determination of carbon monoxide. The temperature and pressure in the room are noted.

To determine the percentage by volume of carbon monoxide in the collected gas, the flask is connected through a flow meter to an NBS indicating tube and the gas passed through the tube at a rate of 70 ml per minute for a definite period (10 to 180 seconds, depending upon the concentration of CO). The color formed in the indicating tube is then compared visually with standard tubes prepared at the same time by passing known amounts of carbon monoxide through them. Standard mixtures of carbon monoxide and air are used for this purpose. Detailed directions for the preparation of standards, reagents, and tubes are given in reference [8]. From the value obtained for the percentage by volume of carbon monoxide in the collected gas, the volume of the collected gas (which is known by previous calibration of the flask), the density of carbon monoxide at the temperature and pressure of the room, and the weight of the sample, it is possible to calculate the percentage of oxygen in the material. The calculation may be made with the following equation:

$$\text{Percentage of } O_2 = \frac{t_s \times S \times V \times d \times 0.571}{t_x \times W},$$

where t_S and t_X are the times of flow in seconds of the standard carbon monoxide mixture and the gas collected from the sample, respectively; S is the percentage by volume of carbon monoxide in the standard mixture; V is the volume of the collecting flask; d is the density of the carbon monoxide; W is the weight of the sample; and the factor 0.571 is the fraction of oxygen in carbon monoxide.

Blank determinations are made by conducting an analysis in the same manner but without a sample. The blank is about 0.001-percent carbon monoxide 24 hours after the apparatus has been assembled, but after several weeks the blank is reduced to about 0.0002 percent of carbon monoxide.

III. Results and Discussion

Pure compounds containing less than 1 percent of oxygen in the molecule are not available. Therefore, two schemes were used to check the method: (1) pure compounds containing low percentages of oxygen were analyzed, and (2) mixtures of cholesterol and polystyrene, which had been analyzed previously, were prepared in varying ratios to yield samples of very small oxygen content. The results are shown in table 1.

The materials listed in table 1 were selected to determine the effect of various elements on the results. They include chlorine, bromine, nitro-

TABLE 1. *Determination of oxygen in purified materials*

Substance	Oxygen	
	Found	Calculated
	% by weight	*% by weight*
Dicetyl ether	3.6	3.44
Do	3.4	3.44
Do	3.5	3.44
Cetyl stearate	6.3	6.28
Do	6.2	6.28
Do	6.4	6.28
Do	6.3	6.28
Cholesterol	4.1	4.14
Do	4.0	4.14
Do	4.1	4.14
Do	3.9	4.14
S-(2-methoxy-5-chloro)benzylthiuronium chloride [1]	6.2	5.99
Do	6.1	5.99
Do	5.9	5.99
Do	6.1	5.99
Phosphoramide, *N,N',N''-tris*(dibromophenyl)	2.0	2.01
Do	1.9	2.01
Do	1.9	2.01
Do	2.1	2.01
Cholesterol-polystyrene mixtures	2.2	2.24
Do	1.9	1.80
Do	1.5	1.51
Do	1.3	1.22
Do	0.58	0.58
Do	.52	.55
Do	.43	.41
Do	.27	.26

[1] This compound is being prepared at the National Bureau of Standards for use as a micronalytical standard. Its structure is probably similar to that of S-benzylthiuronium chloride; however the structure of the latter compound is not definitely known. See Bougault and Charrier, Compt. rend. **218,** 559 (1944).

gen, sulfur, and phosphorus in addition to carbon, hydrogen and oxygen. The values obtained indicate that these elements do not interfere with the method.

Inasmuch as many laboratories do not have available liquid air, the liquid-air trap was replaced with a potassium-hydroxide trap, which removes acidic substances but not unsaturated compounds, and additional analyses were made. The potassium-hydroxide trap consisted of a straight piece of Pyrex tubing, 15 mm in diameter and 18 cm long, filled with solid pellets of potassium hydroxide. Table 2 shows a comparison of the results obtained with this trap and the liquid-air trap. These results indicate that the potassium-hydroxide trap may be substituted for the liquid-air trap without loss of accuracy.

TABLE 2. *Relative effectiveness of liquid-air and potassium hydroxide traps*

Substance	KOH trap	Liquid-air trap
	% O_2 *by weight*	% O_2 *by weight*
Cholesterol	4.1	4.1
Do	4.1	4.0
Do	3.9	4.1
Do	4.0	3.9
5-(2-methoxy-5-chloro)benzylthiuronium chloride	6.0	6.2
Do	5.9	6.1
Do	5.9	5.9
Do	6.1	6.1
Polystyrene	0.034	0.033
Do	.035	.035
Do	.032	.033

Tests were made to determine the length of time required to sweep the system free of air after introduction of the sample. It was found that 30 minutes of reverse flushing is sufficient. However, if oxygen is adsorbed on the sample a longer time may be required as indicated by the results for anthracene listed in table 3. If desired, the removal of adsorbed oxygen may be accelerated by placing the boat containing the sample near the end of the quartz tube and slipping over this section of the tube an electrically heated jacket filled with a liquid that boils at the temperature selected for heating the sample during the flushing period.

Oxygen determinations have been made on various materials, and a few of these are listed in table 3.

TABLE 3. *Determination of oxygen in miscellaneous materials*

Substance	Oxygen
	% *by weight*
Anthracene (reverse flushing for 2 hr)	0.018
Do	.017
Anthracene (reverse flushing for 16 hr)	.015
Do	.012
Diphenyl	.011
Do	.014
Natural rubber (unextracted)	.8
GRS rubber (unextracted)	.9
Butyl rubber (unextracted)	.4
Gutta percha (unextracted)	1.0
Popcorn polystyrene	0.034
Diesel oil (Fischer-Tropsch)	.14
Vistanex (dried 3 hr at 90° C)	.047
Vistanex (dried 3 hr at 90° and 3 hr at 120° C)	.50
Vistanex (dried 48 hr at 150° C)	2.6

The low values reported in the table for the oxygen content of anthracene and diphenyl were obtained on samples that had been carefully purified. Original samples of these materials contained as much as 0.35 percent of oxygen, and it was possible to follow the purification by the gradual reduction in the percentage of oxygen present. The diesel oil was a sample made in Germany by the Fischer-Tropsch process.

The results obtained with Vistanex are very interesting. In connection with another problem, it had been noted previously by one of the authors that polystyrene, when precipitated in a finely divided state, slowly gained in weight when heated at 50° C. This rate of increase in weight was accelerated at 70° C. The results obtained with Vistanex clearly show that its oxygen content increases with increase in temperature and period of heating. Similar results were obtained with dicetyl ether.

IV. References

[1] C. Dufraisse, Rev. gén. caoutchouc **9,** No. 85, 3 (1932); Rubber Chem. and Tech. **6,** 152 (1933).
[2] P. J. Elving and W. B. Ligett, Chem. Rev. **34,** 129 (1944).
[3] M. Schütze, Naturwissenschaften **27,** 822 (1939).
[4] M. Schütze, Z. anal. Chem. **118,** 241 (1939).
[5] M. Schütze, Z. anal. Chem. **118,** 245 (1939).
[6] J. Unterzaucher, Ber. deut. chem. Ges. **73b,** 391 (1940).
[7] V. A. Aluise, R. T. Hall, F. C. Statts, and W. W. Becker, Anal. Chem. **19,** 347 (1947).
[8] M. Shepherd, Anal. Chem. **19,** 77 (1947).

WASHINGTON, February 6, 1948.

U. S. Department of Commerce
National Bureau of Standards

Research Paper RP1890
Volume 40, June 1948

Part of the Journal of Research of the National Bureau of Standards

Infrared Emission Spectra of Flames[1]

By Earle K. Plyler and Curtis J. Humphreys

The infrared emission spectra of a hydrogen flame and of a natural gas flame have been compared in the region from 1.7μ to 24μ. Emission bands have been observed at 1.87μ, 2.78μ, 4.37μ, 6.26μ, and 15μ that are produced by molecules of H_2O and CO_2. Another band at 3.316μ is attributed to methane. From 3.0μ to 3.8μ there are a number of rotational lines, some of which may be produced by OH and others by H_2O molecules. As the temperature of the flame was increased, the rotational lines became more intense. Five lines in the region from 3.4μ to 3.8μ agree closely in position with the predicted rotational lines of the P branch of the 2→1 vibrational band of OH. These lines correspond to values of K equal to 11, 12, 13, 14, and 15. Wave numbers of some of the observed rotational lines were found to show a good correspondence with predicted values for K equal to 11 to 36, for lines extending from 9μ to 24μ. In addition to this series of lines, there are other lines that are produced by the rotational states of H_2O molecule. A discussion is included of the various methods of observing flame spectra.

I. Introduction

In the February 1948 number of the Journal of Research[2] there is an article on the emission spectra from a Bunsen flame. In that work it was shown that nearly all the emission spectra from the Bunsen flame were produced by H_2O and CO_2 molecules. The CO_2 spectrum has bands in the regions of 4.4μ and 15μ. The CO_2 emission in the 15-μ region is composed of at least three bands with frequencies of 667, 668, and 721 cm^{-1}. These frequencies correspond to the changes in known energy levels. The transitions are (01^10) to (00^00), (02^20) to (01^10), and (10^00) to (01^10). A discussion of the 15-μ emission of CO_2 molecule has been given in a recent report.[3] Nearly all the energy in the region of 2.7μ is radiated by the H_2O molecule. Additional observations included the strong band of water vapor at 6.26μ in the emission spectrum, and many rotational lines extending from 10μ to 24μ.

In the region of 2.8μ to 3.2μ, there are 15 lines that have been attributed to the H_2O molecule. In order to measure the spectrum in the 3-μ region under different conditions of burning, a commercial gas-oxygen torch was used. The gas and oxygen were completely mixed before burning to produce a smooth, narrow, quiet flame 5 in. high on a port about 1 mm in diameter. The emission spectra of a gas-oxygen flame and a hydrogen-oxygen flame have been measured and the results compared.

II. Experimental Work

A Perkin-Elmer infrared spectrometer, with interchangeable prisms of LiF, NaCl, and KBr, was used as the resolving instrument. Natural gas containing about 88 percent of methane was burned in a gas-oxygen torch, and the flame was changed by varying the amount of oxygen. This caused the flame temperature to be different, with a corresponding effect on the relative intensities of the bands. Some of the bands would increase in intensity and others would decrease in intensity, as the temperature was increased.

Figure 1 shows the emission bands from the flame of a gas-oxygen torch. Natural gas was burned with O_2 in considerable amounts, giving rise to a hot flame. The zero branch of the H_2O combination band is found to be at 1.87μ, and the P and R branches at 1.95μ and 1.78μ, respec-

[1] The results of this paper were reported, in part, at the meeting of the Optical Society of America in October 1947.
[2] E. K. Plyler, J. Research NBS 40, 113 (1948) RP1860.
[3] E. K. Plyler, Science 107, 48 (1948).

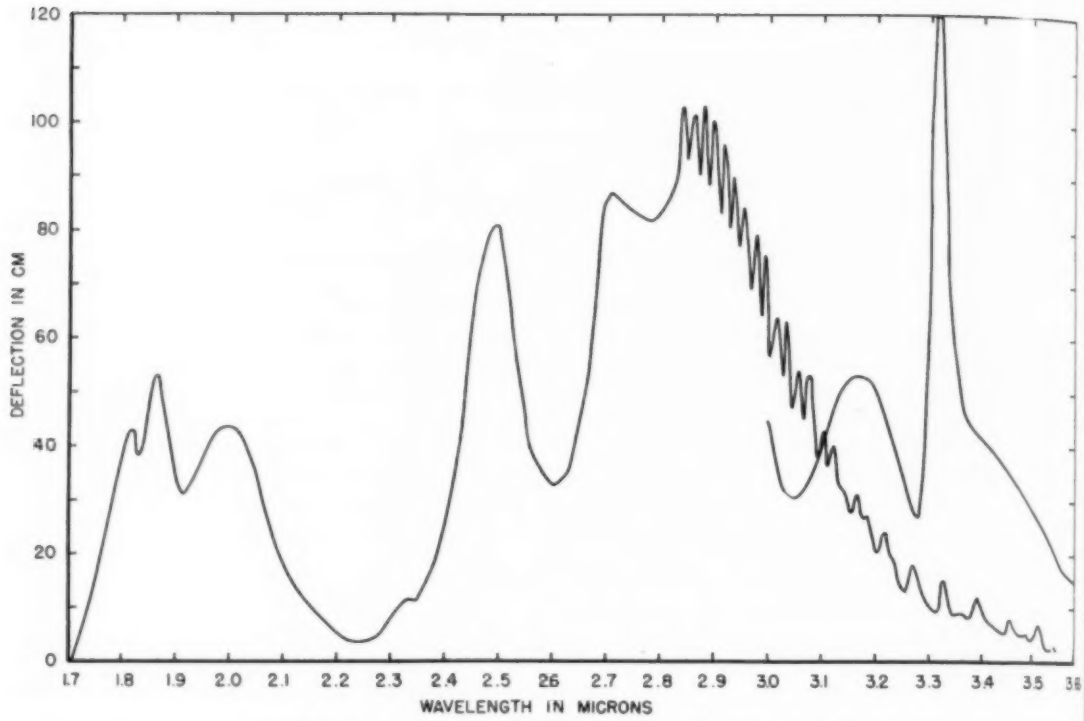

FIGURE 1. *Infrared emission spectrum of a natural gas-oxygen flame.*

The spectrometer slits were 0.18 mm in width, and an LiF prism was used. The methane band at 3.3 μ was measured from a gas-air flame with cone of flame focused on spectrometer slit, and the slits were 0.25 mm in width.

tively are also resolved from the Q branch. However, the resolution of the LiF prism was not sufficient for resolving any of the rotational structure. In the region from 2.84μ to 3.55μ there are many rotational lines. When less oxygen is used in the flame the lines from 2.84μ to 3.1μ stand out more prominently, and the faint lines in the region from 3.1μ to 3.55μ disappear. The intense band with a sharp maximum at 3.315μ was observed when small amounts of oxygen were introduced in the burner and a large cone was present in the flame. The region of the cone was focused on the entrance slit of the spectrometer. The zero branch is sharp and of good intensity. The R branch is observed and is of maximum intensity at 3.16μ, and is well separated from the zero branch.

In figure 2 the emission spectra of the hydrogen flame are shown for the spectral region of 1.7 to 3.9 μ. The 1.87-μ maximum, which is the zero branch of a combination band of the H_2O molecule, is quite intense. The P branch is relatively less intense in the hydrogen flame than in the gas flame. The greater intensity of the gas flame may be caused by the radiation of the CO_2 molecule in the region of 2μ.

The zero branch at 2.71μ is somewhat reduced by the absorption of the CO_2 and H_2O molecules in the air. However, in figures 1 and 2 there has not been any correction applied for the atmospheric absorption. A comparison of the two figures indicates that there is considerable emission from CO_2 in this region. The R branch of the H_2O band has the greatest intensity at 2.5μ and the P branch at about 2.9μ. As shown in figure 2, the rotational lines in the P branch of the 2.7μ-H_2O emission band are well marked, and 19 lines are observed in the region from 2.80μ to 3.25μ. The slits of the spectrometer were 0.185 mm wide, and the flame had considerable oxygen.

When the flame was made hotter by increasing the oxygen by a small amount, these lines were less conspicuous. The flame was adjusted so that

the lines were of greatest contrast to the background, and they were observed with a somewhat narrower slit. Under these conditions it was found that several of the lines had bulges on their sides. It was not possible to completely separate the complex structures with the LiF prism, but it is highly probable that many other lines could be observed in this region if higher resolution were employed.

The curve marked *b* in figure 2 represents the flame spectrum from 3.0μ to 3.4μ when the oxygen is increased. The greater deflections are produced, in part, by increasing the amplication of the thermocouple output by about 50 percent. Under the different flame conditions the rotational components show a considerable variation in intensity. At wavelengths beyond 3.1μ the lines have greater intensity, and it has been possible to extend the observation of rotational structure to 4.8μ. Curve *c* in figure 2 was measured by increasing the slits to 0.25 mm and increasing the amplication by a factor of two compared to the value used in the region from 1.7μ to 3.4μ. The wavelengths of the rotational lines are listed in section III.

The infrared emission in the region from 3.5μ to 5.0μ from the flame was studied, when mixtures of natural gas and oxygen were used. It was found that the emitted energy could be more than doubled by increasing the oxygen. The corrections for the atmospheric absorption and also the self absorption of the flame were calculated from observed data. By passing radiation of one flame through another flame, it was found that the flame absorption amounted to about 20 percent at 4.22μ. This was measured by having one flame focused on the entrance slit and placing another flame in the path between the first flame and the entrance slit. The sum of the energies of the two flames burning separately was compared with the energy of the two flames burning at the same time. The corrected energy curve for the

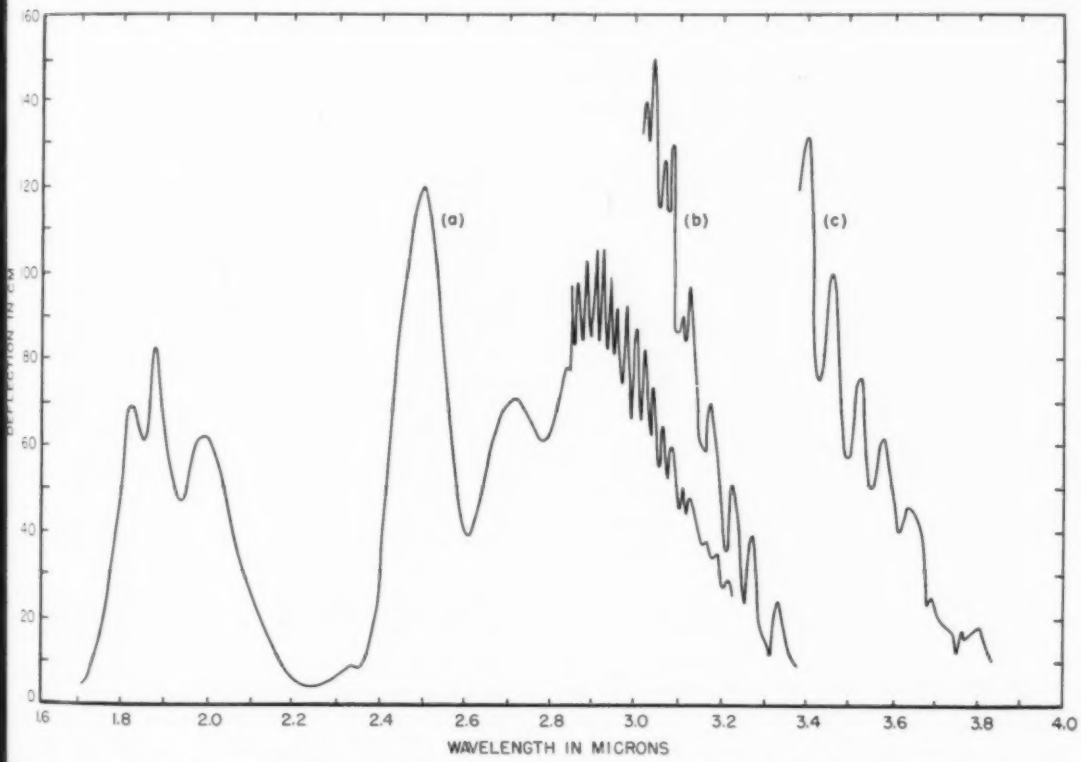

FIGURE 2. *(a), Infrared emission spectrum of a hydrogen-oxygen flame. (b), Hotter flame and amplification increased 50 percent; (c), hotter flame and amplification increased 100 percent.*

4μ to 5μ region did not vary by a significant amount from the curve shown in the previous paper (see footnote 2), and it is not shown here.

In figure 3 is shown the 6.26μ H_2O emission band. This was observed in the hydrogen flame with a considerable amount of oxygen. A rock-salt prism was used in the spectrometer, and the slits were 0.280 mm wide. There is very little emission in the center of the band, and the *R* branch has maximum energy at 5.35μ, and the *P* branch at 6.75μ. The rotational structure is not well resolved, but three strong lines can be seen between 7.5μ and 8.0μ. The energy radiated by the flame is of low intensity. In figure 4 is shown the record of the energy emitted from 10μ to 15μ where it is a maximum. The position of the maximum of intensity within this region varies with the temperature of the flame. The energy emitted by the flame is very much dependent on the amount of oxygen that is introduced. For example, if the flame is hot, with a relatively high proportion of oxygen, the energy is about constant in the 10μ to 15μ region. For cooler flames with less oxygen, the energy increases continuously from 10μ to 15μ. The marked changes in relative intensity of the rotational lines of the water vapor molecule that are produced by flame changes may prove to be a method of measuring flame temperatures. However, no quantitative measurements were carried out on the relation between temperature and emitted energy. All observations were made in the portion of the flame above the cone, except when otherwise noted.

The rapid decrease in intensity of the rotational lines of the H_2O molecule in the region from 13 to 15μ is caused largely by the absorption of the NaCl prism and by CO_2 in the atmosphere. The results shown in figure 4 are for a flame exhibiting maximum intensity at about 12μ. This flame was hotter than one showing constant energy, but the considerable drop in the observed energy in the 14μ to 15μ region is caused by absorption of the NaCl prism. This region of the spectrum was also observed with a KBr prism, and the envelope of the emission lines changed form with the temperature. For the hottest flames, the maximum intensity was observed at about 12μ, and with cooler flames, the maximum intensity was at about 15μ.

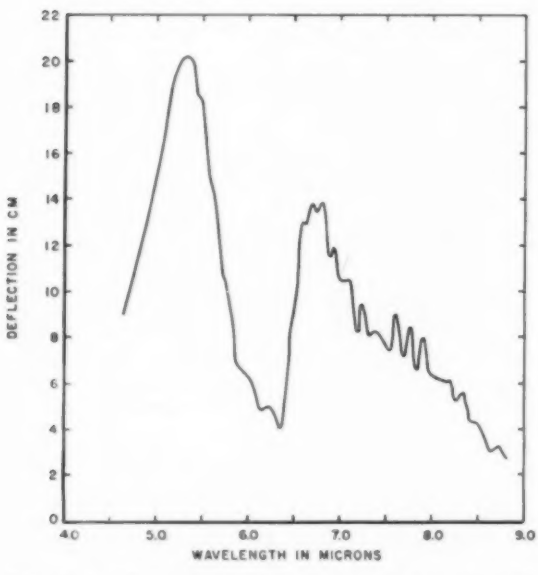

FIGURE 3. *Emission spectrum of the 6.26μ band of the H_2O molecule as obtained from a hydrogen-oxygen flame.*

A rock salt prism was used, and the slits were 0.28 mm in width.

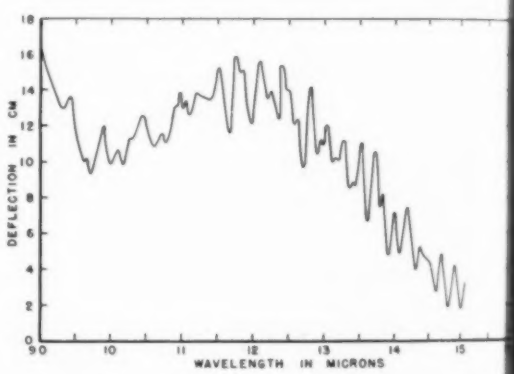

FIGURE 4. *Rotational lines of the hydrogen-oxygen flame from 9 to 15μ.*

The slits were 0.5 mm wide, and an NaCl prism was used.

The region from 15μ to 24μ has been measured with a KBr prism and is shown in figure 5. As the region of 24μ is approached, the energy becomes very small. The spectrum shown in figure represents the observations on the hydrogen flame. Its emitted energy is greater than observed for the natural-gas flame, except in the region of 15μ.

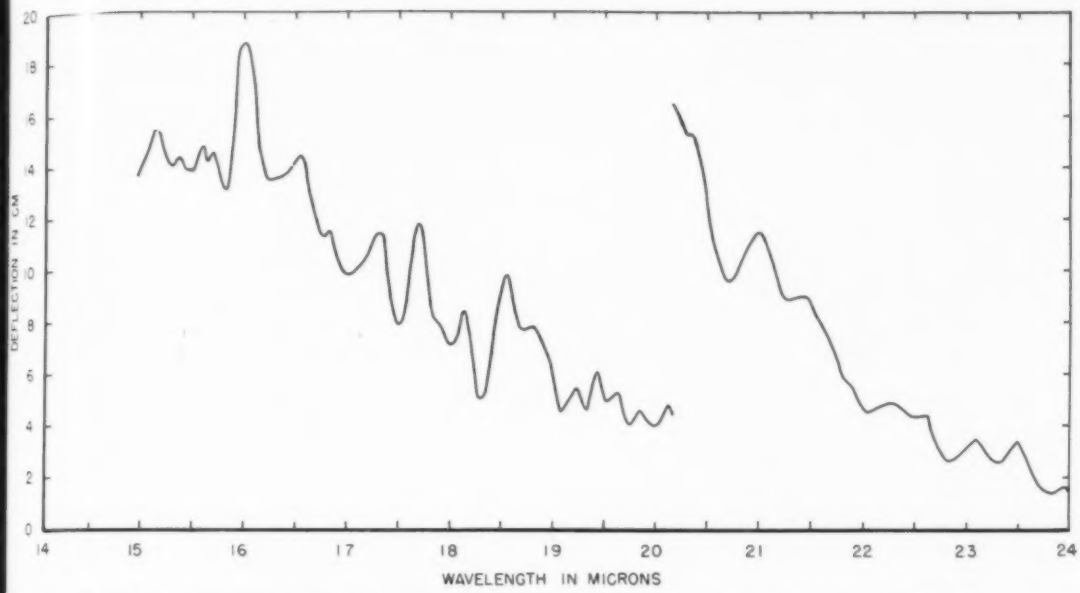

FIGURE 5. *Rotational lines of the hydrogen-oxygen flame from 15 to 24μ measured with a* KBr *prism.*

The slits were 0.53 mm wide from 15 to 20μ and 0.7 mm from 20 to 24μ.

III. Discussion

In the previous paper (see footnote 2), measurements of the Bunsen flame were reported, and the bands produced by the CO_2 and H_2O molecules were noted. Because of some overlapping of the two spectra, certain regions of the spectrum could not be well segregated. For this reason a comparison of the hydrogen-oxygen torch flame with the Bunsen natural-gas—air flame would assist in the study of the emission spectra of the H_2O molecule. This is especially true of the region 1.7μ to 4.9μ. The long wavelength branch of the H_2O band at 2.7μ has been partially resolved, and about 19 lines can be seen in figure 2. By increasing the sensitivity of the instrument and increasing the temperature of the flame, lines are observed to about 3.8μ. The lines from 3.3μ to 3.8μ are probably produced by OH and H_2O molecules, but it has been found possible only in a limited region to make assignments from calculated values for transitions between the energy levels of either H_2O or OH. One exceptional instance will be discussed in another part of this paper. Higher resolution will be necessary in this region in order to permit accurate and complete assignment of lines to series.

It has been found that these lines check very closely with the series of $\Delta j=-1$ and $\Delta K=0$ for the H_2O molecule and give rise to a spacing of about 20 cm^{-1}. However, there are several other series to be expected corresponding to the higher rotational states of the H_2O molecule, which would also give rise to lines in this region. So this one series may only, in part, explain the presence of these lines. The curves *b* and *c* of figure 2 show the effect of temperature on the lines, and the relative intensities are considerably altered. In table 1 the wavelengths and frequencies of the observed rotational lines are listed. Because of the high temperature of the flame, the rotational-vibrational bands have the energy reduced near the center and increased at larger rotational states. This causes the spread in frequency from the *P* to *R* maxima to increase. In the *R* branch there is considerable crowding of the rotational lines.

The band at 3.316 μ in figure 1 was observed at greatest intensity when the axis of a large cone of the flame was focused on the entrance slit of the spectrometer. The *R* branch is readily recognized, but the *P* branch of the band is weak. The zero branch is intense, and the region of maximum intensity is removed from the methane band, observed in absorption, by about 4 cm^{-1}. As

TABLE 1.—*Observed rotational components in the region from 2.8 to 3.7μ*

Wavelength	Wave number	Wavelength	Wave number
μ	cm^{-1}	μ	cm^{-1}
2.827	3,537	3.076	3,250
2.841	3,519	3.100	3,225
2.855	3,502	3.117	3,208
2.874	3,479	3.063	3,161
2.895	3,454	3.216	3,109
2.912	3,434	3.267	3,060
2.929	3,414	3.325	3,007
2.948	3,392	3.388	2,951
2.971	3,365	3.448	2,900
2.992	3,342	3.513	2,846
3.013	3,318	3.568	2,802
3.032	3,298	3.645	2,743
3.056	3,272		

higher temperatures are reached in the methane gas there will be a gradual shift to longer wavelengths for the zero branch of the band.

The authors are indebted to G. H. Dieke of Johns Hopkins Univ., who furnished them with a table of the calculated wave numbers of the vibrational-rotational lines of OH and also the wave numbers for the pure rotational lines.[4] Many lines arise from the 1→0 transition in vibrational levels and also from the 2→1 transition. The wave numbers calculated by Dieke were plotted, and it was found that the overlapping of the different series in the region from about 3,000 to 4,000 cm^{-1} was so great that the available instruments could not separate the different states. However, in the region from 2,500 to 3,000 cm^{-1}, the overlapping is not so great, and a series of five lines that were observed in the hydrogen flame check will with predicted transition in the 2→1 vibrational band. The observed lines are shown in figure 2, c. With low oxygen concentrations in the mixture, these lines are very weak. The flame mixture was adjusted to give the greatest energy in this region, and it was a hot flame. When observations were made in the region of 3μ, it was found that the lines as shown in figure 2 were not as well resolved with a hot flame as with a moderate flame. But as the longer wavelength region of the band is reached, high flame temperatures are necessary to bring out the rotational lines. The 2→1 band has *P*, *Q*, and *R* branches and there are two series. Each line is double. Thus for each value of *K* (rotational levels) there exist four lines with nearly the same wave number. It was not possible with the prism instrument to separate the lines and only one maximum could be observed. In table 2 the calculated values are taken from Dieke's table, and they are averaged values of all four components. The experimental values are correct to 4 cm^{-1}.

TABLE 2. *Calculated and observed wave numbers for rotational lines in the P branch of the 2→1 band of* OH

K	*P* (calculated)	*P* (observed)	*P* (observed)
	cm^{-1}	cm^{-1}	μ
11	2946.3	2,950	3.388
12	2897.9	2,896	3.448
13	2848.9	2,848	3.513
14	2799.2	2,803	3.568
15	2748.8	2,744	3.645

These five lines that appear relatively free from interference or overlapping show such close agreement with predicted positions, that it appears practically certain that they constitute the part of the rotational structure of the *P* branch of the 2→1 band of OH, for *K* values, 11 to 15 inclusive. This structure is observed only because the emission of the H_2O molecules has become relatively weak in this limited interval. For the region of shorter wavelengths, the H_2O emission is so strong as to completely mask the OH spectral structure so that it is not possible to observe lines showing the characteristic intervals for the 2→1 band and the 1→0 band.

In table 3 the wavelengths and wave numbers of the rotational lines from the hydrogen flame are listed. The observations to 15μ were made with an NaCl prism and from 15μ to 24μ with a KBr prism.

This table comprises all of the measured values of the emission maxima that appeared in the recordings of the spectrum of the hydrogen flame shown in figures 4 and 5. This observed spectrum appears to consist of the superposed systems of pure rotational lines of OH and H_2O.

In order to examine the evidence that the rotational OH emission spectrum has been produced, table 4, giving a comparison of the calculated and observed line positions, has been constructed. The calculated wave numbers, corresponding to *K* values 11 to 22, are obtained from Dieke's table

[4] *G. H. Dieke*, Table of OH bands, private communication.

TABLE 3. *Observed rotational lines in the spectrum of the hydrogen flame in the region from 9 to 24 μ*

λ (μ) (observed)	cm⁻¹ (observed)	λ (μ) (observed)	cm⁻¹ (observed)	λ (μ) (observed)	cm⁻¹ (observed)
9.43	1,060	13.43	745	20.11	497
9.63	1,038	13.53	739	20.41	490
9.89	1,011	13.70	730	20.98	477
10.07	993	13.83	723	21.47	466
10.03	970	13.99	714	21.91	456
10.44	958	14.17	706	22.26	449
10.73	931	14.35	697	22.63	442
10.90	917	14.49	690	23.08	433
10.98	911	14.68	681	23.50	426
11.04	905	14.91	671	23.96	417
11.19	894	15.16	659	.....	.....
11.54	867	15.35	652	.....	.....
11.75	851	15.61	641	.....	.....
11.85	844	15.70	637	.....	.....
12.09	827	16.01	625	.....	.....
12.25	816	16.58	603	.....	.....
12.41	806	16.82	595	.....	.....
12.48	801	17.31	578	.....	.....
12.63	791	17.70	565	.....	.....
12.79	781	18.13	552	.....	.....
12.94	772	18.54	539	.....	.....
13.03	767	18.79	532	.....	.....
13.14	761	19.22	520	.....	.....
13.28	753	19.43	515	.....	.....

Actually there are four possible lines for each K, but inasmuch as the resolution available in these experiments did not permit observation of these separate components, the four values are averaged in each instance to give the computed line position. Dicke's calculations were carried out only as far as K-value, 22. We have extended them to K, 36, by extrapolation. It is estimated that the error in this extrapolation cannot exceed 1 cm^{-1}, which is well within the estimated experimental error of the observations for this region of the spectrum, namely 4 cm^{-1}.

Of the 26 entries in table 4, all but 2 show agreement between the observed and calculated positions within the limits of experimental error. In almost all instances of failure to find experimental evidence for an emission line of OH, there is an intense maximum probably originating in H_2O overlapping the calculated position. Some of the listed lines appear only as bulges on the sides of the profiles of other intense maxima, but agreement with the predicted position seems to confirm their reality. The evidence for the reality of this system of rotational lines of OH rests mainly on its completeness rather than on the precision of the

TABLE 4. *Observed and calculated wave numbers of the pure rotational lines of* OH

K	R (calculated)	R (observed)	R (observed)
	cm^{-1}	cm^{-1}	μ
11	431.8	433	23.08
12	465.3	466	21.47
13	498.4	497	20.11
14	530.9	532	18.79
15	562.7	565	17.70
16	593.8	595	16.82
17	624.2	625	16.01
18	653.9	652	15.35
19	682.9	681	14.68
20	711.0	714	13.99
21	738.3	739	13.53
22	764.8	767	13.03
23	790.6	791	12.63
24	815.6	816	12.25
25	839.9	844	11.85
26	863.4	867	11.53
27	886.2	886	11.28
28	908.2	911	10.98
29	929.5	931	10.73
30	950.0	---	-----
31	969.8	970	10.31
32	988.8	993	10.07
33	1007.0	1,011	9.89
34	1024.5	---	-----
35	1041.2	1,038	9.63
36	1057.2	1,060	9.43

observations. The appearance of a small number of scattered combinations dispersed through another complex spectrum might well be regarded as fortuitous, but when the observed system is practically complete, the probability that it is real seems to be overwhelming.

The numerous remaining lines shown in figures 4 and 5 and listed in table 3, are produced by higher rotational states of the H_2O molecule. As mentioned above, some of these overlap or coincide with OH, making it practically impossible to estimate the relative intensities of the lines in the OH system. A noteworthy instance is the very intense maximum at 16.0μ, which undoubtedly receives by far the greater contribution from H_2O, masking an OH line in the same location.

IV. Conclusion

The emission spectra of a gas-oxygen and hydrogen-oxygen flame have been compared in the region from 1.7μ to 3.8μ. Nearly all of the energy in the 1.9μ region is produced by the H_2O molecule. A small increase in the energy of the gas flame in

the 2-μ region may be caused by emission of CO_2. The rotational lines that are observed at about 3μ are present in both flames, but they extend to longer wavelengths in hydrogen-oxygen flames. The intensity of the observed bands can be increased at least twofold by increasing the oxygen. The emission in the region of 10μ can be greatly increased with high-temperature flames. The energy remains about constant from 9μ to 16μ and then decreases gradually to 24μ. With a moderate flame temperature the energy increases from 9μ to 15μ and then decreases as the wavelength is increased.

In this study of the emission of flames, it has been shown that the amount of oxygen that is introduced into the flame has marked influence on the intensity of the band. In the 3-μ region, the relative intensities of the rotational lines may be varied considerably by changing the temperature of the flame. For a quantitative study of emission spectra originating in a flame, it would be necessary to measure the quantity of fuel gas and oxygen that are mixed for burning. A gas-oxygen torch or a regulated burner, giving rise to a steady flame, makes it much easier to obtain smooth traces on the recorder for the energy emitted. The results can be repeated closely. For quantitative determinations, the steady flame is very desirable. However, in many industrial applications, the turbulent flame is the more common type, and the Bunsen burner flame approaches nearer to industrial burner flames. This study has been chiefly concerned with the study of the emission spectra of CO_2 and H_2O in flames. The flames resulting from burning various hydrocarbons and alcohols will also have considerable energy emitted by CO_2 and H_2O molecules. There may be other bands in the observed flame spectra of various fuels that are characteristic of the molecular or atomic groups. The bands are usually of low intensity.

In addition to a controlled burner, a spectrometer of high aperture ratio is needed. This makes it possible to observe low-intensity bands. Because of the decrease in the observed intensity produced by the absorption of H_2O and CO_2 molecules in the air, an instrument that is free from atmospheric absorption is better suited for quantitative measurements. For the study of many problems, an instrument of moderate resolution is satisfactory. In the measurement of the rotational lines within a band, a grating spectrometer is better suited.

The authors express their thanks to G. H. Dieke of Johns Hopkins University for supplying calculated values of the wave numbers of the OH bands and of W. S. Benedict of the National Bureau of Standards for advice in the interpretation of the experimental data.

WASHINGTON, March 12, 1948.

U. S. Department of Commerce
National Bureau of Standards

Research Paper RP1891
Volume 40, June 1948

Part of the Journal of Research of the National Bureau of Standards

Pressure-Volume-Temperature Data for Oxygen

By Cyril H. Meyers

To satisfy the demand for data on oxygen at higher pressures, an equation has been developed that represents the available experimental data within the accuracy of the observed values. Values of the virial coefficients are given for densities in Amagat units in the temperature range −200° to +200° C. Values of pressure in pounds per square inch[2] are tabulated corresponding to temperatures from −50° to +150° F and densities up to 320 times the density at 70° F and 1 atmosphere. These data are also presented in a chart, with pV/RT and pressure as coordinates.

I. Equation of State

The use of progressively higher pressures in high-pressure containers has developed a need for data on oxygen at pressures and densities higher than those at present tabulated. Although an equation for representing the properties of oxygen has been published by Millar and Sullivan [1], that equation is not adequate for the present purpose. Hence an equation has been devised that represents all available experimental PVT data at densities up to the critical density within the limit of experimental accuracy. The equation is of the Kamerlingh Onnes type. Exponential functions of temperature replace the functions used by that author. This equation has the form

$$pV/RT=1+B/V+C/V^2+D/V^4, \qquad (1)$$

where the virial coefficients have the following values:

$$B=(B_1/T)(1-\exp\ (-M/T))+B_2$$

$$C=(C_1/T)(1-\exp\ (-M/T)^3)+C_2$$

$$D=(E_1/T)(1-\exp\ (-M/T)^7)+D_2$$

The omission of the term in $1/V^3$ is in accordance with the practice of Kamerlingh Onnes. The quantities B_1, B_2, C_1, C_2, D_1, D_2, and M are constants. The exponent of (M/T) is in each case, equal to $(2n-1)$ where n is the exponent of V. The practice of Kammerlingh Onnes has been to add terms containing higher powers of V for making the equation applicable at higher densities. No attempt has been made to see whether the form of temperature function used here could be extended to such additional terms.

A study of charts of pV versus $1/V$ for several substances shows that a linear relation exists between the minimum values of pV for the various isotherms and their corresponding values of density. If this linear relation may be extrapolated to low temperatures where the minimum occurs in the region of the subcooled liquid and cannot be reproduced experimentally, then since the density of the condensed phase is finite, the minimum value of pV should also be finite, even though negative at the lower temperatures. The form of temperature functions used in eq 1 have been designed such that their product with T remains finite as T approaches zero; and in this respect are considered to be better than those used for butadiene [2], although the constants for the second virial can be chosen so that over a wide temperature range the two functions will give values very closely in agreement. The form B_1/T^4+B_2, which was used for the third virial in the equation for butadiene, becomes at high temperatures a close approximation to the form used here.

The value of M was determined by a method of successive approximations. The procedure consisted in assuming a value for M, solving for B_1 and B_2 from values of the second virial derived from the experimental data at two temperatures,

[1] Figures in brackets indicate the literature references at the end of this paper.

785784—48——3

those chosen being 0° and 100° C, and calculating the value of the second virial at a third temperature. Successive values of M were chosen until the calculated value of the second virial at the third temperature, in this case the critical temperature, agreed with that derived from experimental data. The value obtained for M was near $1.25T_c$ and hence the number 192.838 was adopted for M. This is five-fourths of 154.27°K, the number reported by the Leiden laboratory for the critical temperature. In consideration of the law of corresponding states, the quantity $1.25T_c$ should be sufficiently approximate to make a good initial choice for fitting data to other substances, although the exact value five-fourths is no longer considered significant.

Although coefficients were determined for the three terms to represent all the observed data for oxygen within the limit of experimental accuracy, yet at the lowest temperatures the choice of a smaller value of M would improve slightly the agreement between calculated and observed values But this change would be at the expense of excessive deviations at higher temperatures. A similar situation was found in attempts to apply the equation to nitrogen.[2] On the other hand, the data for nitrogen above 100° C indicate a larger value of M. This emphasizes the fact that, although eq 1 covers the entire range of data on oxygen, it is only empirical and is applicable to a limited temperature range.

For convenience in computation, the Naperian number e is replaced by the base 10 giving

$$B=(B_1/T)(1-10^{-b})+B_2$$

$$C=(C_1/T)(1-10^{-c})+C_2$$

$$D=(D_1/T)(1-10^{-d})+D_2$$

The numerical values to be used are as follows:

$B_1=-1.04472$ $\quad B_2=0.0009878$

$C_1=647.93\times10^{-6}$ $\quad C_2=1.426\times10^{-6}$

$D_1=-1133.9\times10^{-12}$ $\quad D_2=5.55\times10^{-12}$

$T=°\mathrm{C}+273.16$

$$b=0.434294(M/T)=83.7484/T$$

$$c=0.434294(M/T)^3=3.1143\times10^6/T^3$$

$$d=0.434294(M/T)^7=43.06\times10^{14}/T^7,$$

where

$$0.434294=\log_{10}e$$

and where in the right-hand side of the equatio the temperature T is expressed in degrees Kelvi and the volume V, in Amagat units, that is, t ratio of the volume at the specified state to t volume at 0° C and 1 atm. Since the fracti pV/RT is dimensionless in form, its value independent of the units, and it may be expres in any units so long as they are consistent.

II. Representation of the Experimenta Data

Although this work was undertaken primarily calculate data for use in the compressed g industry in the temperature range −50° to 150° a much wider range has been covered.

Equation 1 with the constants given in the fi section of this paper represents the available da within the experimental error from −145° 200° C, at densities up to 300 or even more Amag units. The accuracy with which eq 1 repres the data is shown by figure 1, in which the coor nates are $(V/V_0)\ (1-pV/RT)$ versus V_0/V, whe V is the specific volume at the pressure p and t temperature T, V_0 is the specific volume at 1 at and 0° C, and R is the gas constant in appropria units. The continuous curves represent valu calculated from eq 1. The sensitivity of the ch to errors in pressure is variable, with the dens becoming infinite at zero density. The effect −117° C of a 0.2 percent error in the pressur illustrated by the distance H between the top the chart and the adjacent dotted curve.

The available measured values of pVT oxygen are represented by the various points figure 1. These data are given in Internatio Critical Tables, [3]. They comprise measureme from three sources namely: (1) Holborn and O at the Physikalische Technische Reichsanstalt (2) Kamerlingh Onnes and his associates Leiden [3, 5], Amagat [6].

(1) The first group consists of nine measu ments at pressures up to 100 atm at each of t

[2] The constants used for nitrogen were $P_1=-0.008223$, $P_2=0.001208$, and $M=157.45=(5/4)\ T_c$, where T_c was assumed to be 125.96°K, and V is in Amagat units. A very good representation of the data in International Critical Tables [3] up to 100° C is obtained, but at 400° C the second virial coefficient is in error by about 0.0002, i. e., about 20 percent. If the exponent is increased to about $-1.8\ T_c/T$ the experimental data above −100° C are very well represented but not those at lower temperatures.

temperatures 0°, 50°, and 100° C. The points marked by × represent these measurements in figure 1. The empirical equation represents these measurements with average deviations from the observed pressures of 0.011, 0.043, and 0.017 percent, respectively.

(2) The second group are less precise and probably less accurate. Except for those observations below −117° C, they are represented in figure 1 by the various kinds of circles. Table 1 shows the pressure range covered by these measurements as well as the accuracy with which the empirical equation represents them. The four columns contain respectively the temperature in degrees C, the number of measurements at that temperature, the pressure range covered in atmospheres, and the average difference between the calculated and observed pressures in percent.

Except for the data at −102.46°C, the average deviations at low temperatures do not exceed those in the temperature range 0° to 20° C, where the equation is more accurately determined by the measurements at the Reichsanstalt. Reference to figure 1 shows that the data at −102.46 deviate consistently from the equation. There is no trend in the deviations at other temperatures to indicate that this is a failure of the equation. It appears rather that the data along this particular isotherm are in error. Likewise the four observed values at −113.97° C and the respective approximate densi-

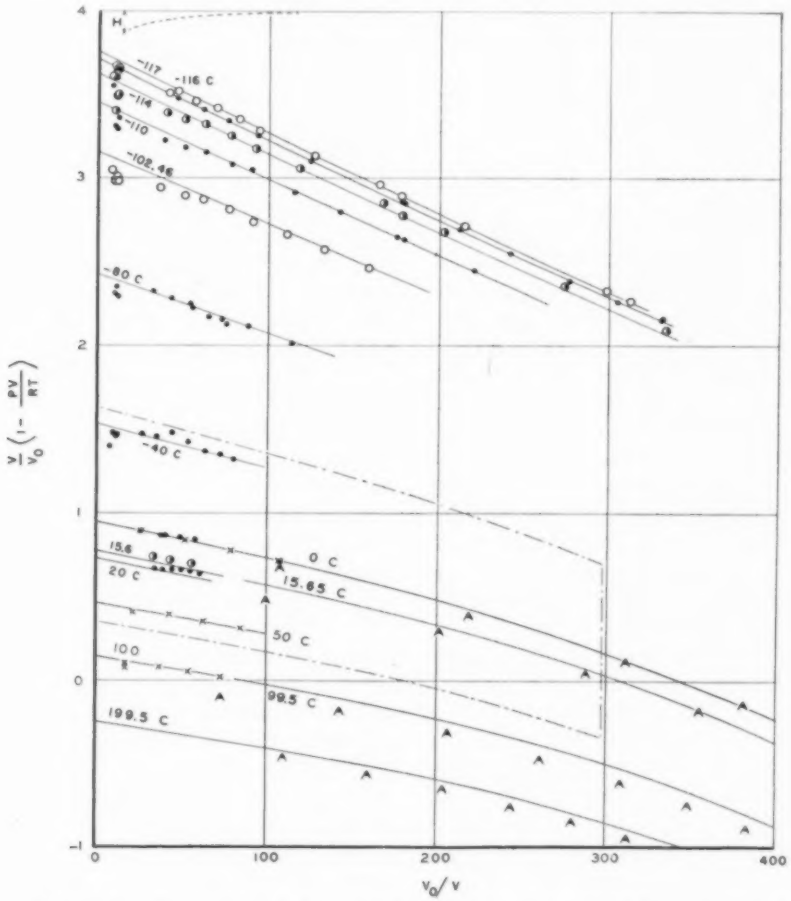

FIGURE 1. *Comparison of observed values with values calculated from equation 1.*

Values observed by Holborn and Otto [4]; various circles, values observed by Onnes et al [5]; A, values observed by Amagat [6]; continuous curves calculated from eq 1; – –, height H between this curve and top of the chart indicates the effect of 0.2 percent error in pressure; – – –, boundary of field covered by table 4.

TABLE 1. *Comparison of values from empirical equation with measurements at Leiden*

Temperature	Number measure	Pressure range	Average deviation
°C		*atm*	*Percent*
−145.39	2	3 to 5	0.10
−137.87	2	5	.08
−124.95	5	3 to 6	.04
−118.58	3	4 to 6	.03
−117.01	4	4 to 6	.11
−116.99	12	20 to 52	.14
−116.01	17	4 to 55	[a].09
−113.97	12	20 to 60	[b].07
−113.94	3	5 to 6	.13
−109.90	3	5 to 7	.09
−109.97	10	20 to 61	.14
−102.49	4	5 to 7	.11
−102.46	8	20 to 60	.23
−80.03	8	21 to 62	.13
−80.00	3	6 to 8	.08
−40.05	7	21 to 61	.09
−70.01	4	6 to 9	.06
−0	5	36 to 54	.05
15.6	3	34 to 56	.17
20	6	34 to 60	.11

[a] One measured value has been excluded. If this value is included the average deviation becomes 0.18%.

[b] Four measured values have been excluded, see text.

ties of 167, 202, 274, and 334, which, according to Leiden Communication 169a, form a complete series of observations (series XXXIII), appear to be even more in error. The relative size of the deviations are such that the error could either be in the temperature or in the calibration of the small end of the piezometer.

(3) The third group of observed data are represented in figure 1 by the letter *A*. A comparison of these data with values calculated from eq 1 are given in table 2. No estimate of their accuracy can be deduced from their precision, since the values given by Amagat were read from smooth curves through the plotted experimental data. However at 100 atm, the values calculated from eq 1 agree with the first groups of data and therefore must be very near the correct value. At this pressure, the deviation from the Amagat data is 0.3 to 0.9 percent. If the Amagat data do not contain errors that increase progressively with the pressure, it seems likely that the pressures calculated from the equation are within 1 or 2 percent of the correct values up to 1,000 atm in the temperature range 0° to 200° C.

There appear to have been no new data on the critical constants for oxygen since the review by

TABLE 2. *Comparison of values from eq 1 with measurements of Amagat*

The body of the table contains the percentage by which the observed pressure exceeds the calculated value.

Pressure	Temperature, °C.				
	0	15.6	15.65	99.5	199.5
atm	*Percent*	*Percent*	*Percent*	*Percent*	*Percent*
100	0.3	.....	0.6	0.9	.....
200	.7	.....	.6	.9	0.4
300	.1	.....	.5	1.0	.6
400	−.5	.....	0	1.9	.8
500	−1.2	.....	−0.4	2.2	1.1
600	−1.5	.....	−.7	2.2	1.2
700	−1.4	.....	−.7	2.4	1.3
800	−0.9	.....	−.7	2.3	1.2
900	−0.4	.....	−.4	2.0	1.1
1,000	0	0.3	.....	1.8	.....
1,200	0.5	.9	.....	.....	.....
1,400	1.1	1.2	.....	.....	.....
1,600	1.9	1.7	.....	.....	.....
1,800	2.5	2.5	.....	.....	.....
2,000	3.3	3.0	.....	.....	.....

Pickering [7]. The critical density as reported is about 301 Amagat units. The critical temperature and pressure reported by Onnes, Dorsman and Holst [8], whose values Pickering chooses, are respectively 154.27° K and 49.71 atm. The pressure calculated from eq 1 at this density and temperature is 48.3 atm., whereas at the same density the calculated temperature corresponding to 49.71 atm. is 154.89° K, and the temperature at which $dp/dV=0$ is 155.27° K. This indicates a higher critical temperature than that reported by Onnes, although too much dependence should not be placed on slopes calculated from eq 1 in the critical region since, with the number of terms used, the equation is not applicable at densities much above those plotted in figure 1.

The measurement by Rossini and Frandsen [9] of the change in internal energy of oxygen between 40 and 0 atm at 28° C gives an excellent check on eq 1. Those authors report 40 (6.51) = 260.4 int j/mole. Through the use of eq 1 and integration of the relation $(\partial E/\partial V)_T = T(\partial p/\partial T)_V - p$, the value 258.8 int j/mole is obtained, which is well within the accuracy claimed for the experimental data.

E. J. Workman [10] has measured in a calorimeter the ratio of the specific heat of oxygen at various pressures up to 130 kg/cm² to the specific heat at 1 atm. A comparative method was used in which the same stream of gas was passed twice

through the calorimeter. Measurements were made at two temperatures, 26° and 60° C, respectively. Through differentiation of eq 1 and assumption that Cp for 1 atm is 7.05 cal/° C mole, the value of this ratio was calculated for the pressure 50 kg/cm.^{2} The third and higher virials were neglected; at the higher pressures it might be necessary to include calculations based on the third virial. The values for the ratio calculated for 26° and 60° C are, respectively, 1.102 and 1.076, whereas Workman gives 1.088 and 1.063, respectively. The cause for this discrepancy of over 1 percent is suggested by Workman's statement [10, p. 1352] as follows: "For example, we can be reasonably certain that in the present apparatus the net heat transfer q arises from an excessive heat conduction along the line leading from the low pressure bath to the heat interchanger." Heat transfer at this place would always be in the direction to yield a low value for the ratio of specific heats.

Equation 1 leads to a value of 94.9×10^{-5} for the second virial coefficient for oxygen at 0° C. This is in very good agreement with C. S. Cragoe's [11] estimate $(95.1\pm0.9)\times10^{-5}$. The value of pV/RT at 0° C and 1 atm derived from eq 1 is therefore $1-94.9\times10^{-5}$, or 0.999051. Cragoe has shown this value to be consistent with measurements at pressures of 1 atm or less. The use of $RT_0=22.4140$ liter atm per mole as given by him leads to a weight of 1.42904 g for the normal liter. This value was chosen by Pickering [12] in his review of the experimental data on the weight of the normal liter.

Equation 1 has been compared with the Beattie Bridgeman equation [13]. The agreement is very close. For unit Amagat density in the temperature range −140° to +200° C, the deviation for pV/RT at the two extreme temperatures is 8 parts in 100,000, this being the maximum deviation. At 0° C, where eq 1 is in agreement with Cragoe's estimated value [11], the Beattie Bridgeman equation gives a value of pV/RT, which is 5 parts in 100,000 smaller. At higher densities, eq 1 is in slightly better agreement with the experimental data.

It may be of interest to note that the value of pV/RT calculated from eq 1 for saturated oxygen vapor at the normal boiling point (−183.0° C) is 0.9713, which is probably as good a value as any now available.

III. Virial Coefficients

Instead of a complete table of pressures over the whole range −200° to +200° C, for which eq 1 might be used, values of the second virial coefficient B are given in table 3 for every 10 deg C, and values of the higher virial coefficients C and D are given graphically for the same temperature range in figures 2 and 3, respectively. These values are for use with the density in Amagat units. If the density in grams per liter is desired,

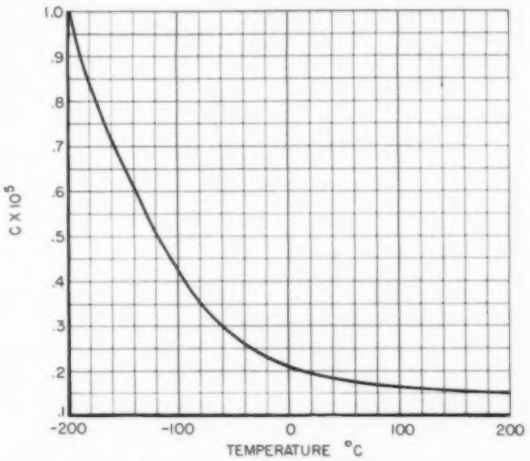

FIGURE 2. *Values of the third virial coefficient C plotted as a function of temperature.*

To be used with densities in Amagat units.

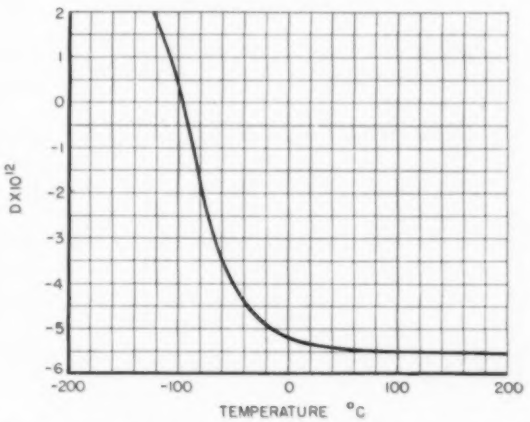

FIGURE 3. *Values of the virial coefficient D plotted as a function of temperature.*

To be used with densities in Amagat units.

the density in Amagat units should be multiplied by the density at 0° C and 1 atm, 1.42904 g/liter.

TABLE 3. *Values of the second virial coefficient B, multiplied by 1,000, for use in eq 1*

(Quadratic interpolation should be used)

Temperature	Temperature, ° C				
	0	10	20	30	40
°C					
−100	−3.0644	−3.4514	−3.8066	−4.4123	−5.0140
−0	−0.9488	−1.0743	−1.2123	−1.3647	−1.5333
0	−.9488	−0.8345	−0.7299	−0.6340	−0.5461
100	−.1420	−.0804	−.0423	+.0027	+.0447
200	+.2488				
	50	60	70	80	90
−100	−5.7225	−6.5648	−7.5774	−8.8112	−10.3388
−0	−1.7208	−1.9299	−2.1642	−2.4278	−2.7247
0	−0.4650	−0.3902	−0.3210	−0.2569	−0.1974
100	.0842	.1213	.1561	.1888	.2197

The quantity pV/RT is dimensionless, and for the left-hand side of the equation, p, V, and T may be in any units as long as the proper value of R is used. If p is in atmospheres, V in Amagat units, and T=° C+273.16, the value of R is 1/(0.999051) (273.16), or 0.00366434.

At low pressures the third and fourth terms are negligibly small, and when the temperature and a pressure not much over 1 atm are given, p/RT may be substituted for $1/V$ in the second term, and

$$pV/RT=1-Bp/RT, \qquad (2)$$

becomes a convenient approximation to eq 1 at such low pressures.

IV. Table and Chart in Engineering Units

In the compressed gas industry, it is customary to express pressures in pounds per square inch, temperatures in degrees Fahrenheit, and densities in units similar to Amagat units, i. e., the ratio of the density at the given condition to the density at 70° F and 1 atm (14.696 lb/in.²). When eq 1 is reduced to these units, the constants represented by letters are

$B_1=-1.74509$ $\qquad B_2=0.0009167$

$C_1=1004.37\times10^{-6}$ $\qquad C_2=1.2280\times10^{-6}$

$D_1=-1513.68\times10^{-12}$ $\qquad D_2=4.1160\times10^{-12}$

$b=150.747/T$ $\qquad T=$°F+459.688

$c=18.163\times10^{6}/T^{3}$ $\qquad R=0.0277631$

$d=2636\times10^{14}/T^{7}$

Table 4 contains pressures that were calculated with the use of these constants in eq 1. Temperatures are given at the ends of the rows; densities are given at the heads of the columns, and pressures in the body of the table. The units are as described in the preceding paragraph except in the third section of the table where a unit of 10 lb/in.² is used to avoid carrying pressures to an unnecessary number of places. An attempt has been made to give a number of decimal places comparable with the accuracy of the experimental data, although some of the values may be given to an extra place.

If the number of pounds mass of gas per cubic foot is desired, the densities in the units given should be multiplied by the density at 70° F and 1 atm, namely 0.082787 lb/ft³. This factor is deduced from three data, namely: (1) the value 0.99933 for pV/RT at 70° F and 1 atm calculated from eq 1, (2) the value 22.4140 liter atm per scale assumed for RT at the ice point, (3) the value 273.16° K assumed for the temperature of the ice point.

The range covered by this table and the extent to which the equation is supported by experimental data in this region is illustrated in figure 3 by an area bounded on the left by the left-hand boundary of the chart, on the right by a vertical dot-dash straight line, and above and below by dot-dash curves.

A chart (fig. 4) has also been prepared that reproduces the data given in table 4 in a form that permits the rapid solution of practical problems. This chart is being printed in a larger size, together with similar charts for nitrogen and hydrogen and with instructions for their use, as Bureau Miscellaneous Publication M191. The coordinates of the chart are $Z=pV/RT$ versus pressure.

On this chart, figure 4, pressures are expressed in pounds per square inch absolute and temperatures in degrees Fahrenheit. Densities are expressed as the ratio of the density at the specified condition to that calculated from the equation for 70° F and 1 atm., i. e., 0.082787 lb/ft³. Readings from the chart indicate that it is drawn to represent the equation within 5 lb/in.² and within 0.0005 for the value of pV/RT. The quantity

TABLE 4. *Absolute pressures for oxygen at various temperatures and densities*

Densities referred to the density at 70° F and 1 atm as unity; density at 70° F and 1 atm=0.082787 lb/ft.³

Temperature	UNIT OF PRESSURE, 1 PSI ABSOLUTE FOR DENSITIES (V_{70}/V)—										
	1	10	20	30	40	50	60	70	80	90	100
°F											
−70	11.3570	112.04	220.79	326.4	429.1	528.9	626.1	720.9	813.3	903.6	991.9
−60	11.6353	114.88	226.62	335.3	441.2	544.5	645.2	743.5	839.7	933.8	1,026.2
−50	11.9136	117.73	232.43	344.3	453.4	560.0	664.1	766.1	866.0	964.0	1,060.3
−40	12.1919	120.57	238.24	353.2	465.5	575.4	683.1	788.7	892.3	994.1	1,094.4
−10	12.4701	123.41	244.05	362.1	477.7	590.9	702.0	811.2	918.5	1,024.2	1,128.4
0	12.7484	126.25	249.86	371.0	489.8	606.4	720.9	833.7	944.7	1,054.2	1,162.4
10	13.0266	129.09	255.66	379.9	501.9	621.8	739.8	856.1	970.9	1,084.1	1,196.2
20	13.3049	131.93	261.46	388.7	513.9	637.2	758.7	878.5	996.9	1,114.0	1,230.0
30	13.5832	134.76	267.25	397.6	526.0	652.6	777.5	900.9	1,022.9	1,143.8	1,263.7
40	13.8614	137.60	273.04	406.5	538.0	667.9	796.3	923.2	1,048.9	1,173.6	1,297.4
50	14.1396	140.43	278.83	415.3	550.0	683.3	815.0	945.5	1,074.9	1,203.3	1,331.0
60	14.4178	143.26	284.61	424.2	562.1	698.6	833.7	967.8	1,100.8	1,233.0	1,364.5
70	14.6960	146.10	290.39	433.0	574.1	713.9	852.5	990.0	1,126.6	1,262.6	1,398.0
80	14.9742	148.93	296.17	441.9	586.1	729.2	871.1	1,012.2	1,152.4	1,292.1	1,431.4
90	15.2524	151.77	301.94	450.7	598.1	744.5	889.8	1,034.3	1,178.2	1,321.6	1,464.8
100	15.5305	154.60	307.71	459.5	610.1	759.7	908.4	1,056.5	1,204.0	1,351.1	1,498.1
110	15.8087	157.43	313.48	468.3	622.1	775.0	927.1	1,078.6	1,229.7	1,380.5	1,531.3
120	16.0869	160.26	319.25	477.1	634.1	790.2	945.7	1,100.7	1,255.4	1,409.9	1,564.5
130	16.3650	163.09	325.02	485.9	646.0	805.4	964.2	1,122.7	1,281.0	1,439.2	1,597.7
140	16.6432	165.92	330.78	494.7	658.0	820.6	982.8	1,144.7	1,306.6	1,468.5	1,630.7
150	16.9213	168.74	336.53	503.5	669.9	835.8	1,001.3	1,166.7	1,332.2	1,497.8	1,663.8

Temperature	110	120	130	140	150	160	170	180	190	200	210
−50	1,078.5	1,163.5	1,247.0	1,329	1,411	1,491	1,572	1,651	1,731	1,811	1,891
−40	1,116.8	1,206.1	1,293.9	1,381	1,467	1,552	1,637	1,722	1,807	1,892	1,977
−30	1,155.1	1,248.6	1,340.8	1,432	1,523	1,613	1,703	1,792	1,882	1,972	2,063
−20	1,193.3	1,290.9	1,387.6	1,483	1,579	1,673	1,768	1,862	1,957	2,053	2,149
−10	1,231.4	1,333.2	1,434.1	1,534	1,634	1,734	1,833	1,932	2,032	2,133	2,235
0	1,269.4	1,375.4	1,480.6	1,585	1,690	1,794	1,898	2,002	2,107	2,213	2,320
10	1,307.3	1,417.5	1,527.0	1,636	1,745	1,854	1,962	2,072	2,182	2,293	2,405
20	1,345.1	1,459.4	1,573.3	1,687	1,800	1,913	2,027	2,141	2,257	2,373	2,490
30	1,382.8	1,501.3	1,619.4	1,737	1,855	1,973	2,092	2,211	2,331	2,452	2,575
40	1,420.5	1,543.2	1,665.5	1,788	1,910	2,033	2,156	2,280	2,405	2,532	2,660
50	1,458.1	1,584.9	1,711.4	1,838	1,965	2,092	2,220	2,349	2,479	2,611	2,744
60	1,495.6	1,626.5	1,757.2	1,888	2,019	2,151	2,284	2,418	2,553	2,690	2,828
70	1,533.1	1,668.0	1,803.0	1,938	2,074	2,210	2,348	2,486	2,626	2,768	2,912
80	1,570.5	1,709.5	1,848.7	1,988	2,128	2,270	2,412	2,555	2,700	2,847	2,996
90	1,607.8	1,750.9	1,894.3	2,038	2,183	2,328	2,475	2,623	2,773	2,925	3,080
100	1,645.0	1,792.2	1,939.8	2,088	2,237	2,387	2,539	2,692	2,847	3,004	3,163
110	1,682.2	1,833.5	1,985.2	2,138	2,291	2,446	2,602	2,760	2,920	3,082	3,247
120	1,719.3	1,874.6	2,030.6	2,187	2,345	2,504	2,665	2,828	2,993	3,160	3,330
130	1,756.4	1,915.7	2,075.8	2,237	2,399	2,563	2,728	2,896	3,066	3,238	3,413
140	1,793.4	1,956.7	2,121.0	2,286	2,453	2,621	2,791	2,963	3,139	3,315	3,496
150	1,830.3	1,997.7	2,166.1	2,336	2,507	2,679	2,854	3,031	3,211	3,393	3,578

TABLE 4. *Absolute pressures for oxygen at various temperatures and densities*—Continued

	UNIT OF PRESSURE, 10 PSI ABSOLUTE, FOR DENSITIES (V_{70}/V)—										
	220	230	240	250	260	270	280	290	300	310	320
−50	197.1	205.3	213.6	222	231	240	249	258	267	278	288
−40	206.3	215.1	223.9	233	242	252	261	271	282	293	304
−30	215.5	224.8	234.3	244	254	264	274	285	296	308	319
−20	224.6	234.5	244.6	255	265	276	287	298	310	322	335
−10	233.8	244.2	254.8	266	277	288	300	312	324	337	350
0	242.8	253.9	265.0	276	288	300	312	325	338	352	366
10	252.0	263.5	275.3	287	300	312	725	339	352	367	381
20	261.0	273.1	285.4	298	311	324	338	352	366	381	397
30	270.0	282.7	295.6	309	322	336	350	365	380	396	412
40	279.0	292.2	305.7	319	334	348	363	378	394	411	427
50	288.0	301.8	315.8	330	345	360	376	391	408	425	443
60	296.9	311.3	325.9	341	356	372	388	405	422	440	458
70	305.9	320.8	335.9	351	367	384	400	418	436	454	473
80	314.8	330.2	346.0	362	379	396	413	431	449	469	488
90	323.7	339.7	356.0	373	390	407	425	444	463	483	504
100	332.6	349.1	366.0	383	401	419	438	457	477	497	519
110	341.4	358.5	376.0	394	412	431	450	470	491	512	534
120	350.3	367.9	385.9	404	423	443	463	483	504	526	549
130	359.1	377.3	395.9	415	434	454	475	496	518	541	564
140	367.9	386.7	405.8	425	446	466	488	509	532	555	579
150	376.7	396.0	415.7	436	457	478	500	522	545	569	594

pV/RT or Z is independent of the units of p, V, and T as long as the appropriate value of R is used. The value of Z at 70° F and 1 atm is 0.99933; at 32° F and 1 atm, 0.999051. For the units given in the chart, the value of R is 0.0277631. RT is then 0.0277631 (° F+459.69). The use of the chart is best illustrated by the following example:

An oxygen cylinder of 1.528 ft³ internal volume is designed to be filled at 70° F to a gage pressure of 2,000 lb/in.².

a. To what pressure may it be filled at 60° F?

b. If properly filled, what will the pressure be if the temperature of the tank should rise to 130° F?

c. How many cubic feet of oxygen under the standard condition of 1 atm and 70° F, will the cylinder deliver, and what weight will be delivered?

d. At 70° F what will the pressure be after 100 ft³ have been delivered?

Solution:

(a) For the purpose of reading on the chart, we may assume that 2,000 lb/in.² gage is equivalent to 2,015 lb/in.² abs. The point on the chart at 70° F and 2,015 lb/in.² abs corresponds to a density of 145.5 and to a value of Z or pV/RT of 0.9415. If we follow the line of constant density for 145.5 down to 60° F, the pressure read directly from the chart is 1,960 lb/in.² abs, or 1,945 lb/in.² gage, i.e. the filling pressure at 60° F. For a more accurate estimate of the filling pressure, we note that at the same point on the chart the value of Z or pV/RT is 0.9335. We now have at 70° F, $p_1V/RT_1=2015V_1/R(70+459.69)=0.9415$, and at 60° F, $p_2V_2/R(60+459.69)=0.9335$. Since $V_1=V_2$, this leads to $p_1T_2/p_2T_1=0.9415/0.9335$ or $p_2=2015(519.69)0.9335/529.69(0.9415)=1960.2$ lb/in.² abs or 1945.2 lb/in.² gage. The direct reading on the chart is in this case in agreement with the more accurate calculated value, although an error in the direct reading as large as 5 lb/in.² may be expected.

(b) If we follow the line of constant density for 145.5 up to 130° F, the pressure read directly from the chart is 2,330 lb/in.² abs.

(c) The number of cubic feet under standard conditions in the tank=145.5(1.528)=222.3 ft

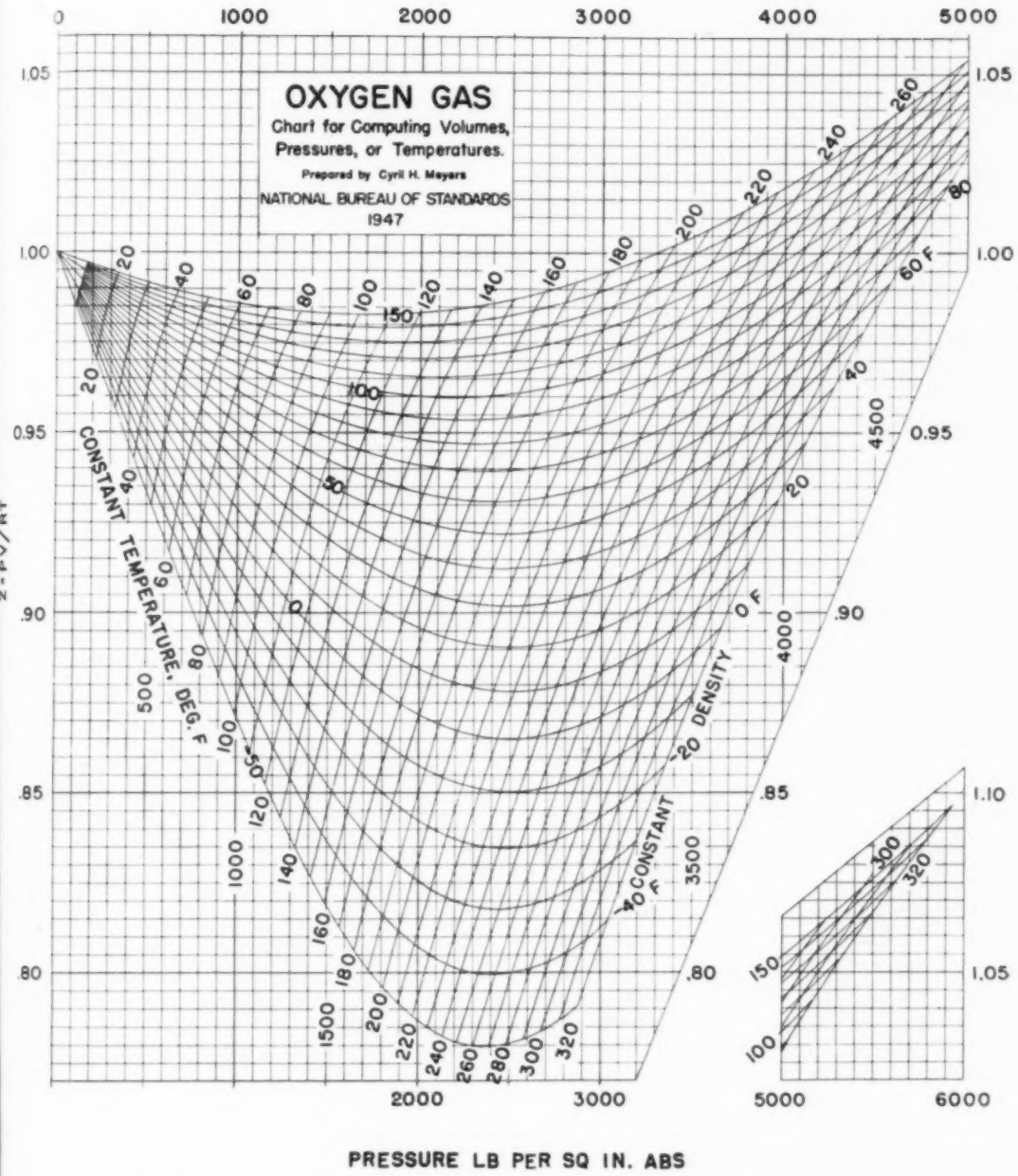

FIGURE 4. *Chart of PVT for oxygen in the temperature range −50° to +150° F.*

The number of cubic feet delivered is 222.3−1.528=220.8 ft³. The weight delivered is 220.8×0.082787=18.28 lb.

(d) After 100 ft.³ have been delivered, the density in the tank is 122.3/1.528=80.0. At this density and 70° F, the pressure read directly from the chart is 1,130 lb/in.² abs.

V. References

[1] R. W. Millar and John D. Sullivan, Bur. Mines Tech. Pap. 424 (1928).

[2] R. B. Scott, Cyril H. Meyers, Robert D. Rands, Jr., Ferdinand G. Brickwedde, and Norman Bekkedahl, J. Research NBS **35,** 39 (1945) RP1661.

[3] International Critical Tables, **3,** 8 and 9 (McGraw-Hill Book Co. Inc., New York, N. Y., 1926).

[4] L. Holborn and J. Otto, Z. Physik. **10,** 367 (1922).

[5] C. A. Crommelin, J. P. Martinez, and H. K. Onnes, Proc. Roy. Acad. Sci. Amsterdam **22,** 108 (1920); Leiden Comm. No. 154a (1918); H. K. Onnes and C. A. Crommelin, Proc. Roy. Acad. Sci. Amsterdam **18,** 515 (1915); Th van Urk & P. G. Nijhoff, Proc. 4th Int. Cong. Refrig. **1,** 65a and 73a (1924); or Leiden Comm. No. 169a and 169c (1924).

[6] E. H. Amagat, Ann. chim. phys. **29,** 68 (1893).

[7] S. F. Pickering, J. Phys. Chem. **28,** 97 (1924).

[8] H. K. Onnes, C. Dorsman, and G. Holst, Proc. Roy. Acad. Sci. Amsterdam **17,** 950 (1915); or Leiden Comm. No. 145b.

[9] Frederick D. Rossini and Mikkel Frandsen, BS J. Research **9,** 733 (1932) RP 503.

[10] E. J. Workman, Phys. Rev. **37₂,** 1,345 (1931).

[11] Carl S. Cragoe, J. Research NBS **26,** 495 (1941) RP1393.

[12] S. F. Pickering, BS Sci. Pap. **21,** 141 (1926) S529.

[13] J. A. Beattie and O. C. Bridgeman, J. Am. Chem. Soc. **50,** 3,136 (1928).

WASHINGTON, January 26, 1948.

U. S. Department of Commerce
National Bureau of Standards

Research Paper RP1892
Volume 40, June 1948

Part of the Journal of Research of the National Bureau of Standards

Reduction of Sphero-Chromatic Aberration in Catadioptric Systems[1]

By Robert E. Stephens

Schmidt and Maksutov catadioptric systems suffer from sphero-chromatic aberrations that are of opposite sign. By the use of a hybrid system, whose corrector is a deep-meniscus lens with an aspheric curve on the external surface, the sphero-chromatic residuals have been reduced and, as a consequence, usuable relative apertures have been increased.

Some time ago a Maksutov camera system of large relative aperture was designed at the National Bureau of Standards for the purpose of ascertaining whether or not such a system, employing as it does only spherical surfaces, could be used to replace a Schmidt system for certain purposes. It was found that the residual zonal spherical aberration was so large that the system was unsatisfactory. On further analysis, however, it was found that the residual sphero-chromatic aberration of the Maksutov system was opposite in sign to that of a comparable Schmidt system and of about the same magnitude. This suggested that a hybrid system, partially corrected by an aspheric surface and partially by a deep meniscus lens, would suffer substantially less from sphero-chromatic aberration than either the Schmidt or the Maksutov type. Such has indeed been found to be the case.

A hybrid Maksutov-Schmidt system consisting of a correcting plate, plane on one side, placed with its vertex at the center of the concave mirror, and a meniscus achromatic lens properly placed, could presumably be designed that would be as free from coma as the best of either of the original types. This has not been attempted by the author. Instead, several systems have been designed in which the aspheric surface is applied to the side of the meniscus lens away from the mirror.

The chromatic aberration of either a Schmidt or a Maksutov system results from the variation of correction for spherical aberration with index of refraction of the correcting plate or meniscus lens. In either of these systems the variation of spherical correction is preponderantly due to changes of the third order spherical aberration of the correcting plate or lens. In a Schmidt system the spherical aberration is perfectly corrected for one wavelength. At other wavelengths there exists simple spherical aberration, undercorrected for longer wavelengths and overcorrected for shorter wavelengths. In a Maksutov system the situation is reversed. Superimposed upon the zonal spherical aberration, which is the best that can be accomplished by the meniscus lens, is overcorrection of spherical aberration at longer wavelengths and under correction at shorter wavelengths. Because of the large angles of incidence existing at the surfaces of the lens in this type system, aberrations of higher order are present to a greater extent than in the Schmidt system, but the differences over a small range of wavelengths are still predominantly of the third order.

For the first trial it was intended to design a system with a relative aperture of $f/0.7$, which would be achromatic at $f/1.0$. However, because of the effect of the corrector upon the equivalent focal length, the achromatic zone turned out to be at $f/0.89$. A first radius and a suitable thickness were assumed for the corrector. The second radius was then given the value that resulted in achromatism at the selected zone. Rays were then traced through the system at the most important wave length and the condition of the spherical aberration determined. Different values were assumed for the first radius until a system

[1] This work has been sponsored by the Bureau of Ships, Navy Department.

of the Maksutov type was found in which the marginal longitudinal spherical aberration was about half that for the uncorrected mirror.

The first surface was then replaced by an aspheric surface [2] such that the optical path lengths for the principal wavelength from all points of an incident plane wave to the chosen focus were made equal. The chosen focus was that corresponding to the ray of the principal wavelength through the achromatic zone of the tentative spherical surface. The resulting aspheric surface is tangent to the tentative surface at the achromatic zone.

The system was then analyzed for residual chromatic aberration by tracing rays at the extreme wavelengths through the system. The longitudinal displacements, from the focus of the rays of the most important wavelength, are shown graphically as a function of height of incidence in figure 2. This should be compared with a similar graph for a Schmidt system of somewhat smaller relative aperture ($f/0.83$) shown in figure 1. The improvement is obviously considerable in spite of the larger relative aperture of the hybrid system.

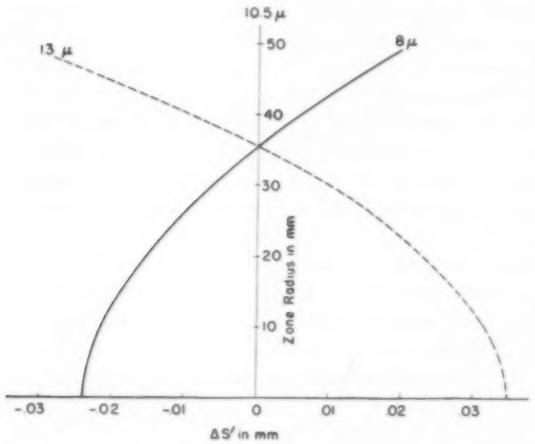

FIGURE 1. *Spherical aberration curves for a Schmidt camera system.*

Equivalent focal length = 83.56 mm.

Although the improvement over previous systems is considerable, the balance of the residual spherochromatic aberration is not optimum. This optimum condition would be attained if the

[2] It is not the purpose of this paper to describe the methods used to compute aspheric surfaces. The procedures used were similar to the exact method of F. A. Lucy, J Opt. Soc. Am. **38**, 251 (1940); and, for finite object distances, H. S. Friedman, J. Opt. Soc. Am., **37**, 480 (1947).

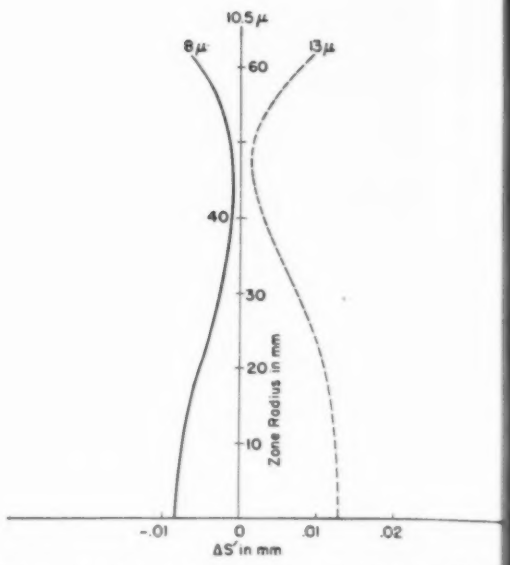

FIGURE 2. *Spherical aberration of first Schmidt-Maksutov hybrid.*

Equivalent focal length = 88.68 mm.

best focus (in the presence of residual aberration) for each of the extreme wavelengths could be made to coincide with the perfect focus of the principal wavelength. If this is impossible, the next best adjustment would be such that the focal ranges [3] for the extreme wavelengths overlap. Accordingly, further trials were made.

In succeeding designs the second radius of the corrector was so chosen that modest overcorrection of chromatic aberration was obtained at the selected zone. Then, when the aspheric surface had been substituted for the tentative first surface, correction of the type illustrated in figure 3 resulted. The residual optical path differences, at the focus of the principal wavelength, were less than one-tenth wavelength for the extreme wavelengths. The coma of the system, as indicated by its maximum offense against the sine theorem of 0.007, is greater than would usually be tolerated but was quite satisfactory for the purpose at hand. Figure 4 shows a drawing of this system.

The systems designed by the author were all for use in the infra-red region between 8μ and 13μ, 10.5μ being chosen as the principal wavelength

[3] A discussion of the "focal range" is given in Glazebrook, Dictionary of applied physics, in the section on the optics of the microscope (written by Conrady), **IV**, 221.

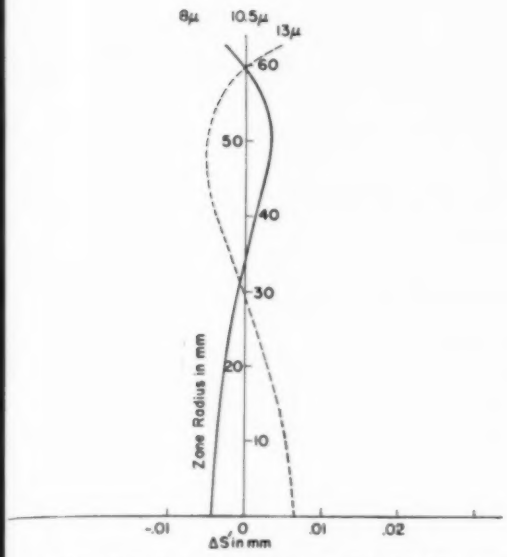

FIGURE 3. *Spherical aberration of Schmidt-Maksutov hybrid in which almost optimum balance of residual spherochromatic aberration has been achieved.*

Equivalent focal length=89.66 mm.

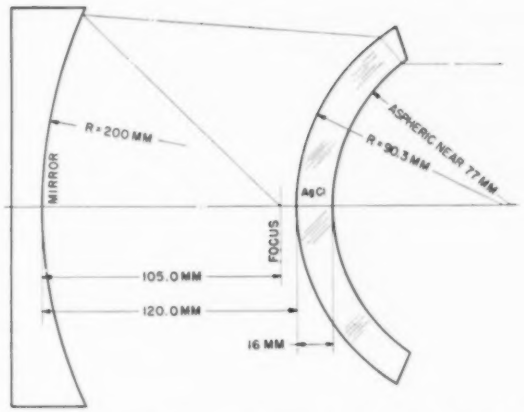

FIGURE 4. *System whose aberrations are shown in figure 3.*

The principles involved in the reduction of the residual spherochromatic aberration should, however, apply equally well to systems for use in the visible or any other spectral range.

WASHINGTON, December 19, 1948.

U. S. Department of Commerce
National Bureau of Standards

Research Paper RP1893
Volume 40, June 1948

Part of the Journal of Research of the National Bureau of Standards

Some Energy Relations in the Systems PbO-B_2O_3 and PbO-SiO_2

By Leo Shartsis and Edwin S. Newman

Heats of solution of a series of glasses in the system PbO-B_2O_3 were measured in 2 *N* nitric acid with a simple vacuum-bottle calorimeter. Heats of solution of a series of glasses in the system PbO-SiO_2, ranging in composition from 6 to 35 percent of SiO_2, were measured in a mixture of HF and 2.5 *N* nitric acid with an electrically calibrated isothermal-jacket calorimeter. From these data, and heats of fusion available in the literature, calculations were made of the heats of reaction of the component oxides in either amorphous or crystalline states in forming glasses in these systems.

I. Introduction

The heat accompanying the glass-forming reactions is of interest to the physical chemist studying glass. Its significance lies in the fact that a knowledge of the energy changes accompanying glass formation should ultimately lead to a better understanding of the glassy state. The heat of glass formation is of practical importance, because it is one of the factors needed in evaluating the efficiency of glass-melting furnaces.

The direct measurement of the heat accompanying the reaction of components to form a glass is very difficult, if not impossible, because the reaction takes place at elevated temperatures and is often very sluggish. For this reason, indirect measurements were made by use of a heat-of-solution method. The reactants were dissolved in a suitable solvent and the heat of solution determined. The finished glass was dissolved in the same solvent in such an amount that its solution was identical with that resulting from the solution of the reactants. The difference between the heat of solution of the reactants and that of the finished glass was the desired heat of reaction. As the calorimetric procedure was conducted near room temperature, the heats of reaction so determined were at room temperature (approximately 25° C). The heats of reaction at elevated temperatures may be calculated from such data combined with the specific heats of the reactants and product over the desired temperature range.

II. The System PbO-B_2O_3

1. Preparation of Glasses

Two series of glasses were used in this study. The first was made specifically for heat-of-solution measurements; the second was made for another project, and portions remaining from that work were used to make additional heat-of-solution measurements. The two series were prepared in essentially the same manner, but details varied somewhat. Only the preparation of the first series will be described.

The raw materials used in melting the glasses were boric acid and PbO [1] of reagent quality. Fifty-gram batches were melted in platinum crucibles heated in an electric muffle to not less than 800° C. For melts high in B_2O_3, temperatures as high as 950° C had to be used. During melting the glasses were homogenized by frequent stirring with a platinum wire mounted at the end of a long glass tube. For very fluid melts (those high in PbO), the mixing was aided by shaking the crucible and moving it with a swirling motion. When it appeared homogeneous the melt was quickly poured onto a clean steel plate. Each glass was ground to pass a No. 60 sieve, well-mixed and remelted.

Glasses containing more than 92 percent of PbO could not be obtained because of crystalliza-

[1] An X-ray pattern made by H. F. McMurdie indicated that this material was litharge, the β or low-temperature form.

tion. Geller and Bunting [1][2] obtained clear glasses containing as much as 94.5 percent of PbO, but they prepared much smaller quantities of material and used a more efficient quenching system.

2. Heat Treatment and Chemical Analysis

Most of the glasses were annealed by heating to 20° C or 30° C below their deformation temperatures [1] for an hour and then cooling very slowly. The heat of solution of a strained glass may be expected to be higher than that of the same glass after annealing. However, the method used was not sufficiently sensitive to detect this difference. Therefore, the remaining glasses were not annealed.

The glasses were analyzed for PbO. The PbO content was determined as the sulphate by several evaporations with HF and H_2SO_4 and heating at 500° to 550° C to constant weight.

3. Calorimetric Materials, Apparatus, and Procedure

A quantity of 2.00 *N* nitric acid was prepared from chemically pure acid and distilled water. About 500 g of analytical reagent grade ZnO was heated for 1 hour at 900° to 950° C, cooled, and ground to pass a No. 100 sieve and stored in a well-stoppered reagent jar. This material was used to determine the effective heat capacity of the vacuum-bottle calorimeter.

Most of the heat-of-solution determinations were made with a simple vacuum-bottle calorimeter [2]. As can be seen (fig. 1), it consists of a wide-mouthed Thermos flask in a container of insulating material. Inserted through holes in the cork stopper are a two-bladed glass stirrer, a Beckmann thermometer, and a glass funnel through which the charge is introduced into the calorimeter. A paper disk marked with six equally spaced broad radial lines was glued to the top of the horizontal member of the friction drive, and a 3-neon bulb (not shown) was used to illuminate it. When the stirrer is operated at a speed of 600 rpm, the lines appear stationary. At higher speeds the lines appear to move in the same direction as the stirrer, whereas at speeds lower than 600 rpm they appear to move in the reverse direction. A speed-adjusting screw permits the speed to be maintained approximately constant.

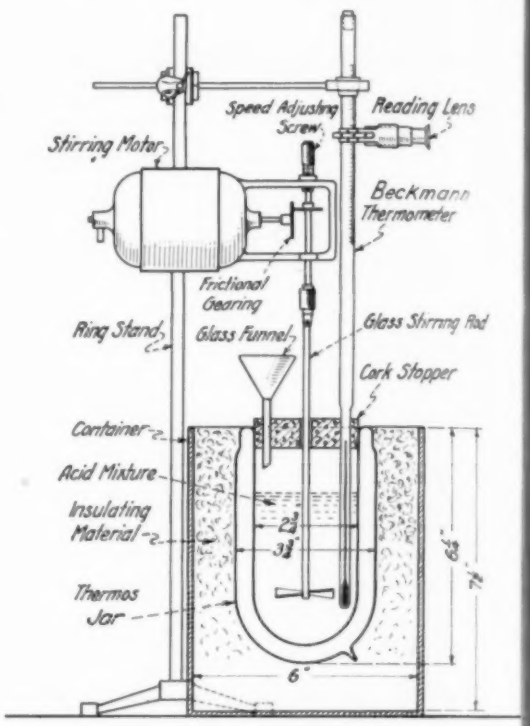

FIGURE 1. *Vacuum-bottle calorimeter.*

As ZnO was used to measure the heat capacity of the calorimeter, its heat of solution in 2.00 *N* HNO_3 was determined with an electrically calibrated calorimeter, which will be described later. As a check on the vacuum-bottle calorimeter, the heats of solution of crystalline PbO and of two PbO-B_2O_3 glasses were also determined with this apparatus.

4. Procedure and Calculations

The acid charge consisted of 425 ± 0.05 g of 2.00 *N* nitric acid. Its temperature was adjusted to 2 or 3 degrees below room temperature before introduction into the calorimeter, so that the initial temperature indicated by the Beckmann thermometer would be at the lower portion of its

[2] Figures in brackets indicate the literature references at the end of this paper.

scale. After the calorimeter was assembled a stirring period of not less than 10 minutes was allowed. The reading of the Beckmann thermometer was then recorded, the clock started, and the sample (powdered to pass a No. 100 sieve) introduced as uniformly as possible in not less than 1 minute or more than 2 minutes. Temperature readings were taken every 5 minutes until the rate of temperature change of the calorimeter was constant for at least three 5-minute intervals. Experiments showed that with a properly designed stirrer and an adequate stirring rate, complete solution was attained in 20 minutes, so that in general the total time of the experiment was 40 minutes, of which the last 20 were used as a rating period.

The calculation of the final temperature was made by extrapolating the constant rate of temperature change of the calorimeter during the rating period back to zero time. The "final" temperature so calculated minus the initial temperature of the calorimeter was taken as the temperature rise of the calorimeter caused solely by the energy evolved by the reaction of the sample with the acid. This corrected temperature rise of the calorimeter was converted to an energy change by multiplying it by the effective heat capacity of the calorimeter and its contents. The errors inherent in such a method of calculation are approximately the same in both heat-of-solution determinations and in the effective heat-capacity determinations and thus tend to compensate each other.

To determine the effective heat capacity of the calorimeter, a heat-of-solution experiment with ZnO as the sample was made. The known heat[3] evolved by ZnO $[-256.9+0.1(T-24)]$ cal/g, T=temperature in deg C—previously determined with an electrically calibrated calorimeter, when divided by the observed temperature rise yielded the heat capacity of the calorimeter. Since the isothermal heat of solution of ZnO varies with temperature, the value at the final temperature of the calibration was used. The effective heat capacity obtained was thus that of the calorimeter and the reactants, i. e., the ZnO and the acid. For subsequent experiments with glasses or oxide mixtures, their heat capacities were substituted for that of the ZnO in the value obtained for the calibration.

The solid material introduced into the calorimeter was at room temperature, which was higher than the initial temperature of the calorimeter. Account was taken of the sensible heat thus carried into the apparatus. This heat is given by the formula $C_s\ (T_R-T_O)$, where C_s is the heat capacity of the solid, T_R is the temperature of the room, and T_O is the initial temperature of the calorimeter. In the determination of effective heat capacity, this amount of heat must be added to that developed by the reaction of the zinc oxide and acid to obtain the total heat input into the calorimeter. For the heat-of-solution measurements, this amount of heat must be deducted from the total heat measured to obtain the quantity solely due to the reaction of the sample with the acid.

5. Data and Discussion

Table 1 gives the data obtained, and figure 2 shows them in graphical form. As the heats of solution of the first two mixtures of PbO (crystal)

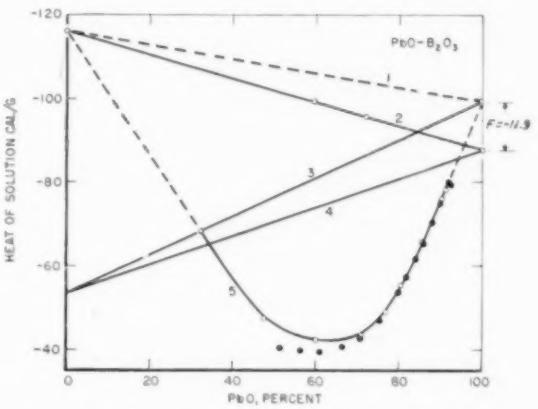

FIGURE 2. *Heats of solution in the system* $PbO\text{-}B_2O_3$.

Mixtures of PbO (gls) and B_2O_3 (gls) (curve 1); mixtures of PbO (c) and B_2O_3 (gls) (curve 2); mixtures of PbO (gls) and B_2O_3 (c) (curve 3); mixtures of PbO (c) and B_2O_3 (c) (curve 4); PbO-B_2O_3 glasses (curve 5). Open circles (except 0 percent of PbO) represent values obtained with 10-g samples; closed circles represent values obtained with samples of 18 to 25 g. The difference between the heat of solution of PbO (gls) and PbO (c), represented by F, is the heat of fusion of PbO at room temperature.

[3] The calory defined as 4.1840 abs J is used in this paper. According to convention, heat evolved is negative.

TABLE 1. *Heats of solution in the system* PbO-B_2O_3

Substance	Vacuum-bottle calorimeter			Precision calorimeter		
	Percentage of PbO	Heat of solution [1,2,3]	Number of determinations	Approximate weight of sample	Heat of solution	Number of determinations
FIRST SERIES						
B_2O_3(c)	0.0	[4] −53.5				
B_2O_3(gls)	.0	−116.1	1	2.25		
Glass	[5] 32.3	−68.3	1	10		
Do	47.5	−47.3	2	10		
Do	59.9	−42.4	3	10		
Do	70.9	−43.5	1	10		
Do	76.8	−49.0	1	10		
Do	80.4	−55.5	5	10	−55.2	1
Do	85.4	−65.7	3	10		
Do	90.1	−76.1	4	10		
Do	91.1	−78.1	2	10		
Do	92.5				−79.3	1
Lithargite	100 (c)	−87.6	4	10	−87.7	2
Oxide mixtures:						
B_2O_3(gls)+PbO(c)	59.6	−99.5	1	10		
Do	72.1	−96.0	1	10		
SECOND SERIES						
Glass	51.3	−40.2	1	18		
Do	56.2	−39.8	2	18		
Do	61.0	−39.4	1	20		
Do	66.5	−40.6	1	20		
Do	70.7	−42.8	2	23		
Do	75.5	−47.1	1	20		
Do	79.9	−53.7	1	20		
Do	82.1	−57.4	2	25		
Do	84.1	−61.7	1	20		
Do	86.0	−65.5	2	25		
Do	88.0	−70.2	2	20		
Do	89.8	−74.9	2	20		
Do	91.9	−79.8	2	23		
Do	[6] 100(gls)	−99.5				

[1] 1 calory=4.1840 abs j.
[2] According to convention, heat evolved is negative.
[3] In 2.60 *N* HNO_3.
[4] Calculated. J. C. Southard, J. Am. Chem. Soc. **63**, 3147 (1941).
[5] Average composition of two immiscible glasses.
[6] Extrapolated.

plus B_2O_3 (glass) tested fell on a straight line between the end members, no other determinations of oxide mixtures were made.

A curve (5, fig. 2) was fitted to the heats of solution of the first series of glasses. The heats of solution of the second series (solid circles in fig. 2) were somewhat lower than those of the first series because the amounts of sample dissolved in the latter were about twice as great as in the former, thus causing the final concentration to be different.

The heats of solution of glasses having high percentages of PbO seemed to be linear with the weight percent of PbO. The equation of a line was fitted by the method of least squares to the data obtained with the vacuum-bottle calorimeter on glasses containing more than 85 percent of PbO. The value at 100 percent of PbO obtained from the equation of this line was −99.5 cal/g. Since the average vacuum-bottle value of the heat of solution of PbO (c) was −87.6 cal/g, the heat of fusion of PbO (c) at room temperature calculated from these data is +11.9 cal/g.

The value for the heat of solution of B_2O_3 (c) was taken as −53.5 cal/g, the difference between the heat of solution of glassy B_2O_3 (−116.1 cal/g) and the heat of crystallization of B_2O_3 (c) at room temperature (−62.6 cal/g [3]). Straight lines were drawn between the values for the heats of solution of B_2O_3 (gls) and PbO (gls), curve 1; B_2O (gls) and PbO (c), curve 2; B_2O_3 (c) and PbO (gls), curve 3; and B_2O_3 (c), and PbO (c), curve 4. These lines represent the heats of solution of mixtures of the oxides. These data, together with the heats of solution of the glasses, enable a calculation to be made of the heats accompanying the following four reactions at approximately 25° C:

$$x\mathrm{PbO(gls)}+(1-x)\mathrm{B_2O_3(gls)}=x\mathrm{PbO}.(1-x)\mathrm{B_2O_3(gls)}+\Delta H_1 \quad (1)$$

$$x\mathrm{PbO(c)}+(1-x)\mathrm{B_2O_3(gls)}=x\mathrm{PbO}.(1-x)\mathrm{B_2O_3(gls)}+\Delta H_2 \quad (2)$$

$$x\mathrm{PbO(gls)}+(1-x)\mathrm{B_2O_3(c)}=x\mathrm{PbO}.(1-x)\mathrm{B_2O_3(gls)}+\Delta H_3 \quad (3)$$

$$x\mathrm{PbO(c)}+(1-x)\mathrm{B_2O_3(c)}=x\mathrm{PbO}.(1-x)\mathrm{B_2O_3(gls)}+\Delta H_4, \quad (4)$$

n which x and $(1-x)$ are the grams of the appropriate oxide necessary to make 1 g of glass and ΔH_1, etc., the heats of glass formation, are variables dependent upon x. These calculations were made by subtracting the heats of solution of the glasses from those of the appropriate oxide mixtures on the assumption that the heat of solution of the mixtures is a linear function of the heats of solution of the component oxides. The results are shown graphically in figure 3. The two curves where PbO (gls) is one of the reactants are hypothetical, because glassy PbO at room temperature is as yet unknown. Table 2 gives values of heats of reaction at such intervals that linear interpolation may be used.

ABLE 2. *Heats of glass formation at room temperatures (approximately 25° C) from oxides in the system* PbO-B_2O_3

Product (glass) percentage of PbO	Reactants			
	$PbO(gls)+B_2O_3(gls)$	$PbO(c)+B_2O_3(gls)$	$PbO(gls)+B_2O_3(c)$	$PbO(c)+B_2O_3(c)$
	Heat of reaction, cal/g of product [1 2]			
	ΔH_1	ΔH_2	ΔH_3	ΔH_4
0	0	0	[3] +62.6	[3] +62.6
5	(−6.6)	(−6.0)	(+52.9)	(+53.5)
10	(−13.1)	(−11.9)	(+43.2)	(+44.4)
15	(−19.7)	(−17.9)	(+33.5)	(+35.3)
20	(−26.2)	(−23.8)	(+23.9)	(+26.3)
25	(−32.8)	(−29.9)	(+14.1)	(+17.1)
30	−39.4	−35.9	+4.4	+8.0
35	−46.0	−41.8	−5.3	−1.1
40	−52.7	−48.9	−15.1	−10.3
45	−58.8	−53.5	−24.4	−19.0
50	−62.3	−57.3	−31.0	−25.0
55	−63.7	−57.1	−35.5	−29.0
60	−63.7	−56.6	−38.7	−31.6
65	−63.2	−55.5	−41.3	−33.6
70	−61.2	−52.9	−42.4	−34.1
75	−56.9	−47.9	−41.2	−32.3
80	−48.3	−38.8	−35.8	−27.3
85	−36.9	−26.8	−27.5	−18.4
90	−25.4	−14.6	−19.1	−9.4
95	−12.7	−1.4	−9.6	+0.7
100	0	+11.9	0	+11.9

alory = 4.1840 abs j.
ording to convention, heat evolved is negative.
Southard, J. Am. Chem. Soc. **63**, 3147 (1941).

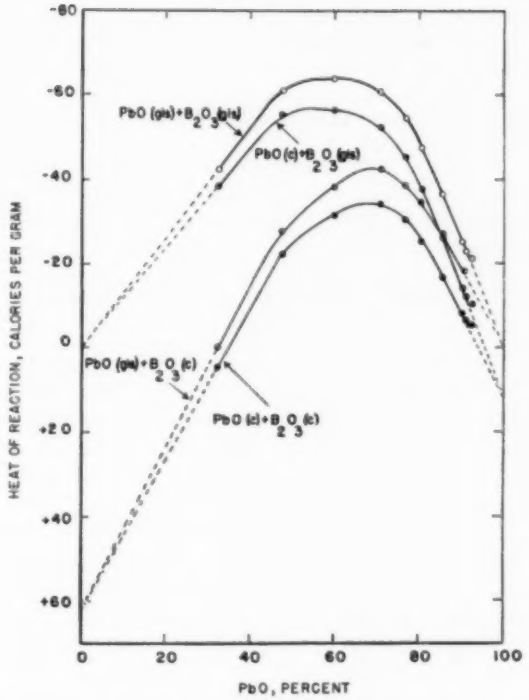

FIGURE 3. *Heats of reaction to form glasses in the system* PbO-B_2O_3.

III. The System PbO-SiO_2

1. Preparation of Glasses

The glasses investigated were prepared by melting, in platinum crucibles, the requisite amounts of PbO and SiO_2. The weights of the melts ranged between 300 and 500 g. They were stirred with a platinum rod and when they seemed homogeneous were poured into iron molds. Glasses containing more than 35 percent of SiO_2 could not be conveniently melted in the apparatus available. Melts containing less than 13 percent of SiO_2 crystallized when poured into molds. In order to prepare glasses containing less than 13 percent of silica, small portions of the crystallized compositions were melted in platinum crucibles and poured into ice water. In this manner glasses containing as little as 6 percent of SiO_2 were

prepared. Microscopic examination of the lowest silica-containing glass thus quenched showed it to contain less than 1 percent of crystalline material.

2. Heat Treatment and Analysis

The glasses were given no further heat treatment. They were analyzed for PbO in the same manner as the PbO-B_2O_3 glasses. Silica was obtained by difference.

3. Calorimetric Materials, Apparatus, and Procedure

A quantity of 2.50 *N* nitric acid was prepared from chemically pure acid and distilled water. Reagent quality hydrofluoric acid (about 48 percent of HF) was used. The calorimetric charge consisted of 50 ml of HF and enough nitric acid to make 648.5±0.05 g of mixed acids.

The calorimeter (fig. 4) used in this work has been previously described [4]. The whole assembly was placed in a water bath whose temperature was kept constant within ±0.005° C by automatic means. The temperature of the calorimeter and water bath were measured with platinum-encased platinum resistance thermometers whose resistances were determined with Mueller temperature bridges.

The Regnault-Pfaundler formula [5] was used in calculating the temperature rise obtained and to guard against arithmetical errors, the temperature rise was also calculated by the second Geophysical Laboratory formula [5], by using the value of the thermal-leakage modulus obtained by the former method.

The effective heat capacity of the calorimeter and contents was measured by introducing a measured amount of electrical energy and measuring the resultant temperature rise.

4. Data and Discussion

Table 3 gives the data obtained, and figure 5 shows them in graphical form. The equation of a straight line was fitted by the method of least squares to the values of heats of solution of compositions containing less than 17 percent of silica. The value at 0 percent of silica (100 percent of PbO) obtained from the equation of this line was −99.2 cal/g. As the value for the heat of solution of PbO (c) was −89.4 cal/g, the heat of

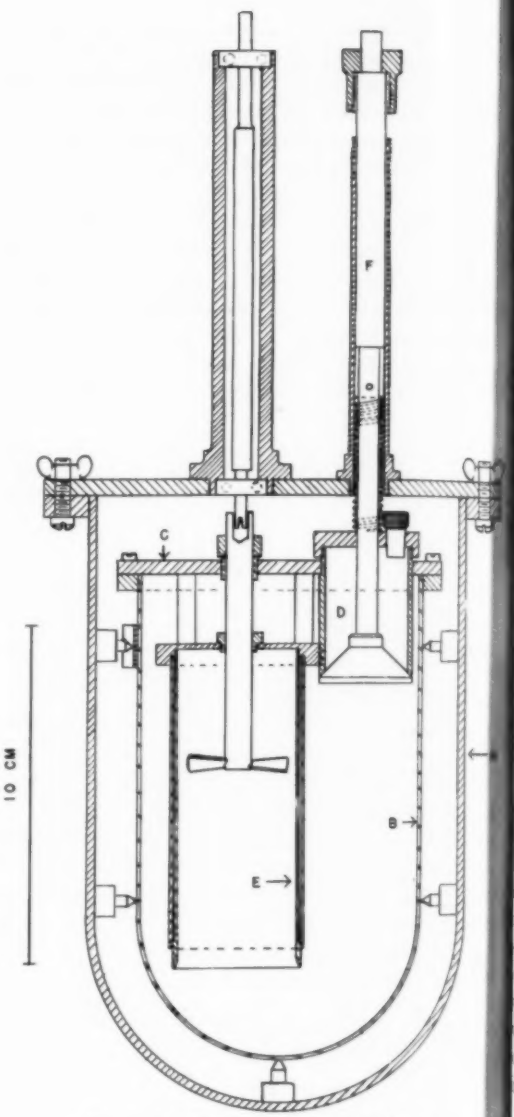

FIGURE 4. *Heat-of-solution calorimeter.*

A, outer jacket; *B*, reaction vessel; *C*, cover of reaction vessel; *D*, valve for introduction of sample; *E*, heater coil; *F*, rod for opening valve.

fusion of PbO (c), at room temperature, calculated from these data is +9.8 cal/g.

The concentration of HF used for the glasses was not sufficient to produce an adequate rate of solution of vitreous silica. A somewhat roundabout method of obtaining its heat of solution in the desired concentration of HF was therefore

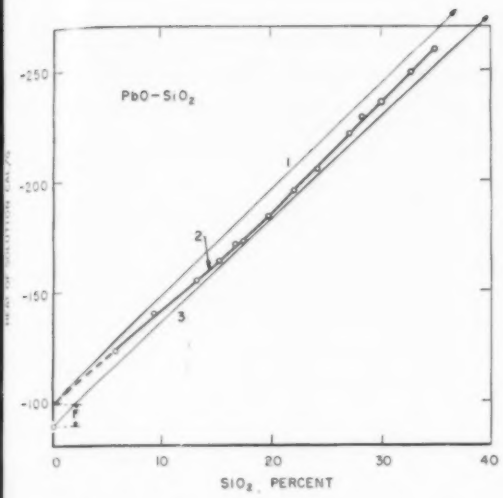

FIGURE 5. *Heat of solution in the system* $PbO\text{-}SiO_2$.

...tures of PbO (gls) and SiO_2 (gls) (curve 1); PbO-SiO_2 glasses (curve 2); ...tures of PbO (c) and SiO_2 (c). The difference between the heat of ...olution of PbO (gls) and PbO (c) (curve 3), represented by *F*, is the ...eat of fusion of PbO at room temperature.

...dopted. The heats of solution of silica gel and ...itreous silica were determined in a high-HF con...entration. The difference between these two ...alues when corrected for the heat of dilution ...aused by the water contained in the gel the is ...nergy difference between these two forms of silica ...nd therefore independent of the solution in which ...t was measured. This difference was then added ...lgebraically to the heat of solution of silica gel ...n the lower concentration of HF, such heat being ...alculated to the ignited weight of the gel and ...orrected for the heat of dilution caused by the ...ater in the gel. The necessary heats of dilution ...ere measured in separate experiments. The heat ...f solution of quartz was calculated by subtract...g −36.8 calories (the value obtained by Mulert [6] for the difference in heat content of amorphous silica and quartz at room temperature) from the heat of solution of vitreous silica.

TABLE 3. *Heats of solution in the system* $PbO\text{-}SiO_2$

Substance	Percentage of SiO_2	Heat of solution [1,2]	Number of determinations	Approximate weight of sample
50 ml HF+sufficient 2.5 (*N*) HNO_3 to make 648.5 g				
		cal/g		*g*
PbO (c)	0.0	−89.4	2	7
PbO (gls)	[3] 0	−99.2		
Glasses	5.9	−123.2	2	7
Do	9.4	−139.8	2	7
Do	13.2	−154.7	2	7
Do	15.3	−163.5	2	7
Do	16.8	−171.4	2	5
Do	17.5	−172.6	2	7
Do	19.8	−183.7	2	7
Do	22.1	−195.4	2	7
Do	24.3	−205.2	2	7
Do	27.1	−221.1	2	7
Do	28.3	−229.4	2	7
Do	30.0	−235.6	9	7
Do	32.7	−248.8	2	7
Do	34.9	−259.3	2	7
Silica gel	100.0	[4] −591.7	2	3
H_2O	0.0	−0.9	1	0.5
SiO_2 (gls)	100.0	[5] −592.4		
SiO_2 (quartz)	100.0	[6] −555.6		
250 ml HF+sufficient 2.5 (*N*) HNO_3 to make 648.5 g				
Silica gel	100.0	[4] −593.7	2	3.0
SiO_2 (gls)	100.0	−592.9	2	2.5
H_2O	0	−11.0	1	0.5

[1] 1 calory = 4.1840 abs j.
[2] By convention, heat evolved is negative.
[3] Extrapolated.
[4] Calculation made on the basis of ignited weight.
[5] Calculated.
[6] O. Mulert, Z. anorg. Chem. **75**, 198 (1912).

With these data and the previously outlined methods, calculations were made of the heats accompanying the following reactions at approximately 25° C:

$$x\mathrm{PbO(gls)} + (1-x)\mathrm{SiO_2(gls)} = x\mathrm{PbO}.(1-x)\mathrm{SiO_2(gls)} + \Delta H_1 \quad (1)$$

$$x\mathrm{PbO\,(c)} + (1-x)\,\mathrm{SiO_2\,(gls)} = x\mathrm{PbO}.(1-x)\mathrm{SiO_2(gls)} + \Delta H_2 \quad (2)$$

$$x\mathrm{PbO\,(gls)} + (1-x)\,\mathrm{SiO_2\,(c)} = x\mathrm{PbO}.(1-x)\mathrm{SiO_2(gls)} + \Delta H_3 \quad (3)$$

$$x\mathrm{PbO\,(c)} + (1-x)\,\mathrm{SiO_2\,(c)} = x\mathrm{PbO}.(1-x)\mathrm{SiO_2(gls)} + \Delta H_4. \quad (4)$$

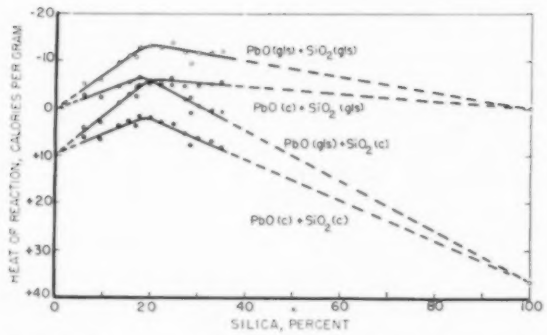

FIGURE 6. *Heats of reaction to form glasses in the system* $PbO\text{-}SiO_2$

TABLE 4. *Heats of glass formation at room temperatures (approximately 25° C) from oxides in the system* $PbO\text{-}SiO_2$

Product (glass) percentage of SiO_2	Reactants			
	PbO(gls)+ SiO_2(gls)	PbO(c)+ SiO_2(gls)	PbO(gls)+ SiO_2(c)	PbO(c)+ SiO_2(c)
	HEAT OF REACTION, CAL/G OF PRODUCT [1,2]			
	ΔH_1	ΔH_2	ΔH_3	ΔH_4
0	0	9.8	0	9.8
5	−3.6	5.7	−1.7	7.6
10	−7.6	1.7	−3.4	5.4
15	−10.6	−2.2	−5.1	3.3
20	−12.7	−4.9	−6.0	2.5
25	−12.3	−5.0	−3.1	4.2
30	−11.8	−4.9	−0.7	6.1
35	−11.2	−4.8	1.7	8.0
100	0	0	[3] 36.8	[3] 36.8

[1] 1 calory = 4.1840 abs j.
[2] According to convention, heat evolved is negative.
[3] O. Mulert Z. anorg. Chem. **75,** 198 (1912).

The results are shown in figure 6. In the absence of data, straight lines were drawn between 35 and 100 percent of silica. Table 4 gives values of heats of reaction at small enough intervals that linear interpolation may be used.

By combining the data from both the systems investigated, a value of +2.4 kcal/mole was obtained for the heat of fusion of PbO at room temperature. This may be compared with a reported value of +2.75 kcal/mole at the melting point [7]. It is to be expected that the heat of fusion at room temperature should be lower than at 1,163° K, the melting temperature.

IV. Summary

The heats of solution of some compositions in the systems $PbO\text{-}B_2O_3$ and $PbO\text{-}SiO_2$ have been measured. From these data and from values of heats of fusion available in the literature, heats of reaction of appropriate oxides to form glasses in these systems have been calculated.

V. References

[1] R. F. Geller and E. N. Bunting, J. Research NBS 18, 585 (1937) RP995.
[2] W. Lerch, Eng. News-Record **113,** 523 (1934).
[3] J. C. Southard, J. Am. Chem. Soc. **63,** 3,147 (1941).
[4] E. S. Newman and L. S. Wells, J. Research NBS 21, 825 (1938) RP1107.
[5] W. P. White, The modern calorimeter (The Chemical Catalog Co., New York, N, Y., 1928).
[6] O. Mulert, Z. anorg. Chem. **75,** 198 (1912).
[7] Bureau of Mines Bull. 393 (1936).

WASHINGTON, January 28, 1948.

U. S. Department of Commerce
National Bureau of Standards

Research Paper RP1894
Volume 40, June 1948

Part of the Journal of Research of the National Bureau of Standards

Divided Flow, Low-Temperature Humidity Test Apparatus[1]

By Arnold Wexler

An apparatus is described, based on the principle of divided flow, for producing air of known relative humidity at temperatures below 0° C with an average error of 3 percent. It was designed primarily for testing and calibrating at low temperature the electric-hygrometer elements used in radiosondes, although any device with a diameter less than 1⅛ in. may be inserted into the test chamber of the apparatus. It is capable of producing rapid and discrete changes in relative humidity at constant temperature, a desirable feature for studying lag characteristics. It is provided with a control for obtaining any air velocity up to 1,500 ft/min.

I. Introduction

An apparatus has been developed for producing r of known relative humidity at temperatures om 0° to −40° C. The primary purpose for ilding this apparatus was to provide a means r investigating the behavior of radiosonde hy- ometers at low temperatures, especially electric- grometer elements of the Dunmore type. In eir use, on radiosondes, the elements are sub- ted to rapidly changing humidity conditions l to air velocities of about 700 ft/min. It was t desirable in studying and calibrating these ments to be able to do so under simulated ditions of use. Therefore, in the design of e apparatus, provision was made to permit id change from one discrete value of relative midity to another, and a device was incorpor- d for controlling the velocity of the air.

II. Theory

The method utilized for producing an atmos- ere of known relative humidity was to divide urately a current of dry air into two streams, e of which was maintained dry and the other urated with respect to ice, and then to recom- e the two. It was employed by Gluckauf [2] in an investigation on absorption hygrometers and by Walker and Ernst, Jr.[3] in a laboratory setup for preparing constant mixtures of air and water vapor. Figure 1 is a simplified schematic diagram of the basic components of the apparatus illustrating the principle of operation. By means of the proportioning valve, V, a flow of moisture-free air is divided into two parts in a known ratio. One part is passed through the saturator, S, over a series of trays containing ice until it is completely saturated. It is then mixed in the mixing chamber, C_M, with the other part that has been maintained dry, and allowed to exhaust through the

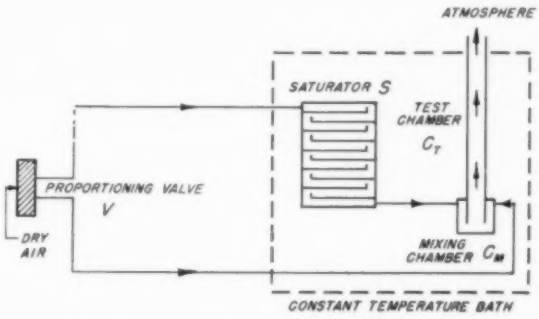

FIGURE 1. *Simplified schematic diagram illustrating the principle of operation of the humidity apparatus.*

This development was financially supported by the Bureau of Ships, rtment of the Navy.

[2] F. Gluckauf, Proc. Phys. Soc. **59**, 344 (1947).

[3] A. C. Walker and E. J. Ernst, Jr., Ind. & Eng. Chem. Anal. Ed. **2**, 134 (1930).

test chamber, C_T, into the atmosphere. The saturator, mixing chamber, and test chamber are kept immersed in a constant temperature bath. In order to subject a hygrometer or other device to air of known and constant relative humidity, it is inserted into the test chamber, C_T.

The relative humidity in the test chamber is a function of (a) the fraction of air that passes through the saturator, (b) the total pressure in the saturator, (c) the total pressure in the test chamber, (d) the saturation pressure, and (e) the partial pressure of the water vapor in the test chamber. Under ideal conditions, which the apparatus approaches with sufficient closeness, all variables except one drop out, and the relative humidity becomes equal to the fraction of air that passes through the saturator. If X is the fraction of air that passes through the saturator, W_S is the ratio by weight of the water vapor to the dry air of the mixture leaving the saturator, and W_C is the ratio by weight of the water vapor to the dry air of the mixture passing through the test chamber, then

$$W_C = XW_S. \tag{1}$$

From Dalton's law of partial pressures, and assuming the perfect gas laws apply, it follows that for an air-water vapor mixture the ratio by weight W of the water vapor to the weight of dry air is

$$W = \frac{M_w}{M_a}\frac{p}{P-p}, \tag{2}$$

where M_a and M_w are the molecular weights respectively of air and water vapor, p the partial pressure of the water vapor in the mixture and P the total pressure of the mixture. Substituting the value of W in eq 2 into eq 1 yields

$$X = \frac{(P_S - p_S)p_C}{(P_C - p_C)p_S}. \tag{3}$$

Relative humidity is defined as the ratio of the actual vapor pressure to the saturation pressure of water. The relative humidity, H, in the test chamber, C_T, is therefore

$$H = \frac{p_C}{p_S}. \tag{4}$$

Combining eq 3 and 4 leads to

$$H = \frac{X}{\left(\frac{P_S}{P_C} - \frac{p_S}{P_C}\right)\frac{P_C}{P_C - p_C}}. \tag{5}$$

If the pressure drops from the saturator to the test chamber and from there to the atmosphere are made small, then $P_S = P_C = P_A$, the atmospheric pressure. At 0° C, $p_S/P_C = p_S/P_A = 0.006$, at −10° C it equals 0.0025, and at −20° C it equals 0.001. Also $P_C/P_C - p_C = P_A/P_A - p_C$, where p_C equals or is less than p_S. Therefore, for the applicable conditions eq 5 reduces without significant error to

$$H = X. \tag{6}$$

III. Description of Apparatus

The essential functional units of the apparatus are (a) the drying system, (b) the proportioning system, (c) the humidifying system, (d) the mixing chamber, (e) the test chamber, (f) the cooling system, and (g) the thermo-regulating system for temperature control. Figure 2 schematically shows these functional units and their component parts.

Air is supplied to the drying system at pressures from 70 to 90 psi. Water from the air at the supply pressure is removed by freezing in the dry ice-varsol bath, *C1*, in which the temperature is well below −70° C. The vapor pressure of the water in the air emerging from the drying system, upon expansion to 1 atmosphere, is probably less than 0.0003 mm Hg. Particles of dirt, ice, or oil are caught by the filter, *A8*.

The dry air is brought to room temperature by means of the electric heater, *A10*, is reduced and controlled in pressure by regulator, *A12*, and then passes through the proportioning system. The pressure regulator also serves to control the speed of air in the test chamber, *A25*, permitting adjustments up to 1,500 ft/min.

The proportioning valve, *A15*, figure 2, which divides the air in a definite ratio consists of six orifices of equal cross-sectional area so arranged that by a turn of the knob of the valve, the incoming air can be divided to produce any of seven ratios, 0, 1/6, 1/3, 1/2, 2/3, 5/6, and 1. These ratios are the fractions of air entering the valve that emerge through one of the exit channels of

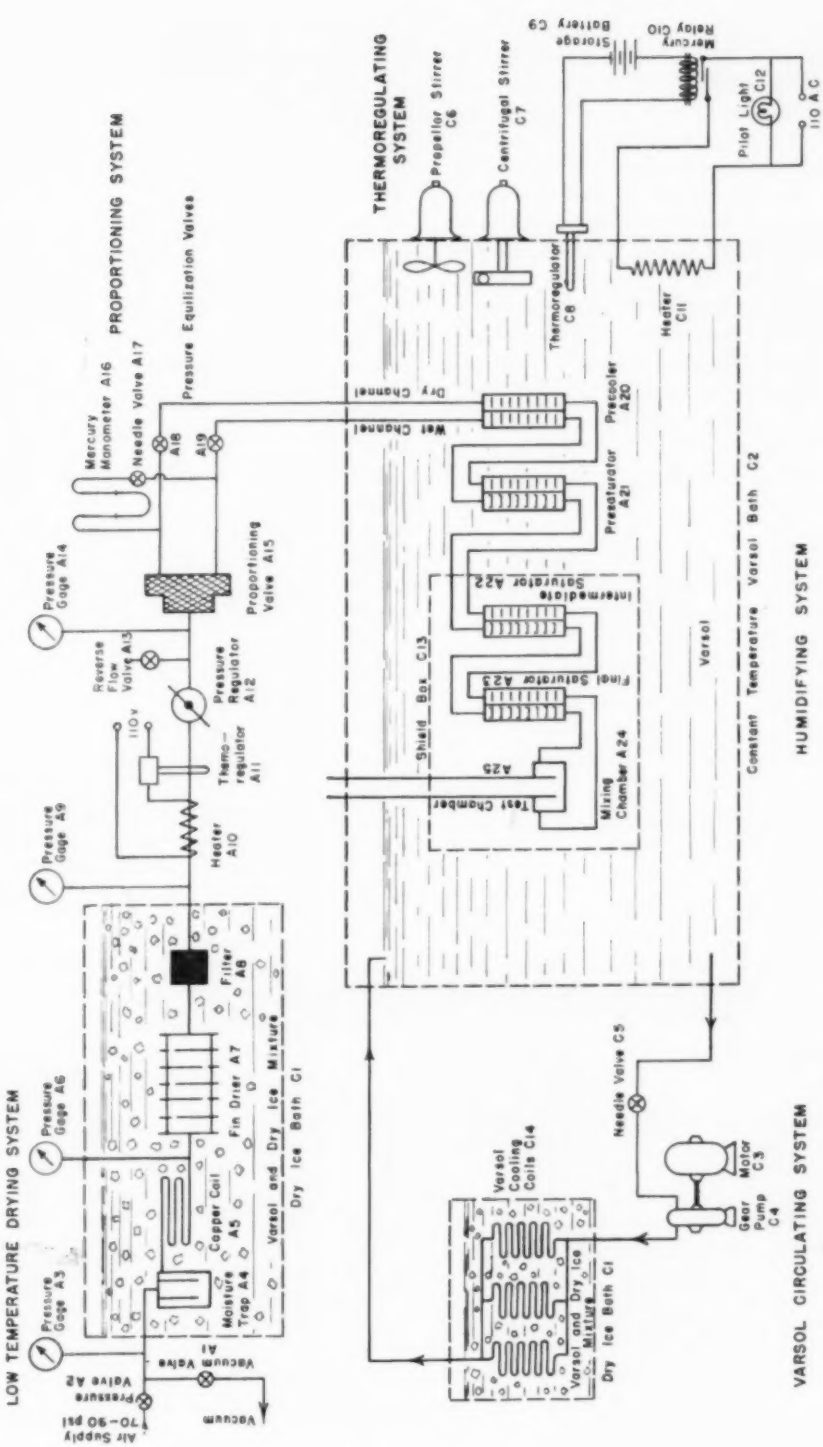

FIGURE 2. *Schematic drawing of the functional units and component parts of the humidity apparatus.*

the valve. If they are considered to apply only to that part of the air that subsequently becomes saturated, then they may be used as the values of X in eq 5 and 6. To assure that the air will divide in accordance with one of these given fixed ratios, the downstream pressures must be equalized. To achieve this, the differential mercury manometer, *A16*, and the two variable resistances (pressure equalization valves), *A18* and *A19*, are installed.

The construction of, and the flow of air through, the proportioning valve are shown in figures 3 and 4. Essentially the valve, *A15*, consists of a brass base, *B*, a brass top, *T*, a steel orifice plate, *P*, and a Bakelite knob, *K*. The incoming air enters the valve through a central hole in the base, *B*, continues through two 3/16-in. diameter holes in the midsection of the orifice plate, *P*, strikes the top, *T*, reverses its flow and again passes through the steel orifice plate, *P*, this time through six 1-mm diameter orifices, and exits in two streams from the base, *B*. The base, *B*, has two circular grooves on a 1½ in. diameter, 3/16-in. wide, ¼ in. deep and separated ¼ in. at the ends. Each groove is connected to an outlet, *O*. The orifice plate, *P*, rests on the base, *B*, in such a fashion that the orifices communicate with either or both grooves, depending upon the angular position of the plate, *P*, with respect to the base, *B*. The surfaces of contact between the plate, *P*, and base, *B*, are ground and lapped and coated with a thin film of stopcock grease to provide a leaktight but rotatable joint. By means of a steel shaft, *S*, that connects the orifice plate, *P*, to the Bakelite knob, *K*, through the valve top, *T*, and a steel packing nut, *N*, that seals the shaft, *S*, in the top, *T*, the orifice plate, *P*, can be rotated to any one of the seven possible settings. Upon turning the knob, *K*, two spring actuated snap pins, *Q*, in the knob, *K*, click and seat in a series of holes on the outer surface of the valve top, *T*, corresponding to the seven desired positions of the orifice plate, *P*, with respect to the valve base, *B*.

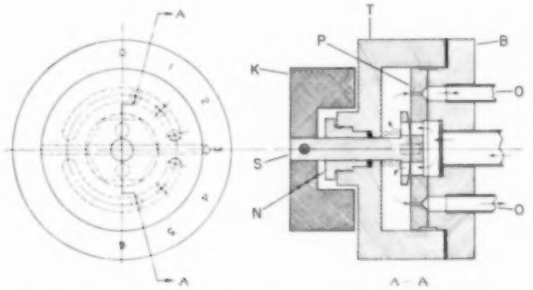

FIGURE 3. *Cross-sectional view of the proportioning valve showing the flow of air.*

P, Brass base; *T*, brass top; *P*, steel orifice plate; *K*, Bakelite knob; *O*, air outlet; *S*, steel shaft; *N*, steel packing nut.

The two air streams, upon leaving the proportioning system, flow through the humidifying system in parallel channels, thermally in contact with one another to allow heat interchange and temperature equilibrium between the two streams to be achieved and maintained. Saturation is ac-

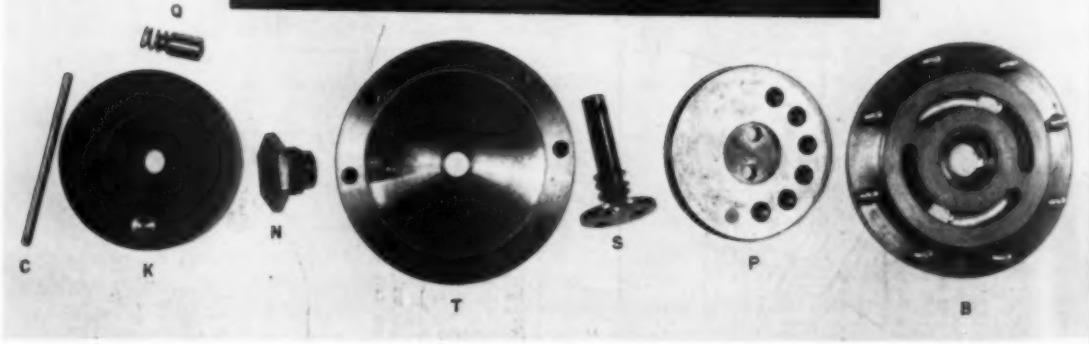

FIGURE 4. *Essential parts of the proportioning valve.*

B, Brass base; *P*, steel orifice plate; *S*, steel shaft; *T*, brass top; *N*, steel packing nut; *K*, Bakelite knob; *Q*, spring-actuated snap pin; *C*, steel pin for fastening *K* to *S*.

complished in four stages. The air to be humidified is first brought to ambient temperature in a precooler, *A20*, figure 2. It then passes through three saturators, *A21*, *A22*, and *A23*. The precooler, *A20*, consists of staggered shelves, one series for each of the two currents of air. Each series is pneumatically isolated from, but in thermal contact with, the other. The saturators are similarly built, except that trays replace one series of shelves. The trays can be filled with water and the water frozen. Thus, in the saturator, in one channel air passes over trays of ice and in the parallel adjoining channel, air passes over shelves. From the final saturator, *A23*, the saturated air and the dry air are centrifugally mixed in the mixing chamber, *A24*, and discharged into the atmosphere through the test chamber, *A25*.

The humidifying system, the mixing chamber, *A24*, and the test chamber, *A25*, are immersed in a varsol bath, *C2*, whose temperature is closely regulated. This is done by circulating the varsol of the bath through cooling coils, *C14*, immersed in dry ice. The bimetal thermoregulator, *C8*, through the relay, *C10*, controls the heater, *C11*, to keep the bath termperature at any desired value. The bath, *C2*, is actively agitated. As an aid in averaging and stabilizing the variations of the bath temperature, the intermediate and final saturators, *A22* and *A23*, the mixing chamber, *A24*, and the test chamber, *A25*, are encased in the copper shield box, *C13*, to provide a unit of high heat content that assumes the mean temperature of the bath. The shield box, *C13*, keeps varsol away from direct contact with the enclosed components.

The thermoregulating system is capable of controlling the temperature of the humidifying system to $\pm 0.05°$ down to $-15°$ C, to $\pm 0.1°$ down to $-30°$ C and to $\pm 0.2°$ down to $-40°$ C for runs up to 10-hr duration. For short periods of time of ½ to 1 hr, the temperature can be maintained to $\pm 0.02°$ C. Calibrated copper-constantan thermocouples and a precision potentiometer are used for measuring the temperature in the apparatus with an accuracy of $\pm 0.02°$ C.

Measurements of the temperatures at the inlets and outlets in the final saturator, *A23*, under various conditions, indicate that at the inlets the two air streams are on the average within 0.07° C of one another, and at the outlets they are on the average within 0.02° C of one another. In the humidifying side of the final saturator, *A23*, the inlet and exit temperatures are on the average within 0.03° C of each other. The temperature in the test chamber is on the average 0.08° C warmer than the air emerging from the final saturator, *A23*.

Since no further saturation can occur subsequent to the exit of the air from the final saturator, *A23*, the pressure at the exit may therefore be considered as the P_S of eq 5. The difference between P_S and atmospheric pressure, P_A, for various test chamber air velocities, is shown in the curve of figure 5. At an air velocity

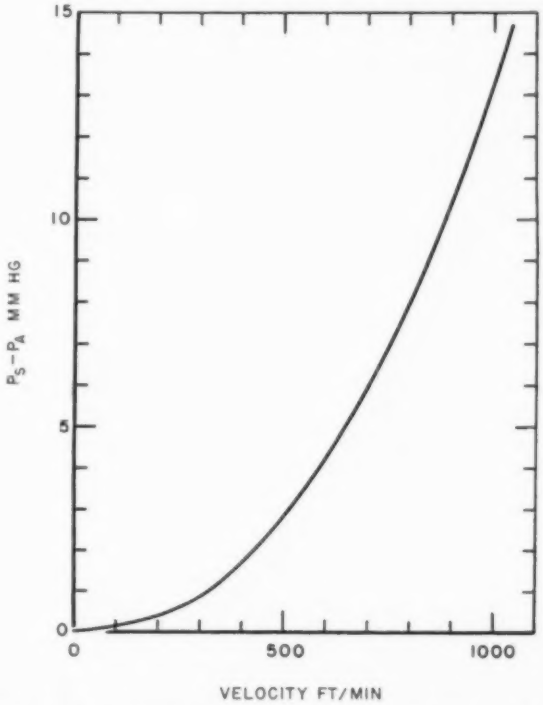

FIGURE 5. *Difference in pressure between the exit of the final saturator, P_s, and atmospheric pressure, P_A, for various test chamber air velocities.*

of 525 ft/min, the assumption that $P_S = P_A$ introduces an error in H of 0.4 percent, at 850 ft/min, the error is 1.2 percent, and at 1,140 ft/min, the error becomes 2.5 percent. If eq 5 instead of eq 6 is used for calculating the relative humidity produced by the apparatus, these errors are avoided.

IV. Calibration

1. Theory

In order to check the over-all performance of the apparatus, a series of tests was made to compare the actual humidity it produces with the humidity given by eq 6. The gravimetric method of moisture determination was selected as the means for measuring the water vapor content of the air in the test chamber under operating conditions. By definition, the relative humidity in the test chamber is

$$H=\frac{p_w}{p_{sw}}, \tag{7}$$

where p_w is the partial pressure of the water vapor in the air, and p_{sw} is the saturation pressure of the water vapor. Assuming that air and water vapor from room temperature to $-60°$ C and at a pressure of 1 atmosphere obey Dalton's law of partial pressures and the perfect gas law, then

$$p_a+p_w=P_C, \tag{8}$$

$$p_wV=\frac{m_w}{M_w}RT_C, \tag{9}$$

and

$$p_aV=\frac{m_a}{M_a}RT_C, \tag{10}$$

where p_a is the partial pressure and P_C is the total pressure of the air in the test chamber, V is the volume, m_w and m_a are the weights of water and air respectively in volume V, M_w and M_a are the molecular weights of water and air, R is the universal gas constant, and T_C is the absolute temperature in the test chamber.

Since the air in the air–water-vapor mixture from the test-chamber exhausts with negligible pressure drop into the atmosphere, then $P_C=P_A$, where P_A is atmospheric pressure. Dividing eq 9 by eq 10 and substituting into eq 8 yields

$$p_w=\frac{P_A}{1+\frac{m_aM_w}{m_wM_a}}. \tag{11}$$

If, from a sample of air taken from the test chamber, the weight of water vapor and air be determined and the pressure measured, the partial pressure of the water vapor could easily be calculated using eq 11, and the relative humidity would follow from eq 7. Figure 6 is a schematic diagram of the setup used for obtaining m_a, m_w, and P_A. A glass probe was inserted into the test chamber and a sample of air withdrawn. The water vapor was removed from the sample by passing it through an absorption tube containing phosphorous pentoxide and accurately weighed. The volume, pressure, and temperature of the same sample of air were measured, and from these data m_a was obtained.

Now

$$m_a=V_ad_a, \tag{12}$$

where d_a is the density of dry air at the pressure and temperature of V_a, the volume of dry air. In this particular setup, V_a was measured by a laboratory wet gas meter at a temperature t_a

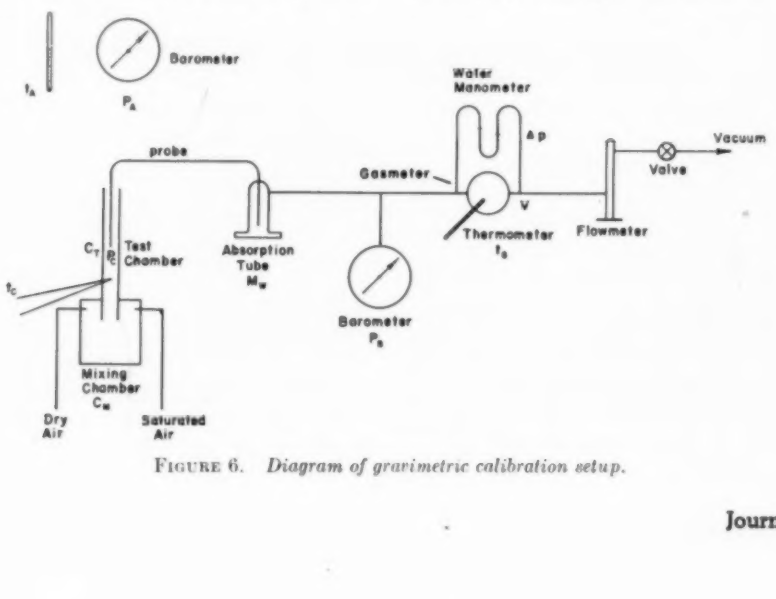

FIGURE 6. *Diagram of gravimetric calibration setup.*

This gasmeter completely saturates the air passing through it so that the partial pressure of the dry air in the gasmeter is given by $P_B - p_g - 1/2\Delta p$, where P_B is the pressure at the inlet to the gas meter, p_g is the saturation pressure of water vapor at the temperature, t_g, of the air in the gas meter, and Δp is the pressure drop across the gas meter. The weight of the dry air in the sample, in terms of observable data and the density of dry air under standard conditions, becomes

$$m_a = \frac{V_a(P_B - p_g - 1/2\Delta p)(0.001293)(273.1)}{760(273.1 + t_g)}. \quad (13)$$

Substituting from eq 13 and 11 into eq 7 yields the desired expression for the relative humidity in the test chamber in terms of known and measurable quantities

$$H = \frac{P_A/p_{sw}}{1 + \dfrac{V_a(P_B - p_g - 1/2\Delta p)(0.00028898)}{m_w(273.1 + t_g)}}. \quad (14)$$

With the proportioning valve set to produce a relative humidity of 100 percent, and the pressure regulator adjusted to give an air velocity in the test chamber of 525 ft/min, a number of gravimetric determinations was made in the temperature range of $-10°$ to $-40°$ C. Then with the air velocity maintained at 525 ft/min, and at an ambient temperature of $-10°$C, a run was made at each setting of the proportioning valve. Finally, at an ambient temperature of $-10°$ C and with the proportioning valve set at 100 percent, two runs were made, one at an air velocity of 850 ft/min and the other at 1,140 ft/min.

2. Procedure and Results

In making a gravimetric determination, the humidity apparatus was set into operation and brought to equilibrium conditions. The sample of air was withdrawn by the glass probe at the rate of 1 liter per minute. An attempt was made to collect 50 mg of water vapor in the absorption tube. This required withdrawing air for periods varying from ½ to 10 hr. The weight of the water was determined with an accuracy of ½ to 1 percent.

For the duration of the run, frequent readings were made at equal time intervals of the temperatures and pressures. The pressure, P_B, at the inlet of the gas meter was determined with an accuracy of ± 0.2 mm Hg and the atmospheric pressure, P_A, was determined with an accuracy of ± 0.1 mm Hg, both by means of precision aneroid barometers. A mercury-in-glass thermometer, accurate to 0.1 deg, gave the temperature, t_g, of the air in the gas meter. A water manometer that could easily be read to ½ mm or better was used to obtain the pressure drop, Δp, across the gas meter.

The results of these determinations are given in table 1, based upon the saturation pressures with respect to ice presented in the Smithsonian Tables,[4] in Wärmetabellen,[5] and in Goff's table.[6] It is estimated that the vapor pressures have been gravimetrically determined with an accuracy of 1 to 2 percent. The difference, D, without regard to sign, between each test result and the setting of the proportioning valve is also given. The differences depend upon the vapor pressure tables used in the computation. The best agreement between the gravimetric determinations and the valve settings of the humidity apparatus is obtained by utilizing the Wärmetabellen values of vapor pres-

TABLE 1. *Gravimetric calibration*

Run number	Saturation temperature	Air velocity	Proportioning valve setting	Relative humidity					
				Smithsonian		Wärmetabellen		Goff	
				Result	D	Result	D	Result	D
	°C	ft/min	°C	°C	°C	°C	°C	°C	°C
1	−10.30	525	100	100.6	0.6	101.6	1.6	101.5	1.5
8	−11.09	525	100	97.3	2.7	98.2	1.8	98.1	1.9
9	−11.01	525	100	94.9	5.1	95.8	4.2	95.7	4.3
10	−11.30	525	100	94.1	5.9	95.0	5.0	94.9	5.1
1a	−14.57	525	100	98.9	1.1	100.0	0.0	100.0	0.0
5	−28.65	525	100	96.6	3.4	99.1	.9	97.6	2.4
6	−28.61	525	100	98.0	2.0	100.3	.3	99.1	0.9
7	−40.94	525	100	94.4	5.6	99.6	.4	94.4	5.6
11	−39.77	525	100	96.0	4.0	99.1	.9	96.3	3.7
2	−10.30	525	83.3	81.3	2.0	82.2	1.1	82.0	1.3
3	−10.10	525	66.7	63.3	3.4	63.9	2.8	63.8	2.9
4	−10.02	525	50.0	49.7	0.3	50.2	0.2	50.2	0.2
12	−10.50	525	33.3	32.9	.4	33.2	.1	33.2	.1
13	−10.48	525	16.7	15.4	1.3	15.5	1.2	15.5	1.2
14	−10.01	525	0	0.4	0.4	0.4	0.4	0.4	0.4
15	−10.36	850	100	94.2	5.8	95.6	4.4	95.5	4.5
16	−10.75	1,140	100	102.3	2.3	103.3	3.3	104.6	4.6
1b	−14.42	525	66.7	64.2	2.5	64.9	1.8	64.9	1.8
Avg	.....	.....	.....	.....	2.7	.....	1.7	.....	2.4

[4] Smithsonian Meteorological Tables, 5th ed. (1939).

[5] L. Holborn, K. Scheel, and F. Henning, Wärmetabellen der Physikalisch-Technischen Reichsanstalt (1919).

[6] John A. Goff, ASHVE Journal Section: Heating, piping, and air conditioning, 355 (June 1945).

sure. The average difference between the valve settings and the test results for the temperature range of −10° to −40° C and for air velocities up to 1,140 ft/min, based on the Warmetabellen is 1.7 percent, on Goff's table is 2.4 percent, and on the Smithsonian tables is 2.6 percent. These results show that the humidity apparatus, over the temperature and velocity ranges tested, produced air having a relative humidity that averaged within 3 percent of the orifice ratio setting of the proportioning valve.

V. Discussion

This apparatus is particularly suited for the investigation and calibration of hygrometers, psychrometers, and dewpoint apparatus at temperatures below 0° C. The rotation of the proportioning valve and the adjustment of the pressure equalization valves are the only operations necessary for changing the relative humidity. The time involved is usually a matter of 1 or 2 seconds. This readily permits any device under test to be subjected to a sudden discontinuous change in relative humidity, a desirable advantage in the study of lag characteristics. The air velocity in the test chamber can easily be adjusted to any value up to 1,500 ft/min within several seconds by adjusting the pressure regulator. The size of an object that can be tested is limited by the inside diameter of the test chamber, which is 1⅛ in. For applications where high air velocities are not necessary, the diameter of the test chamber may be increased to allow larger devices to be inserted.

There is no provision in the apparatus for introducing discrete and rapid changes in ambient temperature. To change the ambient temperature may require up to an hour to reach equilibrium conditions.

There are two ways in which this apparatus may be used to produce known dewpoints. If the proportioning valve is set to 100, then the emerging air will have a dewpoint equal to the test chamber temperature, or, more closely, to the temperature of the air in the final saturator. A change in dewpoint is made by altering the bath temperature. On the other hand, if recourse to standard vapor-pressure tables and eq 4 is made, then for any given bath temperature, several vapor pressures, equivalent to dewpoints at temperatures below that of the bath, are obtainable by rotation of the proportioning valve. The dewpoints thus obtained may have an average error of 0.3 deg C based on an average error in the humidity of 3 percent.

The author thanks R. B. Kennard, for designing the proportioning valve and preliminary models, and E. G. Clarke for constructing some of the units, especially the saturators.

Washington, March 3, 1948.

U. S. Department of Commerce
National Bureau of Standards

Research Paper RP1895
Volume 40, June 1948

Part of the Journal of Research of the National Bureau of Standards

Gradual Damping of Solitary Waves

By Garbis H. Keulegan

This paper treats the problem of the damping by viscous action of translation waves. A short exposition is given of Boussinesq's boundary layer theory for wave motion, and expressions for the damping of rectangular and solitary waves are derived. Scott Russell's experimental results for solitary waves are compared with the theory, and satisfactory agreement is found to exist. This fact makes it legitimate to apply the formulas developed to correct in model tests on harbors or in other tests of a like nature for the dissipative effects that occur in shallow-water waves.

I. List of Symbols

$A = \omega h_1 / H$.
B = breadth of channel.
e = base of natural logarithms.
(E_1/dt) = rate of dissipation of energy of the wave.
(E_2/dt) = rate of decrease of energy of the wave.
δE_1 = energy in column of unit length and of width dx.
$F(\ )$ = function of.
g = acceleration of gravity.
h or h_1 = height of wave above undisturbed surface.
h_{01} = initial height of wave above undisturbed surface.
H = depth of undisturbed water.
k = constant defined by eq 35.
K = constant defined by eq 44.
L = length of wave.
$n = kx$.
N = an integral defined by eq 41.
p = the pressure in the liquid.
q = a variable.
s = a variable, also the distance travelled by the wave.
t = time.
x = coordinate parallel to solid surface in direction of motion.
y = coordinate parallel to solid surface at right angles to direction of motion.
z = coordinate perpendicular to solid surface.
u, v, w = velocity components of particles in the boundary layer parallel to x, y, z, respectively.
u_0, v_0, w_0 = velocity components of particles in the potential region parallel to x, y, z, respectively.
V = particle velocity in the potential region.
X = x-component of body force per unit mass due to gravity.
Y = y-component of body force per unit mass due to gravity.
Z = z-component of body force per unit mass due to gravity.
$Y(\ )$ = function of.
α = a variable, also a damping coefficient.
β = a variable.
κ = a constant defined by eq 17.
μ = viscosity of the water.
ν = kinematic viscosity of the water.
ρ = density of the water.
ϕ = a dissipation function.
ω = velocity of wave propagation.

II. Introduction

In the propagation of translation waves in still water, the main source of dissipation of the energy is the thin layer of liquid next to the solid boundaries of the channel; that is, in the boundary layer. The motion in the layer is laminar, and the determination of the velocities in it can be made by resorting to the ordinary equations of viscous motion. The motion of the liquid outside of the layer is potential, and there the values of the velocities are exactly those that would be obtained from the ordinary theory, assuming that the laminar layer is absent. The errors involved in the use of this method can be ignored, since the variation of pressure in a cross section of the laminar layer is negligible. In fact, the gradual decrease of height of a solitary wave, the only wave of translation, which under ideal conditions, travels without change of form, can be explained on the basis of this dissipation, at least, when the wave is of moderate proportions. The purpose of this paper is to develop a method of computing this energy dissipation and to compare the results with ex-

perimental data as a means of verifying the accuracy of the theory.

III. Dynamical Equation of the Laminar Layer

The theory of the laminar layers with reference to wave motion was initiated by Boussinesq, and the essential elements of his method will now be given [1].[1]

Consider the unsteady motion of a liquid near a flat solid boundary. For the sake of generality it will be supposed that the motion is two-dimensional. We select the rectangular system of axes x, y, z, where z is normal to the solid surface. The velocity components of particles along these axes are u, v, and 0, respectively. At the solid boundary, that is, at $z=0$, u and v vanish. In the motion of waves u, $\partial u/\partial x$, and similar quantities are small, and hence their products may be neglected. Owing to the thinness of the layers and their great lengths, only shears parallel to the solid boundaries are of consequence. Thus, the equation of motion for the liquid in the layer may be written as

$$\left.\begin{aligned}\frac{\partial u}{\partial t}&=-\frac{1}{\rho}\frac{\partial p}{\partial x}+X+\nu\frac{\partial^2 u}{\partial z^2},\\ \frac{\partial v}{\partial t}&=-\frac{1}{\rho}\frac{\partial p}{\partial y}+Y+\nu\frac{\partial^2 v}{\partial z^2},\end{aligned}\right\} \tag{1}$$

and

$$0=-\frac{1}{\rho}\frac{\partial p}{\partial z}+Z,$$

where ν is the kinematic viscosity, ρ is the density of the liquid, p is the pressure, and X, Y, Z are the components of the body forces per unit mass due to gravity. The third equation indicates that in the boundary layer the pressure p, the part due to disturbances, does not vary along the normals to the boundary. The pressure, p, in the viscous layer is the same function of x and y as in the potential region next to the viscous layer.

Denoting the limiting values of u and v at the boundary of the layer by u_0 and v_0, these last being the velocities in the potential region, we have for this region

$$\left.\begin{aligned}\frac{\partial u_0}{\partial t}&=-\frac{1}{\rho}\frac{\partial p}{\partial x}+X,\\ \frac{\partial v_0}{\partial t}&=-\frac{1}{\rho}\frac{\partial p}{\partial y}+Y.\end{aligned}\right\} \tag{2}$$

[1] Figures in brackets indicate the literature references at the end of this paper.

Subtracting these equations from the corresponding ones in eq1, we obtain

$$\frac{\partial(u-u_0)}{\partial t}=\nu\frac{\partial^2(u-u_0)}{\partial z^2}, \tag{3}$$

and

$$\frac{\partial(v-v_0)}{\partial t}=\nu\frac{\partial^2(v-v_0)}{\partial z^2}, \tag{4}$$

with the boundary conditions

$$\left.\begin{aligned}u-u_0&=-u_0 \qquad z=0\\ u-u_0&=0 \qquad z=\infty\end{aligned}\right\} \tag{5}$$

and

$$\left.\begin{aligned}v-v_0&=-v_0 \qquad z=0\\ v-v_0&=0 \qquad z=\infty\end{aligned}\right\}. \tag{6}$$

These are the basic boundary equations as derived by Boussinesq. In the form given above they are applicable to a progressive wave of oscillation in a channel or to a standing wave in a rectangular basin.

The limiting value, $z=\infty$, appearing in the boundary conditions is introduced for convenience in the mathematical analysis. Physically the boundary layer is very thin, and the velocities u and v attain the values u_0 and v_0, respectively, at small finite distances away from the solid boundaries. Moreover, if the waves examined are progressive oscillatory waves moving in a rectangular channel and the layer next to the bottom is considered, the axis of z is taken vertical and the x axis is in the same direction as the channel axis. For this case $v=0$, and u_0 is a function of x, z, and t. When the boundary layer of one of the vertical walls is considered, the axis of z is taken normal to the wall, the axis of y is vertical, and, as before, the axis of x is parallel to the channel axis. Now u_0 and v_0 are the velocities in the potential region outside of the layer and are functions of x, y, and t only. The case of the standing waves in a rectangular channel or in a rectangular basin is interpreted in the same manner.

As we shall be interested primarily in translation waves, we need consider only

$$\frac{\partial(u-u_0)}{\partial t}=\nu\frac{\partial^2(u-u_0)}{\partial z^2}, \tag{7}$$

ith th boundary conditions

$$\left.\begin{aligned} u-u_0&=-u_0 \qquad z=0\\ u-u_0&=0 \qquad z=\infty \end{aligned}\right\}. \tag{8}$$

ow u_0 is the uniform velocity in the cross section nd is a function of x and t, assuming that the ave travels in the direction of x positive or x egative.

In the approximate theory of waves, if h is the perelevation of the wave surface, measured from e undisturbed water surface, and H is the depth f the water in the channel, for a wave traveling in e direction of x positive:

$$u_0=\omega\frac{h}{H}, \tag{9}$$

here ω is the velocity of wave propagation given y

$$\omega=\sqrt{gH}. \tag{10}$$

or a wave of translation having any arbitrary orm but a small wave height, and for a solitary ave, independently of height, for waves traveling the direction of x positive, we have

$$h=h(x-\omega t), \tag{11}$$

nd

$$u=u_0(x-\omega t). \tag{12}$$

The meaning of these expressions is that the hape of waves does not change with translation. viously there are two methods available for the scription of the waves. We may observe the riation of the wave height with time at a fixed int $x(x=0)$, or we may observe the variation of wave height with x at a fixed time $t(t=0)$. We select the second method of observation, and n the main problem resolves itself into de- rmining the velocities in the boundary layer the entire length of the wave at a given time, t. om this point of view, the basic equation now is, placing $\partial/\partial t$ in eq 7 by $-\omega(\partial/\partial x)$

$$\frac{\partial(u-u_0}{\partial x}=-\frac{\nu}{\omega}\frac{\partial^2(u-u_0)}{\partial z^2}, \tag{13}$$

h the boundary conditions

$$\left.\begin{aligned} u-u_0&=-u_0 \qquad z=0\\ u-u_0&=0 \qquad z=\infty \end{aligned}\right\} \tag{14}$$

In general, for t constant, it will be assumed that

$$u_0=F(x). \tag{15}$$

IV. Distribution of the Velocities in the Viscous Layer.

The expression

$$u-u_0=-e^{-z\sqrt{\frac{\kappa\omega}{2\nu}}}\cos\left[\kappa(\alpha-x)-z\sqrt{\frac{\kappa\omega}{2\nu}}\right], \tag{16}$$

where κ and α are independent of z and x, as is well known, is a solution of eq 13 and satisfies the second equation of the boundary conditions, eq 14. Putting $z=0$, and remembering that $u=0$ at $z=0$, we obtain

$$u_0=\cos\left[\kappa(\alpha-x)\right]. \tag{17}$$

Thus we conclude that when the velocity of u_0 in the potential region of the water is periodic and is given by eq 17, velocity u in the laminar layer is given by eq 16.

To obtain the velocities in the viscous layer when the wave consists of a long intumescence, we require a general solution with the value of u_0 given by eq 15. The general solution may be constructed from the elementary solution, eq 16. Multiplying its right-hand member by $F(\alpha)d\alpha$ and integrating between the limits, $+\infty$ and $-\infty$, we obtain

$$u-u_0=-\int_{-\infty}^{+\infty}F(\alpha)e^{-z\sqrt{\frac{\kappa\omega}{2\nu}}}\cos\left[\kappa(\alpha-x)-z\sqrt{\frac{\kappa\omega}{2\nu}}\right]d\alpha,$$

which still is a solution of eq 13 and satisfies the second condition of eq 14. Since the permissible values of κ are positive numbers, we finally take

$$u-u_0=-\frac{1}{\pi}\int_0^{\infty}d\kappa\int_{-\infty}^{+\infty}F(\alpha)e^{-z\sqrt{\frac{\kappa\omega}{2\nu}}}$$

$$\cos\left[\kappa(\alpha-x)-z\sqrt{\frac{\kappa\omega}{2\nu}}\right]d\alpha, \tag{18}$$

and this is the desired solution. For, when we make $z=0$, $u=0$, we have

$$-u_0=-\frac{1}{\pi}\int_0^{\infty}d\kappa\int_{-\infty}^{+\infty}F(\alpha)\cos\left[\kappa(\alpha-x)\right]d\alpha,$$

and, therefore, according to the rule of the Fourier integral, it gives $u_0=F(x)$, indicating that the first condition in eq 14 is also satisfied.

785784—48——5

Although eq 18 gives the distribution of velocities in the boundary layer for the most general case, it is desirable to transform the solution into a form more directly manageable for calculation. That is, it is better to change the double integral into a single integral by effecting an integration with respect to κ. With a view to making use of the two well-known definite integrals,

$$\int_0^\infty e^{-q^2} \cos (2s^2+qs)sds=0, \tag{19}$$

and

$$\int_0^\infty e^{-q^2} \cos (2s^2-qs)sds=\frac{\pi}{8} qe^{-\frac{q^2}{4}}, \tag{20}$$

eq 18 is broken into two parts, as follows:

$$u-u_0=-\frac{1}{\pi}\int_{-\infty}^{x} F(\alpha)d\alpha\int_0^\infty e^{-z\sqrt{\frac{\kappa\omega}{2\nu}}} \cos\left[\kappa(\alpha-x)-z\sqrt{\frac{\kappa\omega}{2\nu}}\right]d\kappa$$

$$-\frac{1}{\pi}\int_{x}^{+\infty} F(\alpha)d\alpha\int_0^\infty e^{-z\sqrt{\frac{\kappa\omega}{2\nu}}} \cos\left[\kappa(\alpha-x)-z\sqrt{\frac{\kappa\omega}{2\nu}}\right]d\kappa. \tag{21}$$

In the first double integral in eq 21 $\alpha \leq x$, and this suggests the transformations

$$\kappa(\alpha-x)=-2s^2$$

$$z\sqrt{\frac{\kappa\omega}{2\nu}}=qs,$$

and

$$d\kappa=\frac{4s}{x-\alpha}ds.$$

Introducing these transformations in the first double integral of eq 21, the integral changes to

$$-\frac{4}{\pi}\int_{-\infty}^{x} \frac{F(\alpha)d\alpha}{x-\alpha}\int_0^\infty e^{-q^2} \cos (-2s^2-qs)sds,$$

and therefore vanishes by virtue of eq 19. In the second double integral of eq 21, $\alpha \leq x$, and this suggests the transformation

$$\kappa(\alpha-x)=2s^2,$$

$$z\sqrt{\frac{\kappa\omega}{2\nu}}=qs,$$

$$d\kappa=\frac{4s}{\alpha-x}ds,$$

$$\alpha-x=\frac{\omega}{\nu}\frac{z^2}{q^2},$$

and

$$d\alpha=-\frac{2\omega z^2}{\nu q^3}dq.$$

Introducing these transformations in the second double integral of eq 21 and making use of eq 20, the final result is

$$u-u_0=-\frac{1}{\pi}\int_0^\infty F\left(x+\frac{\omega z^2}{\nu q^2}\right)e^{-\frac{q^2}{4}}dq,$$

or putting $q=2\beta$,

$$u-u_0=-\frac{2}{\pi}\int_0^\infty F\left(x+\frac{\omega z^2}{4\nu\beta^2}\right)e^{-\beta^2}d\beta, \tag{22}$$

which is the desired solution and may be compared with the Duhamel solution of the heat-conduction equation [2].

V. Loss of Energy in the Laminar Layer

As it is assumed that the laminar layer in the vicinity of the solid boundaries is thin and of considerable length, it suffices to express the dissipation function in the form

$$\phi=\mu\left(\frac{\partial u}{\partial z}\right)^2,$$

where μ is the viscosity of the liquid. Consider a rectangular column of indefinite height, the cross section being of unit length and of width dx. Denoting the rate of dissipation of energy in the column by $d/dt\ \delta E_1$,

$$\frac{d}{dt}(\delta E_1)=\mu dx\int_0^\infty \left(\frac{\partial u}{\partial z}\right)^2 dz. \tag{23}$$

Now, since u_0 is independent of z,

$$\int_0^\infty \left(\frac{\partial u}{\partial z}\right)^2 dz=\int_0^\infty \left[\frac{\partial(u-u_0)}{\partial z}\right]^2 dz.$$

Integrating the right-hand member by parts, we have, since $u-u_0=-u_0$ when $z=0$, and $u-u_0=0$ when $z=\infty$,

$$\int_0^\infty \left(\frac{\partial u}{\partial z}\right)^2 dz=u_0\left(\frac{\partial u}{\partial z}\right)_0-\int_0^\infty (u-u_0)\frac{\partial^2(u-u_0)}{\partial z^2}dz$$

where $(\partial u/\partial z)_0$ is the gradient of velocity at the wall. In view of eq 13,

$$\int_0^\infty \left(\frac{\partial u}{\partial z}\right)^2 dz = u_0\left(\frac{\partial u}{\partial z}\right)_0 + \frac{\omega}{\nu}\frac{\partial}{\partial x}\int_0^\infty \frac{(u-u_0)^2}{2}dz.$$

Substituting in eq 23,

$$\frac{d}{dt}(\delta E_1) = \mu dy dx u_0\left(\frac{\partial u}{\partial z}\right)_0 + \rho\omega dy dx \frac{\partial}{\partial x}\int_0^\infty \frac{(u-u_0)^2}{2}dz.$$

When this expression is integrated between the limits $x=+\infty$ and $x=-\infty$, the result gives the rate of energy dissipation in the entire length of the laminar boundary layer. Denoting this loss by dE_1/dt, the integration gives

$$\frac{dE_1}{dt} = +\mu dy \int_{-\infty}^{+\infty} u_0\left(\frac{\partial u}{\partial z}\right)_0 dx, \qquad (24)$$

since at the infinite distances, $x=\infty$ and $x=-\infty$, the velocities u and u_0 both vanish. This formula is from Boussinesq [1]. The interpretation of the formula is that for the determination of the rate of dissipation of energy in the entire wave it is sufficient to consider the gradient of the laminar velocities at the solid boundary and the velocities in the region outside of the boundary layers.

This result can be extended to limited waves with a new interpretation. Let the posterior and anterior feet of the wave be at the points x_1 and x_2, respectively. Since the thickness of the viscous layer at the front of the wave; that is, at point x_2, is negligibly small, the expression for the rate of dissipation of energy for the limited wave per unit width of channel may now be written, since it is independent of z, as

$$\int_{x_1}^{x_2} u_0\left(\frac{\partial u}{\partial z}\right)_0 dx = \mu\int_{x_1}^{x_2} dx\int_0^\infty \left(\frac{\partial u}{\partial z}\right)^2 dz + \rho\frac{\omega}{2}\int_0^\infty u_1^2 dz,$$

where u_1 is the laminar velocity at the point x_1. The interpretation of the two integrals on the right-hand side of the equation is as follows. The first integral (double) represents the rate of energy dissipation in the laminar boundary layer under the wave. The second integral represents the kinetic energy left behind in the channel as the wave travels onward. As far as the wave is concerned, the energy left behind is lost, so that also in the case of a limited wave the integral on the left-hand side represents the rate of loss of energy of the wave per unit width of channel.

VI. Gradual Extinction of Rectangular Waves

The rectangular wave constitutes the simplest example of a translation wave, and the application of the above theories to obtain the expression for the gradual damping of the wave with distance involves no difficulty. In a rectangular wave the superelevation is constant, and the wave length is finite.

Denote the constant superelevation of the wave by h_1, the length by L, and the particle velocities in the potential region by V. Assuming that the wave is traveling in the direction of positive x, we have

$$u_0 = V = \omega\frac{h_1}{H};\quad \omega = \sqrt{gH}. \qquad (25)$$

Suppose that at time $t=0$, the front of the wave is at the station $x=L$ (see fig. 1). Then for the

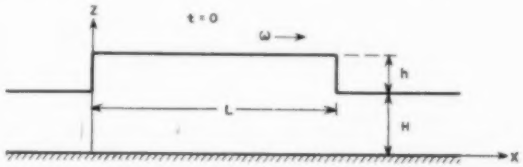

FIGURE 1. *Surface profile of rectangular wave*

description of the function F appearing in eq 15, we have

$$\begin{aligned} u_0 &= F(x) = 0, && x \geqq L, \\ u_0 &= F(x) = V, && 0 \leqq x \leqq L, \\ u_0 &= F(x) = 0, && x \leqq 0. \end{aligned} \qquad (26)$$

Accordingly, using eq 22, we find the boundary layer velocities to be

$$u - V = -\frac{2V}{\sqrt{\pi}}\int_{\frac{z}{2}\sqrt{\frac{\omega}{\nu(L-x)}}}^\infty e^{-\beta^2}d\beta, \qquad (27)$$

when x lies in the range 0 to L, and

$$u = -\frac{2V}{\sqrt{\pi}}\int_{\frac{z}{2}\sqrt{\frac{\omega}{\nu(L-x)}}}^\infty e^{-\beta^2}d\beta + \frac{2V}{\sqrt{\pi}}\int_{\frac{z}{2}\sqrt{\frac{\omega}{-\nu x}}}^\infty e^{-\beta^2}d\beta, \qquad (28)$$

when $x<0$. Since, in the present example, the

rate of dissipation of the energy of the wave per unit width of channel reduces to

$$\frac{dE_1}{dt}=\mu\int_0^L u_0\left(\frac{\partial u}{\partial z}\right)_0 dx, \tag{29}$$

by the use of eq 23, it is sufficient to consider only eq 27. Differentiating the latter equation with respect to z and remembering that V is independent of z,

$$\frac{\partial u}{\partial z}=\frac{V}{\sqrt{\pi\nu(L-x)/\omega}}\,e^{\frac{-z^2\omega}{4\nu(L-x)}}.$$

Putting $z=0$, the velocity gradient at the solid boundary is

$$\left(\frac{\partial u}{\partial z}\right)_0=\frac{V}{\sqrt{\pi\nu(L-x)/\omega}}.$$

Substituting in eq 24 and remembering that $u_0=+V$,

$$\frac{dE_1}{dt}=\mu\int_0^L\frac{V^2dx}{\sqrt{\pi\nu(L-x)/\omega}}.$$

Integrating and afterwards substituting from eq 25, we have finally

$$\frac{dE_1}{dt}=\frac{2}{\sqrt{\pi}}\rho g^{5/4}H^{-3/4}h_1^2L^{1/2}\nu^{1/2}, \tag{30}$$

which is the value of the energy lost per unit time and per unit width of the channel. As was explained previously, the loss is made up of two parts. One part represents the dissipation of energy in the boundary layer under the wave; the other part represents the kinetic energy left in the liquid and in the vicinity of the solid boundary as the wave leaves a given station.

The energy of the wave, half potential and half kinetic, is given by

$$E_2=g\rho h_1^2L,$$

when computed for unit width of channel. The variation of the energy with the time is

$$\frac{dE_2}{dt}=2g\rho h_1L\frac{dh_1}{dt}. \tag{31}$$

Denoting the distance traveled by the wave by s,

$$\frac{dh_1}{dt}=\frac{dh_1}{ds}\frac{ds}{dt},$$

and as ds/dt represents the velocity of the wave

$$\frac{dh_1}{dt}=\sqrt{gH}\frac{dh_1}{ds}.$$

Substituting this in eq 31,

$$\frac{dE_2}{dt}=2\rho g^{3/2}H^{1/2}Lh_1\frac{dh_1}{ds}. \tag{32}$$

By the principle of the conservation of energy, the decrease of the wave energy per unit time must equal the dissipation of energy per unit time. Accordingly the right-hand members of eq 30 and 32 are equal to each other in absolute value but they are of opposite sign. With the grouping of the terms after the comparison is made, we have

$$\left(\frac{h_1}{H}\right)^{-1}d\left(\frac{h_1}{H}\right)=-\frac{1}{\sqrt{\pi}}\left(\frac{L}{H}\right)^{-1/2}\sqrt{\frac{\mu}{g^{1/2}H^{3/2}}}\,d\left(\frac{s}{H}\right),$$

which is the differential equation giving the rate of decrease of the wave height with the distance of travel. The equation was derived by assuming that the channel is very wide and the effect of the side walls could be neglected. If the channel is narrow, however, the second term in the right-hand member must be multiplied by $(1+2H/B)$, where B denotes the width of the channel. That is, in a channel of finite width,

$$\left(\frac{h_1}{H}\right)^{-1}d\left(\frac{h_1}{H}\right)=-\frac{1}{\sqrt{\pi}}\left(1+\frac{2H}{B}\right)\left(\frac{L}{H}\right)^{-1/2}\left(\frac{\nu}{g^{1/2}H^{3/2}}\right)^{1/2}d\left(\frac{s}{H}\right).$$

The solution of the equation is, subject to the assumption, $h=h_{01}$ when $s=0$,

$$\frac{h_1}{H}=\frac{h_{01}}{H}e^{-\alpha\frac{s}{H}}, \tag{33}$$

where

$$\alpha=\frac{1}{\sqrt{\pi}}\left(1+\frac{2H}{B}\right)\left(\frac{L}{H}\right)^{-1/2}\left(\frac{\nu}{g^{1/2}H^{3/2}}\right)^{1/2}. \tag{34}$$

Accordingly, the decrease of wave height with distance is given by an exponential, and a logarithmic decrement that is independent of the height of the wave exists. For waves traveling in water of constant depth, the damping decreases with increase of wave length, with the increase of channel width, and with the decrease of kinematic viscosity.

VII. Gradual Extinction of Solitary Waves

Denoting the superelevation of the crest by h_1, the superelevation of the wave profile for t constant ($t=0$) is given approximately [3] by

$$h=h_1 \operatorname{sech}^2 kx, \tag{35}$$

where

$$k=\frac{1}{H}\sqrt{\frac{3h_1}{4H}}. \tag{36}$$

The dimensionless plot of the wave profile, when the depth of water is twice the crest elevation, is shown in figure 2. Using eq 9 and 12, we may

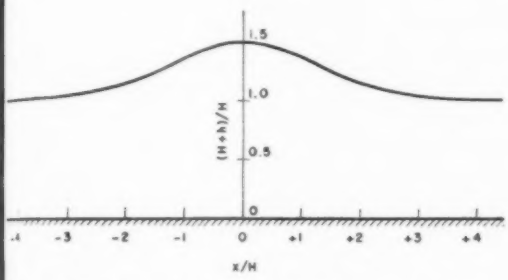

FIGURE 2. *Surface profile of solitary wave,* $(h_1=H/2)$.

write for the particle velocities in the potential region the expressions, assuming that the wave is traveling in the direction of x negative,

$$u_0=A \operatorname{sech}^2 kx;\ A=\omega\frac{h_1}{H}. \tag{37}$$

In the region of the viscous boundary layers, using eq 22,

$$u-u_0=-\frac{2A}{\sqrt{\pi}}\int_0^\infty \operatorname{sech}^2\left(kx+\frac{k\omega z^2}{4\nu\beta^2}\right)e^{-\beta^2}d\beta \tag{38}$$

Differentiating with respect to z and remembering that u_0 is independent of z,

$$\frac{\partial u}{\partial z}=+\frac{4A}{\sqrt{\pi}}\int_0^\infty \operatorname{sech}^2\left(kx+\frac{k\omega z^2}{4\nu\beta^2}\right)\tanh\left(kx+\frac{k\omega z^2}{4\nu\beta^2}\right)\frac{k\omega z}{2\nu\beta^2}\,e^{-\beta^2}d\beta.$$

The limiting value of the integral when z approaches zero cannot be obtained directly, and a transformation of variables becomes necessary. Putting

$$kx=n,$$

and

$$\sqrt{\frac{k\omega}{4\nu}}\frac{z}{\beta}=\alpha,$$

so that

$$-\sqrt{\frac{k\omega}{4\nu}}\frac{z}{\beta^2}\,d\beta=d\alpha,$$

we have

$$\frac{\partial u}{\partial z}=+\frac{4A}{\sqrt{\pi}}\sqrt{\frac{k\omega}{\nu}}\int_0^\infty \operatorname{sech}^2(n+\alpha^2)\tanh(n+\alpha^2)e^{-\frac{k\omega}{4}\frac{z^2}{\alpha^2}}d\alpha.$$

This gives for $z=0$

$$\left(\frac{\partial u}{\partial z}\right)_0=\frac{4A}{\sqrt{\pi}}\sqrt{\frac{k\omega}{\nu}}\int_0^\infty \operatorname{sech}^2(n+\alpha^2)\tanh(n+\alpha^2)\,d\alpha. \tag{39}$$

The rigorous determination of the definite integral appearing in the right-hand side is difficult, and sufficiently accurate results can be obtained if the indicated integration is replaced by the process of summation. Writing

$$Y(n)=\int_0^\infty \operatorname{sech}^2(n+\alpha^2)\tanh(n+\alpha^2)d\alpha, \tag{40}$$

the desired summation for a specific $Y(n)$ was carried out by assigning to the interval $d\alpha$ the value 0.1. The results of such determinations are given in table 1. The graph of $Y(n)$ is shown in figure 3. Since $Y(n)$ is proportional to the velocity gradient at the channel bed, the curve may be interpreted as giving the variation of this velocity gradient along the wave. The velocity gradient at the wall reverses its sign at $n=-0.55$. The maximum value of the velocity gradient at $n=0.35$.

TABLE 1.—*Numerical values of the function* $Y(n)$

n	$Y(n)$	n	$Y(n)$
4.0	0.0000	−0.2	0.1858
3.0	.0066	−.4	.0812
2.5	.0167	−.6	−.0187
2.0	.0440	−.8	−.1017
1.6	.0916	−1.2	−.1495
1.2	.1725	−1.6	−.1408
0.8	.2988	−2.0	−.1132
.6	.3526	−2.5	−.0820
.4	.3798	−3.0	−.0598
.2	.3639	−4.0	−.0355
.0	.2975	−5.0	−.0243

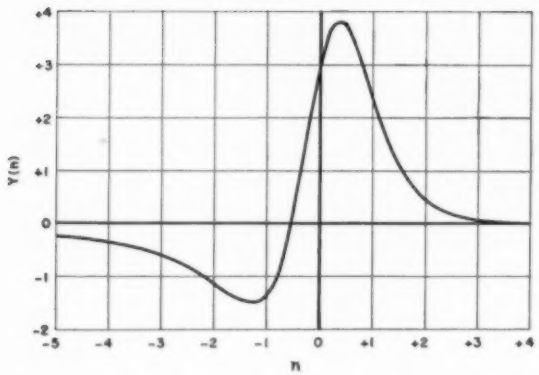

FIGURE 3. *Variation of velocity gradient at wall with distance from center of wave.*

For the case when the wave height is half of the undisturbed water depth, the reversal occurs at the point, $x=-0.9H$. The maximum occurs at the point, $x=0.57H$; that is, ahead of the wave crest. The crest position is given by $x=0$ or $n=0$.

In view of the substitutions from the eq 37, 39, and 40, and the transformation, $kx=n$, the formula for the rate of dissipation of energy, eq 23, reduces to

$$\frac{dE_1}{dt}=-\frac{4\mu A^2}{\sqrt{\pi}k}\sqrt{\frac{k\omega}{\nu}}\int_{-\infty}^{+\infty}Y(n)\ \mathrm{sech}^2\ n dn,$$

which may be written also as

$$\frac{dE_1}{dt}=\frac{4A^2}{\sqrt{\pi}}\rho\sqrt{\frac{\omega\nu}{k}}N, \tag{41}$$

where

$$N=\int_{-\infty}^{+\infty}Y(n)\ \mathrm{sech}^2\ n dn.$$

The method of summations, selecting $n=0.1$, gave for N the value 0.316, or approximately $1/\pi$. Using the value of k from eq. 36 and A from eq. 37 and remembering that $\omega=\sqrt{gH}$, the above expression for the rate of dissipation of energy per unit width of channel becomes

$$\frac{dE_1}{dt}=4\pi^{-3/2}\left(\frac{4}{3}\right)^{1/4}\rho\nu^{1/2}g^{5/4}h_1^{7/4}. \tag{42}$$

As regards the energy of the solitary wave for unit width, we have

$$E_2=\frac{8\rho}{3\sqrt{3}}g(Hh_1)^{3/2}.$$

Differentiating with respect to t, and remembering that

$$\frac{dh_1}{dt}=\sqrt{gH}\frac{dh_1}{ds},$$

we find for the rate of decrease of the energy of the wave

$$\frac{dE_2}{dt}=\frac{4}{\sqrt{3}}\rho g^{3/2}H^2h_1^{1/2}\frac{dh_1}{ds}. \tag{43}$$

By the principle of conservation of energy, the right-hand members of the eq. 42 and 43 are equal in absolute value, but they are of opposite signs. Making the comparison and rearranging the terms, we obtain

$$\left(\frac{h_1}{H}\right)^{-5/4}d\left(\frac{h_1}{H}\right)=-\frac{1}{3}\sqrt{\frac{\nu}{g^{1/2}H^{3/2}}}d\left(\frac{s}{H}\right).$$

This equation is derived by assuming that the channel is very wide, and, therefore, the effect of the vertical side walls can be neglected. If, however, the channel is narrow, the second term in the left-hand member must be multiplied by $[1+(2H/B)]$, where B denotes the width of channel. That is, in a channel of finite width,

$$\left(\frac{h_1}{H}\right)^{-5/4}d\left(\frac{h_1}{H}\right)+\frac{1}{3}\left(1+\frac{2H}{B}\right)\sqrt{\frac{\nu}{g^{1/2}H^{3/2}}}d\left(\frac{s}{H}\right)=0$$

The integration gives, denoting the initial value of the crest height by h_{10},

$$\left(\frac{h_1}{H}\right)^{-1/4}-\left(\frac{h_{10}}{H}\right)^{-1/4}=K\frac{s}{H}, \tag{44}$$

where the coefficient of damping has the value

$$K=\frac{1}{12}\left(1+\frac{2H}{B}\right)\sqrt{\frac{\nu}{g^{1/2}H^{3/2}}}. \tag{45}$$

This gives the variation of the crest height of a solitary wave with the distance traversed.

Comparing eq 33 and 44, it is seen that the extinction of a limited wave takes place in a manner very different than it does with an unlimited wave. Although in the former case the extinction is characterized by a logarithmic decrement independent of height, this is not true of the solitary wave. The reason for this is to be found in the fact that the effective wavelength of a solitary wave is a function of the crest height. With

the decrease of the crest height, the effective length increases [4]. We may now accept the general statement that a logarithmic decrement independent of the wave height exists only for a wave that maintains a constant wavelength during extinction. Thus the damped oscillations of a liquid in a U-tube, of a standing wave in a rectangular basin and the damping of progressive oscillatory wave are characterized by a logarithmic decrement independent of the magnitude of the oscillations.

VIII. John Scott Russell's Experiments on Solitary Waves

To test the validity of the theoretical results above given, John Scott Russell's experimental data on solitary waves will be considered [5]. Although his tests were made to determine the law of velocity of propagation of solitary waves, the representation of data is such that they can be used also to determine the law of damping of waves. The experiments were made more than a century ago in a wooden rectangular channel, 1 ft. wide and 20 ft. long. Altogether some 55 tests are shown for various water depths and for various methods of wave generation.

Regarding the tests, Scott Russell states: "The original experiments are themselves given at the end of this paper for the purpose of enabling anyone who may be disposed to make use of them for any future purpose, either of framing or testing a theory, to make use of them much in the same way as if he had himself made the experiments." The farsightedness and disinterestedness of the investigator is evidence of a scientific attitude of the highest type and are cited by the present writer, to whom Russell's data have proven invaluable, as a model that other investigators might well follow.

Unfortunately the temperature of the water of the tests is not stated. Because of this, the desired comparison between theory and experiment will be made by deducing the temperatures of water from the observed damping of the waves and comparing these values with the prevailing temperatures on the dates of the experiments.

In consulting the original data, it was seen that the tests could be grouped together and average values obtained for individual water depths H. The method of arriving at average values may be explained by considering the measurement for $H=17.9$ cm. It was thought that five individual tests with this depth ought to be sufficient. The original data furnish values of h^1, the height of the wave, and s, the distance travelled. From these, the ratios h^1/H and s/H were formed and plotted. Since in these tests the initial heights h_{10} were not the same, the plotting gave separate curves. Keeping one of the curves fixed, the others were shifted by different amounts parallel to the axis of abscissas so as to give a more or less congruent picture. The positions of the observed points after the shiftings are shown in figure 4. The centers of gravity of the points within selected increments of the abscissas were obtained and are given in table 2. Similar determinations were made for other depths and these are given likewise in table 2.

TABLE 2. *Extinction of solitary waves; average values from Russell's experiments*

$H=2.69$ cm		$H=7.61$ cm		$H=10.02$ cm	
s/H	h_1/H	s/H	h_1/H	s/H	h_1/H
367	0.420	66	0.380	117	0.354
535	.265	255	.305	424	.286
741	.137	397	.265	693	.212
962	.112	605	.197	930	.168
1,060	.087	790	.152	1,156	.128
1,170	.057	950	.130	1,398	.099
1,300	.050	1,178	.097	1,597	.076
1,502	.055	1,470	.067	1,742	.060
1,740	.035	1,780	.053	1,984	.047
2,100	.020	2,270	.043	2,503	.030
Waves 27, 28, 29, 31, 33, 34, 35		Waves 25, 26, 40, 41, 42		Waves 1, 2, 4, 7, 8, 12, 13, 15, 19, 21	
$H=12.92$ cm		$H=15.80$ cm		$H=17.90$ cm	
s/H	h_1/H	s/H	h_1/H	s/H	h_1/H
114	0.342	84	0.235	96	0.131
388	.262	351	.181	291	.110
623	.211	525	.148	493	.097
765	.174	657	.128	683	.087
907	.148	870	.095	889	.071
1,088	.125	1,085	.076	1,097	.063
1,325	.098	1,278	.064	1,288	.048
1,672	.068	1,435	.054	1,494	.045
1,970	.053	1,605	.049	1,706	.041
2,515	.027	1,790	.042	1,910	.032
Waves 43, 44, 46, 47		Waves 48, 49, 50		Waves 51, 52, 53, 54, 55	

The data for $H=17.9$ cm from table 2 are plotted in figure 5. The smooth curve drawn through the points gives the adjusted values of

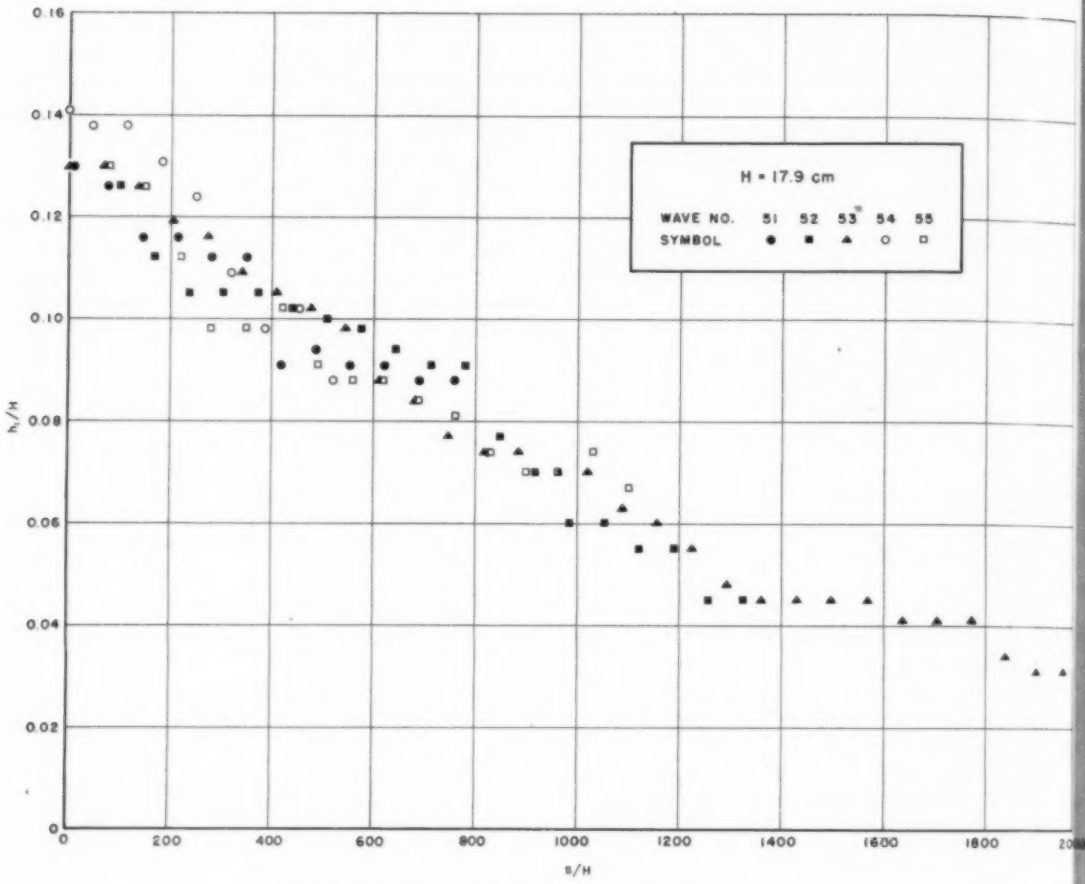

FIGURE 4. *Data from Scott Russell's experiments on solitary waves.*

the wave heights. The quantities h_1/H and s/H were read from the smooth curve. Values of the fourth root of H/h_1 were determined and are plotted in figure 6 with a convenient shift in the origin of s/H. The remaining data from table 2 were treated in a similar manner, and the resulting curves are shown in the figures 6 and 7.

The distribution of the points is linear, a circumstance that accords very well with eq 44. The slopes of the lines determine the coefficients of damping, K. The viscosities of the water can be obtained from eq 45, using the observed values of K, the corresponding values of H, and putting B, the width of flume, equal to 30.48 cm. The individual determinations of water temperature are shown in table 3, and the average value is found to be 15.8° C.

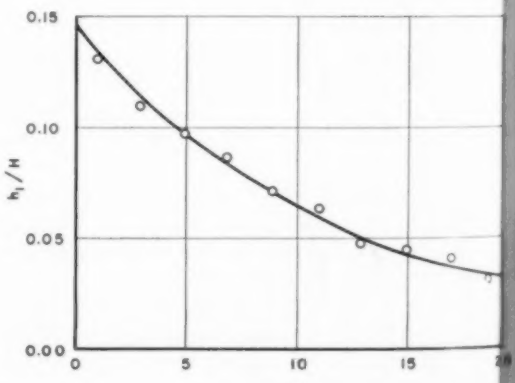

FIGURE 5. *Decrease in height of a solitary wave with distance traversed.*
H=17.9 cm.

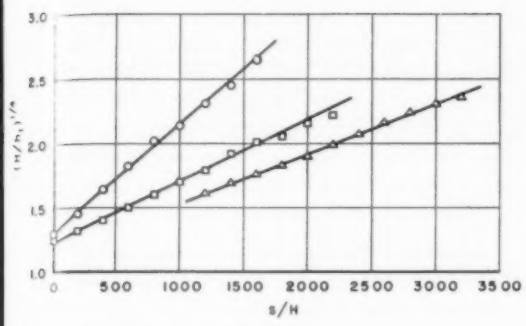

FIGURE 6. *Coefficient of damping of solitary waves.*

○, H=2.69 cm, K=9.0x10^{-4}; □, H=7.61 cm, K=4.85x10^{4}; △, H=17.90 cm, K=3.85x10^{4}.

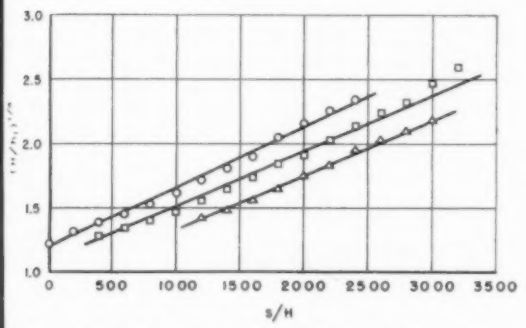

FIGURE 7. *Coefficient of damping of solitary waves.*

○, H=10.02 cm, K=4.67x10^{-4}; □, H=12.92 cm, K=4.25x10^{4}; △, H=15.80 cm, K=4.25x10^{4}.

TABLE 3. *Determination of water temperatures in Russell's experiments*

H	K	ν	θ
Cm			°*C*
2.69	9.00x10^{-4}	0.01168	14.2
7.61	4.85	.01046	18.6
10.02	4.67	.01133	15.4
12.92	4.25	.01132	15.4
15.80	4.25	.01215	12.7
17.90	3.85	.01048	18.5

This average temperature of 15.8° C can be compared with the prevailing mean air temperatures at the time of the experiments. The Russell experiments were made in Edinburgh during the period, August 3 to 8, 1837. It may be said that when water has been introduced from an outside reservoir into a wooden flume of small depth inside a laboratory, during the latter months of summer, the working temperature of the water of the flume is best approximated by the morning air temperature, rather than the minimum or maximum daily air temperatures. Through the courtesy of the Meteorological Office, Air Ministry, Edinburgh, the air temperatures for the dates corresponding to Russell's experiments were communicated to the Liaison Officer, Meteorological Office, U. S. Weather Bureau, Washington, D. C. The data later were transmitted to the author by the Chief of the Division of Climatological and Hydrologic Services, U. S. Weather Bureau. The author wishes to express his appreciation of these favors. The Royal Society of Edinburgh have permitted a copy to be made of the pertinent part of Mr. Adie's original register for 1837, and the part of the data relating to the temperatures is given in table 4. It is the opinion of the Edinburgh Meteorological Office that the morning and the evening readings of the dry bulb were taken at 10 a. m. and 10 p. m. Accordingly, the temperatures described as the morning temperatures should be close to the water temperatures of the Russell experiments. The average of the morning temperature for the 7 days is about 14.6° C. This agrees reasonably well with the average temperatures obtained from the analysis of the wave data; that is, 15.8° C.

TABLE 4.—*Edinburgh temperatures, August 1837*

Day of month	Morning	Evening	Minimum	Maximum
	° *F*	° *F*	° *F*	° *F*
1	60	53	49	57
2	55	53	50	55
3	61	55	48	59
4	52	49	48	57
5	54	53	44	58
6	56	54	46	60
7	60	56	44	66

The favorable agreement between the two temperatures and the fact that the inverse of the fourth root of the wave height varies linearly with the distance of the travel of the waves are proofs enough to show that the present theory of viscous action is sufficient to evaluate the wave dissipation for the water depths considered. The next step in the investigations of this type should be to determine what depths of water will result in a type of dissipation other than that caused by viscosity.

IX. Application to Model Harbor Tests

To the extent that the theoretical formula for the damping of solitary waves is satisfactory, at least when the waves are moving in shallow water, we can apply the results of the above theory to model tests of wave action. The models are of the type in which the depths of water involved are small and in which the pattern of the individual waves can be approximated as a succession of solitary waves. No serious error is made by replacing the ordinary pattern of the shallow-water oscillatory waves by a succession of solitary waves if this is done for the purpose of evaluating the energy dissipation. The method has the advantage that the wavelengths do not enter into the computations, so that the comparisons may be made on the basis of wave height only.

One problem that most readily suggests itself and is susceptible to approximate analysis is the model test of wave action in a harbor. Ordinarily the heights of the waves approaching a model harbor are determined on the basis of Froudian scales after the respective heights of the prototype waves have been selected. For the actual model these values of the initial wave heights must be increased over those determined by the Froude law in order to correct for the energy dissipation in the model harbor. In the prototype the dissipation is not large, so that it can be ignored, and this fact facilitates the determination of the proper model wave heights. The exact determination of the desired model wave heights in the approaches to the model harbor depends on the length and depth proportions of the harbor. The evaluation of the energy dissipation may be made step by step for various consecutive segments of the model. The average of the time rate of dissipation for the entire harbor area can then be evaluated. The height of the approaching waves is increased to such an extent that the increased flow of energy just balances the energy dissipation in the harbor.

The author expresses his appreciation to Herbert N. Eaton, Chief of the Hydraulics Section, for his editorial review of the paper and for constructive suggestions; also to George W. Patterson, his former colleague, for advice and the review of the mathematical methods used in the paper.

X. References

[1] J. Boussinesq, Complément à une étude intitulée ≪Essai sur la théorie des eaux courantes≫, et à un mémoire ≪Sur l'influence des frottements sur les mouvements reguliers des fluides≫. Journal de mathématiques pures et appliquées, série 3e, **4**, 335 (1878).

[2] A. G. Webster, Partial differential equations of mathematical physics, p. 172 (B. G. Teubner, Leipzig, 1927).

[3] G. H. Keulegan and G. W. Patterson, J. Research NBS **24**, 47 (1940) RP1272.

[4] H. Lamb, Hydrodynamics, (ed 5) p. 401 (Cambridge University Press, Cambridge, Eng., 1924).

[5] Report of the Committee on Waves, appointed by the British Association at Bristol in 1836, and consisting of Sir John Robinson, Secretary of the Royal Society of Edinburgh, and John Scott Russell, Report of the seventh meeting of the Brit. Assn. Adv. Sci. p. 417 (John Murray, London, 1838).

WASHINGTON, January 27, 1948.

INDEX TO VOLUME 40

A

Page

Adams, Gerald B., Galen B. Schubauer, Effect of support on the performance of vane anemometers, RP1872 ... 275
Air, absorption of X-rays in, RP1883 ... 393
Air of known relative humidity, apparatus for producing, RP1894 ... 401
Airplane mapping lenses, RP1858 ... 93
Alternating-current bridges, theory of Wagner ground balance for, RP1869 ... 245
Alumina or aluminum oxide in portland cement, phase studies, RP1867 ... 225
Anemometers, vane, effect of support on performance, RP1872 ... 275
Annealing, effect on pH response of the glass electrode, RP1859 ... 105
Annealing of glass, RP1856 ... 67
Antimony-124, disintegration, RP1877 ... 315
Attenuator, waveguide-below-cutoff, theory and design, RP1868 ... 235
Austenitic steels, stainless, stabilization, RP1878 ... 321

B

Barium crown glass, effect of some oxides on refraction and liquidus, RP1881 ... 361
Bates, Roger G., Gladys D. Pinching, Second dissociation constant of oxalic acid from 0° to 50° C and the pH of certain oxalate buffer solutions, RP1885 ... 405
Beckedahl, Norman, Fred A. Quinn, Jr., Elmer W. Zimmerman, Vulcanization of synthetic rubbers by the Peachey process, RP1850 ... 1
Bennett, John A., Herbert C. Vacher, Calibration of X-ray measurement of strain, RP1874 ... 285
Bloom, Evelyn G., Fred L. Mohler, Jonathan H. Lengel, C. Edward Wise, Metastable transitions in mass spectra of fifty-six hydrocarbons, RP1888 ... 437
Bogue, Robert H., William R. Eubank, Preliminary study of portions of the systems Na_2O–CaO–Al_2O_3–Fe_2O_3 and Na_2O–CaO–Fe_2O_3–SiO_2, RP1867 ... 225
Bone char, sulfur in, RP1871 ... 263
Bone, Thomas H., Percy A. Sigler, Martin N. Geib, Measurement of the slipperiness of walkway surfaces, RP1879 ... 339
Borates, compounds of, with carbohydrates, RP1862 ... 129
Boric acid-lead oxide system, heats of solution and reaction, RP1893 ... 471
Brenner, Abner, Eugenia Kellogg, Magnetic measurement of the thickness of composite copper and nickel coatings on steel, RP1875 ... 295
Burkhead, Polly, Charles W. Jennings, Physical properties of electrodeposited chromium, RP1854 ... 61
Brewster, Joseph F., Horace S. Isbell, Nancy B. Holt, Harriet L. Frush, Behavior of certain sugars and sugar alcohols in the presence of tetraborates—correlation of optical rotation and compound formation, RP1862 ... 129
Bridge, Wheatstone, best galvanometer location, RP1884 ... 401
Bridges, theory of Wagner ground balance for alternating-current, RP1869 ... 245
Burkhead, Polly, Abner Brenner, Charles W. Jennings, Physical properties of electrodeposited chromium, RP1854 ... 31
Bunsen flame, infrared radiation, RP1860 ... 113

C

Capacitance of condenser microphones, measurement of, RP1869 ... 245
Carbohydrates, reactions of with borates, RP1862 ... 129
Catadioptric systems, reduction of sphero-chromatic aberration in, RP1892 ... 467
Cathodic protection of iron and steel pipe from underground corrosion, RP1876 ... 301
Cement, portland, phase studies, RP1867 ... 225
Chemical durability of some barium crown glasses containing beryllium and lanthanum oxides, PR1881 ... 361
Chromium-nickel, steel, effect of low temperature, RP1882 ... 375
Chromium plating, properties, RP1854 ... 31
Cook, G. S., E. L. R. Corliss, Cavity pressure method for measuring the gain of hearing aids, RP1857 ... 85
Cook, Richard K., Theory of Wagner ground balance for alternating-current bridges, RP1869 ... 245
Copper and nickel on steel, thickness determination, RP1875 ... 295
Corliss, E. L. R., G. S. Cook, Cavity pressure method for measuring the gain of hearing aids, RP1857 ... 85
Corrosion of zinc in dry-cell electrolytes, effect of inhibitors on, RP1870 ... 251
Corrosion, underground, of iron and steel, RP1876 ... 301
Coverplates for steel columns, mechanical properties:
RP1861 ... 121
RP1880 ... 347
Cromwell, Frances Jane, D. J. McAdam, Jr., G. W. Geil, Influence of low temperatures of the mechanical properties of 18:8 chromium-nickel steel, RP1882 ... 375
Curtiss, Leon F., Irving Feister, Disintegration of antimony-124, RP1877 ... 315

D

Darr, John H., Samuel J. Rosenberg, Stabilization of austenitic stainless steel, RP1878 ... 321
Deitz, Victor, Helen R. Higginson, Cola Parker, Determination of sulfur in bone char, RP1871 ... 263
Denison, Irving A., Melvin Romanoff, Behavior of experimental zinc-steel couples underground, RP1876 ... 301
Density of oxygen gas, RP1891 ... 457
Dibeler, Vernon H., Fred L. Mohler, Dissociation of SF_6, CF_4, and SiF_4 by electron impact, RP1853 ... 31
Dissociation constant of oxalic acid, RP1885 ... 405
Dissociation of SF_6, CF_4, and SiF_4 by electron impact, RP1853 ... 25
Dry cells, electric correlation of gel strength of paste walls and shelf life, RP1870 ... 251

E

Electric dry cells, correlation of gel strength of paste walls and shelf life, RP1870 ... 251
Electric dry cells, effect of inhibitors on corrosion of zinc in, RP1863 ... 151
Electrode, glass, effect of annealing on pH response, RP1859 ... 105
Electrodeposition of chromium, RP1854 ... 31
Electron impact, dissociation of SF_6, CF_4, and SiF_4 by, RP1853 ... 25
Equation of state for oxygen, RP1891 ... 457
Eubank, William R., Robert H. Bogue, Preliminary study of portions of the systems Na_2O-CaO-Al_2O_3, and Na_2O-CaO-Fe_2O_3-SiO_2, RP1867 ... 225
Expansivity of glass, RP1856 ... 67

F

Fano, U., Electric quadrupole coupling of the nuclear spin with the rotation of a polar diatomic molecule in an external electric field, RP1866 ... 215
Feister, Irving, Leon F. Curtiss, Disintegration of antimony-124, RP1877 ... 315
Ferric oxide in portland cement, phase studies, RP1867 ... 225
Flames, infrared emission spectra, RP1890 ... 449
Freeman, J. J., Theory and design of a cavity attenuator, RP1868 ... 235
Fructose, optical rotation of in the presence of tetraborates, RP1862 ... 129
Frush, Harriet L., Horace S. Isbell, Joseph F. Brewster, Nancy B. Holt, Behavior of certain sugars and sugar alcohols in the presence of tetraborates—correlation of optical rotation and compound formation, RP1862 ... 129

G

Page

Galvanometer, locating of for maximum sensitivity, RP1884 ... 401
Gardner, Irvine C., Francis E. Washer, Lenses of extremely wide angle for airplane mapping, RP1858 ... 93
Gases, measurement of water vapor in, RP1865 ... 169
Gas flames, spectra, RP1890 ... 449
Geib, Martin N., Percy A. Sigler, Thomas H. Boone, Measurement of the slipperiness of walkway surfaces, RP1879 ... 339
Geil, G. W., D. J. McAdam, Jr., Frances Jane Cromwell, Influence of low temperatures of the mechanical properties of 18:8 chromium-nickel steel, RP1882 ... 375
Gel strength of paste walls of dry cells, RP1870 ... 251
Glass, barium crown, effect of some oxides on properties, RP1881 ... 361
Glass electrode, effect of annealing of pH response, RP1859 ... 105
Glass, expansion of, RP1856 ... 67
Glass, surface tension, RP1855 ... 61
Glucose, optical rotation of in the presence of tetraborates, RP1862 ... 129
Grauer, Oscar H., Edgar H. Hamilton, Zeno Yabowsky, C. H. Hahner, Changes in the index of refraction and liquidus of a barium-crown glass produced by the partial substitution of the oxides of beryllium, calcium, lithium, lanthanum, thorium, and boron, RP1881 ... 361
Greenspan, Martin, Ambrose H. Stang, Perforated cover plates for steel columns; summary of compressive properties, RP1880 ... 347

H

Hahner, C. H., Edgar H. Hamilton, Oscar H. Grauer, Zeno Yabowsky, Changes in the index of refraction and liquidus of a barium-crown glass produced by the partial substitution of the oxides of beryllium, calcium, lithium, lanthanum, thorium, and boron, RP1881 ... 361
Hamer, Walter J., Correlations of the gel strength of paste walls and the shelf life of electric dry cells, RP1870 ... 251
—, *Morehouse, Clarence K., George W. Vinal*, Effect of inhibitors on the corrosion of zinc in dry-cell electrolytes, RP1863 ... 151
Hamilton, Edgar H., Oscar H. Grauer, Zeno Yabowsky, C. H. Hahner, Changes in the index of refraction and liquidus of a barium-crown glass produced by the partial substitution of the oxides of beryllium, calcium, lithium, lanthanum, thorium, and boron, RP1881 ... 361
Hearing aid, gain, RP1857 ... 85
Heat of combustion of phenyl-beta-napthylamine, RP1873 ... 281
Heats of reaction of the lead oxide-boric acid and lead-oxide-silicon dioxide systems, RP1893 ... 471
Heats of solution and reaction of the lead oxide-boric acid and lead-oxide-silicon dioxide systems, RP1893 ... 471
Higginson, Helen R., Victor Deitz, Cola Parker, Determination of sulfur in bone char, RP1871 ... 263
Holt, Nancy B., Horace S. Isbell, Joseph F. Brewster, Harriet L. Frush, Behavior of certain sugars and sugar alcohols in the presence of tetraborates—correlation of optical rotation and compound formation, RP1862 ... 129
Hubbard, Donald, Gerald F. Rynders, Effect of annealing and other heat treatments on the pH response of the glass electrode, RP1859 ... 105
Humidity test apparatus, RP1894 ... 479
Humphreys Curtis J., Earle K. Plyler, Infrared emission spectra of flames, RP1890 ... 449
Hydrocarbons, metastable transitions in mass spectra of 56, RP1888 ... 437
Hydrogen, spectra, RP1890 ... 449
Hygrometer elements, electric, apparatus for calibrating, RP1894 ... 479

I

Infrared radiation from a Bunsen flame, RP1860 ... 113
Ionization constant of oxalic acid, RP1885 ... 405
Iron and steel, soil corrosion, RP1876 ... 301
Isbell, Horace S., Joseph F. Brewster, Nancy B. Holt, Harriet L. Frush, Behavior of certain sugars and sugar alcohols in the presence of tetraborates—correlation of optical rotation and compound formation, RP1862 ... 129

J

Jaffe, Bernard S., Ambrose H. Stang, Perforated cover plates for steel columns; compressive properties of plates having ovaloid, elliptical, and "square" perforations, RP1861 ... 121
Jennings, Charles W., Abner Brenner, Polly Burkhead, Physical properties of electrodeposited chromium, RP1854 ... 31
Jessup, Ralph S., Donald E. Roberts, Heat of combustion of phenyl-beta-naphthylamine (*N*-phenyl-2-naphthylamine), RP1873 ... 281

K

Page

Kellogg, Eugenia, Abner Brenner, Magnetic measurement of the thickness of composite copper and nickel coatings on steel, RP1875 ... 29
Keulegan, Garbis H., Gradual damping of solitary waves, RP1895 ... 87
Kolter, F. Ralph, Location of the galvanometer branch for maximum sensitivity of the Wheatstone bridge, RP1884 ... 401

L

Lead oxide-boric acid system, heats of solution and reaction, RP1893 ... 471
Lead oxide-silicon dioxide system, heats of solution and reaction, RP1893 ... 471
Lengel, Jonathan H., Evelyn G. Bloom, Fred L. Mohler, C. Edward Wise, Metastable transitions in mass spectra of fifty-six hydrocarbons, RP1888 ... 437
Lime or calcium oxide in portland cement, phase studies, RP1867 ... 225
Liquidus of a barium crown glass; effect of oxides of beryllium, calcium, lanthanum, lithium, thorium, and boron upon the, RP1881 ... 361

M

Madorsky, Samuel L., Sidney Straus, Pyrolytic fractionation of polystyrene in a high vacuum and mass spectrometer analysis of some of the fractions, RP1886 ... 417
Magne-gage measurements of coatings of copper and nickel on steel, RP1875 ... 29
Magnetic measurement of electrodeposits of copper and nickel, RP1875 ... 29
Magnetic properties of 18:8 stainless steel, RP1882 ... 375
Maksutov camera, sphero-chromatic aberration, RP1892 ... 469
Mannitol, optical rotation of in the presence of tetraborates, RP1862 ... 129
Mass spectra of 56 hydrocarbons, metastable transitions in, RP1888 ... 437
Mass spectrometer analysis of pyrolytic fraction of polystyrene, RP1886 ... 417
McAdam, Jr., D. J., G. W. Geil, Frances Jane Cromwell, Influence of low temperatures of the mechanical properties of 18:8 chromium-nickel steel, RP1882 ... 375
McCulloch, Francis W., William W. Walton, and W. Harold Smith, Determination of small amounts of oxygen in organic compounds, RP1889 ... 461
Mechanical properties of 18:8 stainless steel, RP1882 ... 375
Metastable transitions in mass spectra of 56 hydrocarbons, RP1888 ... 437
Meyers, Cyril H., Pressure-volume-temperature data for oxygen, RP1891 ...
Minsimer, Joshua K., Charles G. Weber, Merle B. Shaw, Martin J. O'Leary, Resin bonding and strength development in offset papers, RP1887 ... 427
Mohler, Fred L., Evelyn G. Bloom, Jonathan H. Lengel, C. Edward Wise, Metastable transitions in mass spectra of fifty-six hydrocarbons, RP1888 ... 437
—, *Vernon H. Dibeler*, Dissociation of SF_6, CF_4, and SiF_4 by electron impact, RP1853 ...
Molecular rotation spectra, hyperfine structure of, RP1866 ...
Molecules, long chain, volume effect in, RP1852 ...
Morehouse, Clarence K., Walter J. Hamer, George W. Vinal, Effect of inhibitors on the corrosion of zinc in dry-cell electrolytes, RP1863 ... 151

N

Newman, Edwin S., Leo Shartsis, Some energy relations in the systems PbO–B_2O_3 and PbO–SiO_2, RP1893 ... 471
Nickel and copper coatings, magnetic measurement of thickness, RP1875 ... 29
Nuclear energy of antimony-124, RP1877 ...
Nuclear quadrupole moments, effect of, RP1866 ...

O

Offset papers, strength of, RP1887 ... 427
O'Leary, Martin J., Charles G. Weber, Merle B. Shaw, Joshua K. Minsimer, Resin bonding and strength development in offset papers, RP1887 ... 427
Organic compounds, determination of oxygen in, RP1889 ... 461
Oxalate buffer solutions, pH of, RP1885 ...
Oxides of Li, Be, Ca, B, La, and Th, effect properties of a barium crown glass, RP1881 ... 361
Oxides in portland cement, phase studies, RP1867 ... 225
Oxygen, determination of small amounts of inorganic compounds, RP1889 ... 461
Oxygen, molecular, thermodynamic functions for, RP1864 ... 157
Oxygen, pressure-volume-temperature data, RP1891 ...
Ozone over Organ Mountains, N. M., measurement, RP1851 ...

P

Page

Papers, resin-bonding and strength development, RP1887 ... 427
Parker, Viola, Victor Deitz, Helen R. Higginson, Determination of sulfur in bone char, RP1871 ... 263
Paste walls of dry cells, correlation of strength with shelf life, RP1870 ... 251
Perforated cover plates for steel columns, mechanical properties:
RP1861 ... 121
RP1880 ... 347
Phase equilibria of mineral oxides in portland cement, RP1867 ... 225
Phenyl-beta-naphthylamine, heat of combustion, RP1873 ... 281
N-phenyl-2-naphthylamine, heat of combustion, RP1873 ... 281
pH of oxalate buffer solutions, RP1885 ... 405
pH response of glass electrode, effect of annealing, RP1859 ... 105
Pinching, Gladys D., Roger G. Bates, Second dissociation constant of oxalic acid from 0° to 50° C and the pH of certain oxalate buffer solutions, RP1885 ... 405
Plyler, Earle K., Curtis J. Humphreys, Infrared emission spectra of flames, RP1890 ... 449
Infrared radiation from a Bunsen flame, RP1860 ... 113
Polystyrene, pyrolytic fractionation, and mass spectrometer analysis, RP1886 ... 417
Portland cement, phase studies, RP1867 ... 225
Pressure properties for oxygen, RP1864 ... 163
Pressure-volume-temperature data on oxygen, RP1891 ... 457
Printing papers, strength of, RP1887 ... 427
Pyrolysis of polystyrene and mass spectrometer analysis, RP1886 ... 417

Q

Quinn, Fred A., Jr., Norman Pekkedahl, Elmer W. Zimmerman, Vulcanization of synthetic rubbers by the Peachey process, RP1850 ... 1

R

Radiation, infrared, from Bunsen flame RP1860 ... 121
Refraction of a barium crown glass, effect of some oxides on, RP1881 ... 361
Ruhl, Ralph, Elmer R. Weaver, Measurement of water in gases by electrical conduction in a film of hygroscopic materials and the use of pressure changes in calibration, RP1865 ... 169
Roberts, Donald E., Ralph S. Jessup, Heat of combustion of phenyl-beta-naphthylamine (*N*-phenyl-2-naphthylamine), RP1873 ... 281
Romanoff, Melvin, Irving A. Denison, Behavior of experimental zinc-steel couples underground, RP1876 ... 301
Rosenberg, Samuel J., John H. Darr, Stabilization of austenitic stainless steel, RP1878 ... 321
Rubbers, synthetic, vulcanization by the Peachey process, RP1850 ... 1
Rudders, Gerald F., Donald Hubbard, Effect of annealing and other heat treatments on the pH response of the glass electrode, RP1859 ... 105

S

Saunders, James P., Arthur Q. Tool, Expansion effects shown by some Pyrex glasses, RP1856 ... 67
Schmidt camera, sphero-chromatic aberration, RP1892 ... 467
Schauer, Galen P., Gerald P. Adams, Effect of support on the performance of vane anemometers, RP1872 ... 275
Shartsis, Leo, Edwin S. Newman, Some energy relations in the systems $PbO-B_2O_3$ and $PbO-SiO_2$, RP1893 ... 471
Shartsis, Leo, Spinner, Alden W. Smock, Surface tension of compositions in the systems $PbO-B_2O_3$ and $PbO-SiO_2$, RP1855 ... 61
Shaw, Merle P., Charles G. Weber, Martin J. O'Leary, Joshua K. Missimer, Resin bonding and strength development in offset papers, RP1887 ... 427
Shelton, Percy A., Martin N. Geib, Thomas H. Poone, Measurement of the slipperiness of walkway surfaces, RP1879 ... 339
Silica or silicon dioxide in portland cement, phase studies, RP1867 ... 225
Silicon dioxide-lead oxide systems, heats of solution and reaction, RP1893 ... 471
Simon, Robert, Note on volume effect in coiling molecules, RP1853 ... 21
Slipperiness of walkway surfaces, RP1879 ... 339
Smith, W. Harold, William W. Walton, Francis W. McCulloch, Determination of small amounts of oxygen in organic compounds, RP1889 ... 443
Smock, Alden W., Leo Shartsis, Sam Spinner, Surface tension of compositions in the systems $PbO-B_2O_3$ and $PbO-SiO_2$, RP1855 ... 61
Soda or sodium oxide in portland cement, phase studies, RP1867 ... 225
Solution corrosion of iron and steel, RP1876 ... 301
Solutol, optical rotation of in the presence of tetraborates, RP1862 ... 129
Sucrose, optical rotation of in the presence of tetraborates, RP1862 ... 129

Page

Spectra, beta and gamma ray, of antimony-124, RP1877 ... 315
Spectra of flames, infrared emission, RP1890 ... 449
Sphero-chromatic aberration, reduction in, RP1892 ... 467
Spinner, Sam, Leo Shartsis, Alden W. Smock, Surface tension of compositions in the systems $PbO-B_2O_3$ and $PbO-SiO_2$, RP1855 ... 61
Stainless steels, austenitic, stabilization, RP1878 ... 321
Stair, Ralph, Measurement of ozone over the Organ Mountains, New Mexico, RP1851 ... 9
Stang, Ambrose H., Bernard S. Jaffe, Perforated cover plates for steel columns; compressive properties of plates having ovaloid, elliptical, and "square" perforations, RP1861 ... 121
—, *Martin Greenspan*, Perforated cover plates for steel columns: summary of compressive properties, RP1880 ... 347
Steel and iron, soil corrosion, RP1876 ... 301
Steel columns, properties of perforated cover plates for:
RP1861 ... 121
RP1880 ... 347
Steel, measurement of thickness of coatings of copper and nickel on, RP1875 ... 295
Steel, stainless, 18-8, effect of low temperature, RP1882 ... 375
Steels, austenitic stainless, stabilization, RP1878 ... 321
Stephens, Robert E., Reduction of sphero-chromatic abberation in catadioptric systems, RP1892 ... 467
Strain, X-ray measurement, RP1874 ... 285
Straus, Sidney, Samuel L. Madorsky, Pyrolytic fractionation of polystyrene in a high vacuum and mass spectrometer analysis of some of the fractions, RP1886 ... 417
Sucrose, optical rotation of in the presence of tetraborates, RP1862 ... 129
Sulfur in bone char, RP1871 ... 263
Surface tension of glass, RP1855 ... 61

T

Taylor, Lauriston S., Frank H. Day, Absorption of X-rays in air, RP1883 ... 393
Temperature, low, effect on properties of 18-8 stainless steel, RP1882 ... 375
Tensile tests of 18-8 stainless steel, RP1882 ... 375
Tetraborates, effect of on the optical rotations of carbohydrates, RP1862 ... 129
Thermodynamic functions for molecular oxygen in the ideal gas state, RP1864 ... 163
Tool, Arthur Q., James P. Saunders, Expansion effects shown by some Pyrex glasses, RP1856 ... 67

U

Ultraviolet measurements of ozone over Organ Mountains, New Mexico, RP1851 ... 9
Underground corrosion, cathodic protection of iron and steel from, RP1876 ... 301

V

Vacher, Herbert C., John A. Pennett, Calibration of X-ray measurement of strain, RP1874 ... 285
Vane anemometers, effect of support on performance, RP1872 ... 275
Vinal, George W., Clarence K. Morehouse, Walter J. Hamer, Effect of inhibitors on the corrosion of zinc in dry-cell electrolytes, RP1863 ... 151
Volume effect in coiling molecules, RP1852 ... 21
Vulcanization of synthetic rubbers by the Peachey process, RP1850 ... 1

W

Walkway surfaces, slipperiness, RP1879 ... 339
Walton, William W., Francis W. McCulloch, W. Harold Smith, Determination of small amounts of oxygen in organic compounds, RP1889 ... 443
Washer, Francis E., Irvine C. Gardner, Lenses of extremely wide angle for airplane mapping, RP1858 ... 93
Water vapor in gases, measurement, RP1865 ... 169
Waveguide-below-cutoff attenuator, theory and design, RP1868 ... 235
Waves, solitary, damping of, RP1895 ... 487
Weaver, Elmer R., Ralph Ruhl, Measurement of water in gases by electrical conduction in a film of hygroscopic materials and the use of pressure changes in calibration, RP1865 ... 169
Weber, Charles G., Merle B. Shaw, Martin J. O'Leary, Joshua K. Missimer, Resin bonding and strength development in offset papers, RP1887 ... 427
Wexler, Arnold, Divided flow, low-temperature humidity test apparatus, RP1894 ... 479

Page

Wheatstone bridge, sensitivity, RP1884 401
Wise, C. Edward, Evelyn G. Bloom, Fred L. Mohler, Jonathan H. Lengel, Metastable transitions in mass spectra of fifty-six hydrocarbons, RP1888 437
Woolley, Harold W., Thermodynamic functions for molecular oxygen in the ideal gas state, RP1864 163

X

X-ray measurement of strain, RP1874 285
X-rays, absorption in air, RP1883 393

Page

Zabowsky, Zeno, Edgar H. Hamilton, Oscar H. Grauer, C. H. Hahner, Changes in the index of refraction and liquidus of a barium crown glass produced by the partial substitution of the oxides of beryllium, calcium, lithium, lanthanum, thorium, and boron, RP1881 361
Zimmerman, Elmer W., Norman Bekkedahl, Fred A. Quinn, Jr., Vulcanization of synthetic rubbers by the Peachey process, RP1850 1
Zinc anodes for protection of iron and steel from underground corrosion, RP1876 301
Zinc in dry-cell electrolytes, effect of inhibitors on corrosion of, RP1863 151

Engineering
Library

Journal of Research

of the

National Bureau of Standards

JUNE 1948

VOLUME 40 NUMBER 6

PERIODICALS OF THE NATIONAL BUREAU OF STANDARDS

Journal of Research

The National Bureau of Standards is the principal agency of the Federal Government for fundamental research in physics, chemistry, and engineering. It has the custody of the national standards of physical measurement in terms of which all working standards in research laboratories and industry are calibrated, and carries on necessary research leading to improvement in such standards and methods of measurement. It also has a general responsibility for basic research in physics, chemistry, and engineering, and for developments of improved methods for testing materials and equipment. It determines physical constants and properties of materials, tests and calibrates standard measuring apparatus and reference standards, and studies technical processes. The results of the Bureau's research and investigations are published in the JOURNAL OF RESEARCH.

Research Papers

Reprints of individual articles appearing in the JOURNAL OF RESEARCH. They are made available to serve the needs of research workers, technical groups, and others for the separate papers relating to the special subjects in which they are interested.

Technical News Bulletin

Contains short but complete summaries of research, development, and testing in progress at the Bureau, accounts of the Bureau's national and international activities, scientific and technical announcements of new plans and programs, and a list of publications by members of the staff. It is a prompt and reliable source of official information of value to those who desire to keep in touch with the general activities of the Bureau.

Basic Radio Propagation Predictions

The CRPL–D series, Basic Radio Propagation Predictions, is issued as a monthly publication for those concerned with radio communication in determining the best sky-wave frequencies over any path at any time of day for average conditions for the month of prediction, which is made 3 months in advance. Charts of extraordinary-wave critical frequency for the F2 layer, of maximum usable frequency for a transmission distance of 4,000 km, and of percentage of time occurrence for transmission by sporadic E in excess of 15 Mc, for a distance of 2,000 km, are included.

ANNUAL SUBSCRIPTION Send order, with remittance, to Superintendent of Documents, U. S. Government Printing Office, Washington 25, D. C.	United States, Canada, Cuba, Mexico, Newfoundland, Republic of Panama	Other countries
JOURNAL OF RESEARCH of the National Bureau of Standards:		
12 monthly issues (2 volumes), paper covers	$4.50	$5.50
Bound volume (½ year, 1 volume), blue buckram	3.00	3.50
RESEARCH PAPERS	(*)	(*)
TECHNICAL NEWS BULLETIN, 12 monthly issues	1.00	1.35
BASIC RADIO PROPAGATION PREDICTIONS, 12 monthly issues	1.00	1.25

*The prices of the separate Research Papers appearing in this JOURNAL are given in the Contents. If 100 or more copies of any separate are ordered, a discount of 25 percent is allowed. Those who desire copies of separate Research Papers should send their orders and remittances without delay to the Superintendent of Documents, U. S. Government Printing Office, Washington 25, D. C. This will aid him to determine the number of copies to be printed for sale. Research Papers are not printed from electrotypes and usually no more reprints can be had when the first and only printing is exhausted.

Published with approval of Bureau of the Budget